Universidade de Aveiro Departamento de Química
Ano 2018

Joana Cruz Almeida

Nanopartículas magnéticas à base de ferrites para tratamento de água contendo crómio

Magnetic nanoparticles based on ferrites for treatment of water containing chromium

Universidade de Aveiro Departamento de Química
Ano 2018

Joana Cruz Almeida

Nanopartículas magnéticas à base de ferrites para tratamento de água contendo crómio

Magnetic nanoparticles based on ferrites for treatment of water containing chromium

Dissertação apresentada à Universidade de Aveiro para cumprimento dos requisitos necessários à obtenção do grau de Mestre em Química, realizada sob a orientação científica do Doutor Tito da Silva Trindade, Professor Associado com Agregação do Departamento de Química da Universidade de Aveiro, e da Doutora Maria Eduarda da Cunha Pereira, Professora Associada do Departamento de Química da Universidade de Aveiro.

o júri

presidente

Doutora Helena Isabel Seguro Nogueira
Professora auxiliar do Departamento de Química da Universidade de Aveiro

Doutor Tito da Silva Trindade
Professor Associado com Agregação do Departamento de Química da Universidade de Aveiro

Doutor Carlos Alberto Garcia do Vale
Investigador Principal do Centro Interdisciplinar de Investigação Marinha e Ambiental (CIIMAR) da Universidade do Porto

agradecimentos

Gostaria de agradecer ao Doutor Tito Trindade e à Doutora Eduarda Pereira pelo apoio, disponibilidade, orientação e conhecimentos transmitidos ao longo da realização deste trabalho.

À Daniela Tavares pela disponibilidade em ajudar e apoio incansável, mas também pelo seu interesse, sugestões, esclarecimento de dúvidas, simpatia e amizade manifestados ao longo de todo o trabalho.

Ao Drº Bruno Henriques e à Drª Cláudia Lopes por toda a ajuda, conhecimento, conselhos, simpatia e disponibilidade.

A todos os meu colegas de laboratório pelo companheirismo, simpatia e ajuda.

A todas as pessoas que me ajudaram com diversas técnicas, no departamento de Química, no departamento de Cerâmica e do Vidro e no Laboratório Central de Análises.

Ao Celso Cardoso por todo o apoio, paciência e ajuda, em todos os momentos.

Aos meus pais pela educação e valores transmitidos, por todo o apoio e compreensão manifestada durante todo o meu percurso académico e por todos os sacrifícios que fizeram para me proporcionarem esta oportunidade.

palavras-chave Crómio, Nanomateriais, Sorção, Tratamento de águas

resumo

As atuais políticas ambientais visam diminuir os níveis de elementos vestigiais potencialmente tóxicos nos ecossistemas aquáticos e promover a reutilização da água após o tratamento adequado das águas residuais. O crómio é um elemento de risco presente nos efluentes de várias indústrias, cujos níveis devem ser reduzidos para alcançar os objetivos destas políticas. Nos últimos anos foram desenvolvidos novos materiais e técnicas de baixo custo e alta eficiência para a remoção de crómio. A maior parte do trabalho de investigação realizada diz respeito ao uso de nanomateriais para sorção de crómio a partir de soluções sintéticas, monoelementares e com concentrações irrealistas deste elemento (já que concentrações muito altas permitem que os procedimentos experimentais não tenham problemas com contaminação ou quantificação). Este trabalho compila os trabalhos publicados até à data sobre a aplicação de vários nanomateriais no tratamento de águas contaminadas com crómio. Com base nesta revisão de literatura, foram identificados os principais fatores que influenciam a eficiência de remoção, assim como as lacunas de conhecimento.

Os nanomateriais magnéticos têm ganho interesse como sorventes por permitirem a remoção dos contaminantes das águas por separação magnética. Neste trabalho, foram sintetizadas NPs de magnetite, ferrite de manganês e ferrite de cobalto. As NPs magnéticas foram caracterizadas através de várias técnicas como: DRX, FTIR, TEM/STEM, análise química, método BET, estudos magnéticos e ponto isoelétrico.

Das condições estudadas, verificou-se uma eficiente remoção de Cr(III) com $CoFe_2O_4$ (percentagens de remoção superiores a 95%) no caso em que a remoção ocorreu a pH 6 (a partir de água salina e água salina contendo matéria orgânica dissolvida) e a pH 10 (a partir de água ultra-pura, água mineral, água salina e água salina contendo matéria orgânica dissolvida). Este material mostrou-se promissor para o tratamento de águas residuais e efluentes industriais. A cinética dos processos de remoção foi avaliada recorrendo a três modelos cinéticos de adsorção: pseudo-1ª ordem, pseudo-2ª ordem e Elovich, avaliando-se qual o modelo matemático que descrevia melhor os dados experimentais obtidos. Concluiu-se que a interação entre o Cr(III) e as NPs é de natureza química.

keywords Chromium, Nanomaterials, Sorption, Water Treatment

abstract

Current environmental policies aim to reduce the levels of toxic substances in aquatic ecosystems and to promote the water reuse after appropriate treatment of wastewaters. Chromium is a hazard element present in effluents of various industries that should be reduced to achieve the objectives of these policies. New materials and low-cost techniques of high efficiency in the removal of chromium have been developed in the recent years. Most of the reported research concerns the use of surface functionalized nanomaterials for sorption of chromium dissolved either in synthetic or mono-elemental spiked solutions, and with unrealistic concentrations of chromium (since very high concentrations allow experimental procedures not to have problems with contamination or quantification). The present work compiles the research undertaken so far on the application of various nanomaterials in the treatment of chromium contaminated waters. On the basis of this literature review, major factors influencing the removal efficiency are examined and gaps of knowledge are identified.

Magnetic nanomaterials have gained interest as sorbents by allowing the removal from the water of the materials containing contaminants by magnetic separation. In this work, magnetite, manganese ferrite and cobalt ferrite NPs were synthesized. The NPs were characterized using various techniques as follows: XRD, FTIR, TEM/STEM, Chemical Analysis, BET Method, Magnetic Studies and Isoelectric Point.

Chromium removal by $CoFe_2O_4$ NPs with percentages above 95% was verified for the removal at pH 6 (from saline water and saline water with dissolved organic matter) and pH 10 (from ultra-pure, mineral, saline water and saline water with dissolved organic matter). This material proved to be promising for the treatment of wastewaters and industrial effluents. The kinetics of these adsorption experiments was evaluated using three kinetic adsorption models: pseudo-1st order, pseudo-2nd order and Elovich, evaluating which one of these mathematical models has a better adjustment to the experimental data. It was concluded that the interaction between Cr(III) and NPs is of chemical nature.

List of Contents

List of Figures

List of Tables

Chapter 1

Introduction and objectives

1.1. Introduction

Present life style requires the exploitation of Earth's resources beyond their sustainability causing the reduction or depletion of limited resources (Kitzes et al., 2008). Concerns about environmental issues started with the Industrial Revolution, discharge of industrial effluents, either inadequately treated or untreated, into aquatic systems leading to the increase of hazardous inorganic and organic contaminants in natural waters such as in rivers, lakes, estuaries and coastal areas (Verdonschot et al., 2013). Because of the non-degradation character of many contaminants, they are transfer to the food chains with impact on the ecosystem services and reducing the resource safety (Jin et al., 2016; Thekkudan et al., 2016). Volume of dumped debris in water systems increased with the urbanization often surpassing the self-cleaning capacity and purification of aquatic systems. These discharges may increase in the future as population tends to migrate and concentrate in urban areas, as response to modern life and adversities related to climate changes.

Trace elements have been removed from wastewaters by conventional methods, such as chemical precipitation, ion exchange, membrane filtration, coagulation/flocculation and electrochemical treatment (Fu and Wang, 2011). However, these methods have little efficiency, produce large volume of wastes, and some of them are expensive. Alternatives for treatment of water contaminated by metals are sorption methods (Kurniawan et al., 2006). Efficiency of sorption can be influenced by pH, temperature, amount of sorbent, initial metal concentration, and the presence of other contaminants (Babel and Kurniawan, 2003; Dubey et al., 2016; Valle et al., 2017). Since sorption is mainly a surface phenomenon (mentioned as adsorption in literature), sorbents must have a high surface area per unit mass; this process can be more or less effective depending on the specific surface area (m^2/g), porosity, temperature and pore distribution size. Nanomaterials, i.e., materials and structures with at least one dimension of 1-100 nm (Francisquini et al., 2014), tend to exhibit unique physical and chemical properties. For example, its mechanical, optical, magnetic and chemical properties, which depend heavily on shape, size, surface characteristics and inner structure are much different from those of particles and macroscopic surfaces of similar composition due to size effects and surface (Martins and Trindade, 2012; Quina, 2004; Trindade and Thomas, 2013). We are in the presence of a nanoparticle when this rule is found for the three dimensions (ISO, 2012). Most chemical reactions of the contaminants occur in the surface of the material, hence higher surface area to volume ratio of

nanomaterials leads to much higher chemical activity. So, it is not necessary a large amount of material to remove efficiently a relatively large amount of contaminants. Moreover, it is possible to coat nanomaterials with several types of specific ligands to increase the affinity for target compounds. Adsorption is hence favoured in nanomaterials due to their catalytic potential, high reactivity promoting a fast sorption kinetics, large surface area, easy separation, and considerable number of active sites for interactions with contaminants (Lopes et al., 2013).

Chromium is among the most toxic trace elements released to surface and ground waters due to its widespread use in industrial applications such as leather tanning, metallurgy, electroplating and refractory (Jin et al., 2016; Lin, 2002). Investigations have been carried out to illustrate and remediate the chromium-bearing contamination, as indicated from the significantly increase of published articles about chromium toxicity over the last 10 years (Jin et al., 2016).

The main objective of this research work is to study the application of magnetic nanoparticles in the treatment of chromium-contaminated waters, so this element will be discussed in more detail in the next Chapters.

In this work the problematic related with the discharge to the environment of the trace element chromium will be evaluated, mainly the processes to remove this element from contaminated waters using different nanomaterials and laboratory conditions.

1.2. Methods towards the removal of trace elements from contaminated waters

There is a need to improve the ecological state of waters. In this way, depending on the type of contaminant, the level of pollution, and the resources and expertise available, there are several conventional methods for potential toxic trace elements removal from wastewaters (Fu and Wang, 2011), including chemical precipitation, ion exchange, membrane filtration, coagulation/flocculation and electrochemical treatment.

The conventional methods are cheap but little effective, or efficient and expensive, or efficient at high metal concentrations but inefficient for more realistic concentrations, or usually difficult to apply due to the large volume of waste produced during treatment (Figueira, 2010). Then, sorption has been the most recognized and alternative method for removal of contaminants from water (Ray and Shipley, 2015).

1.2.1. Sorption mechanisms towards the removal of trace elements from contaminated waters

Removal of trace elements from contaminated waters by sorption methods corresponds to the transfer of the sorbate from the liquid fraction to the surface of the sorbent. This process has similarities with ion exchange process in the way they can be grouped as sorption processes, since both consist in contaminant removal through its transportation from the solution to the surface of a solid material. Depending on the attractive forces between the sorbent and the sorbate, this becomes bound by physical (physiosorption) and/or chemical (chemisorption) interactions (Kurniawan et al., 2006). While in the physiosorption the sorbate bonds to the sorbent surface by weak forces, such as Van der Waals interactions, which is a reversible process, the chemisorption is frequently irreversible due to the presence of strong chemical bonds between the sorbent and the sorbate. Sorption process is hence efficient, easy to use, and economically more favourable than many other methods. In addition, in certain conditions sorption is reversible, and thus sorbents can be regenerated by suitable desorption process. A large variety of sorbents are available to remove trace elements from waters (Fu and Wang, 2011), including nanomaterials with various types of coatings and chemical functionalizations (Batool et al., 2014; Hua et al., 2012; Thekkudan et al., 2016; Xu et al., 2012). Sorption mechanisms by a nanomaterial sorbent are a function of various factors, such as the characteristics of the sorbent and sorbate and the physical-chemical conditions (Lopes et al., 2013). Various studies concerning the sorption process dependence upon the experimental parameters have been reported in the literature (Babel and Kurniawan, 2003; Dubey et al., 2016; Valle et al., 2017). About pH, it has been found that the optimum pH value is specific for each sorbate, since the pH of solution affects the surface charge of both sorbate and sorbent, and its interaction will only be promoted if they have opposite charge; for temperature, in general, higher temperatures favour the metal ions uptake and this may be indicative of chemisorption (Gode, 2007); in relation to the amount of sorbent, the sorption rate decreases with the decrease of mass of sorbent per volume of solution ratio because this leads to the saturation of the specific sites due to the excess amount of metal ions per amount of sorbent; lastly, the initial metal concentration is inversely proportional to the removal percentage: for the same conditions, as higher the initial concentration, lower is the ratio between free sites on the sorbent surface and metal ions and, consequently, the contaminant removal decreased. Regarding the presence of other

contaminants, in general, waters and effluents are constituted by varied species, pollutant or not, that can interfere with sorption because of the competition for sorption sites.
Results of sorption experiments are usually fitted to mathematical models to obtain information about the sorbent performance.

Kinetic models – The sorption kinetics reflects the speed that the sorbate is removed by the sorbent, from the moment they come into contact (t_0) until the moment at which the sorbent cannot retain more sorbate, i.e., the equilibration time (t_e). Within this period, the concentration of sorbate on the sorbent material (q_t) progressively increases as concentration in the liquid fraction (C_t) decreases relative to the initial value (C_0). When equilibrium is attained, the sorbate concentration on the sorbent achieves its maximum (q_e), while the concentration of free sorbate is in its minimum (C_e). The total amount of sorbate retained by the sorbent material in a certain time *t* (q_t) and when equilibrium is attained (q_e) can be determined from the following mass balance equations:

$$q_t = \frac{(C_0 - C_t)}{\mathrm{m}} * V \quad (1)$$

$$q_e = \frac{(C_0 - C_e)}{\mathrm{m}} * V \quad (2)$$

where m is the mass of sorbent existing in a given volume V of solution.
Among the various kinetic models available in the literature, the kinetic models of pseudo 1st order (or model of Lagergren) and pseudo 2nd order are two simple mathematical models, widely used. The pseudo 1st order model is expressed by the following equations:

$$\frac{dq_t}{\mathrm{dt}} = k_1(q_e - q_t) \xrightarrow[t=0(q_t=0)\ to\ t=t(q_t=q_t)]{integration} q_t = q_e(1 - e^{-k_1 t}) \quad (3)$$

where k_1 (1/h) is the rate constant of the model. This model has the disadvantage of not to adjust well to the experimental data particularly near the equilibrium (Figueira et al., 2011; Lopes et al., 2013; Tavares et al., 2014).

The pseudo 2nd order model generally adjusts better to the experimental data throughout the entire period of the sorption process (Figueira et al., 2011):

$$\frac{dq_t}{\mathrm{dt}} = k_2(q_e - q_t)^2 \xrightarrow[t=0(q_t=0)\ to\ t=t(q_t=q_t)]{integration} q_t = \frac{q_e^2 k_2 t}{1 + q_e k_2 t} \quad (4)$$

where k_2 (1/h) is the kinetic constant of the model (Lopes et al., 2013; Tavares et al., 2014).

Another common kinetic model is the Elovich's model firstly used to describe the sorption of gas onto solid systems. However, more recently, this model has also been applied to the sorption processes of contaminants from aqueous solutions (Qiu et al., 2009). This model is based on the following equation:

$$\frac{dq_t}{\mathrm{dt}} = \alpha e^{-\beta q_t} \xrightarrow[t=0(q_t=0)\ to\ t=t(q_t=q_t)]{integration} q_t = \left(\frac{1}{\beta}\right)\ln(1+\alpha\beta t) \quad (5)$$

where α and β are, respectively, the initial sorption rate, and the desorption constant.

In order to evaluate the effectiveness of the process, the removal percentages are calculated using the equation 6. The variation of ion concentration along the contact time with the sorbent material are expressed in terms of normalized concentrations (equation 7), which allows the comparison of the removal by various sorbates for a given sorbent, or using the same sorbate but different sorbents, regardless of the initial sorbate concentration.

$$Removal\ (\%) = \frac{(C_0 - C_t)}{C_0} * 100 \quad (6)$$

$$C_t' = \frac{C_t}{C_0} \quad (7)$$

1.3. Specificity of nanomaterials as sorbents

In this research work the main focus will be the use of magnetic nanoparticles to improve the quality of waters contaminated with chromium and so a special attention is addressed to this topic.

Nanomaterials have been explored in three main environmental issues (Quina, 2004): i) prevention of contamination or indirect harm to the environment, using catalytic nanomaterial that increases the efficiency and the selectivity of industrial processes; ii) wastewater treatment, using nanoparticles to sorb trace elements and organic substances; iii) detection and monitoring of contamination, using selective and sensitive sensors. Nanomaterials should satisfy some criteria to be used as sorbents for toxic trace elements removal from wastewater (Wang et al., 2012): nontoxic; high sorption capacities and selectivity to the low concentration of contaminants; easy removal of the sorbed contaminant from the surface of the nanomaterial; recycled. Until now, a variety of nanomaterials such as carbon nanotubes, carbon based material composites, graphene, nano metal or metal oxides, and polymeric sorbents fulfil these criteria and have been studied in the removal of toxic trace elements from aqueous solutions (Wang et al., 2012).

The association of sorption ability and magnetic properties in certain nanomaterials have also been explored in the past years envisaging a new class of nanosorbents (Mokadem et al., 2016; Zhang et al., 2016). Magnetic nanosorbents offer the great advantage of allowing fast recovery by employing magnetic separation technologies. A number of nanosorbents comprising magnetite nanoparticles have been reported by laboratories where this work was performed, which include core/shell nanoparticles for the removal of trace metal ions (Tavares et al., 2013) and magnetic bionanocomposites for the removal of organic contaminants (Fernandes et al., 2017; Salgueiro et al., 2013). This type of nanotechnology is of particular relevance for water purification processes that occur in closed systems such as in water treatment units. The successful implementation of magnetic nanosorbents depends, among other factors, on their efficiency for the selective uptake of contaminants, which requires further developments concerning the type of surface chemistry involved.
Eventhough several materials can be used to requalify contaminated waters, the use of magnetic nanoparticles with a core of ferrite have several advantages and will be further explored in this research work.

1.3.1. Magnetic nanoparticles

The magnetic nanoparticles have had a growing interest, mainly because of its affordable price and to the ease and speed of separation from aqueous solutions using an external magnetic field.

Synthesis – Particles can be prepared with high control of size and/or morphology by the concerted interaction of atoms or molecules during the synthesis process. By adjusting the experimental variables – such as reagent concentration, temperature, pH, presence of additives, properties of the solvent, addition of nucleating seeds – the characteristics of colloidal particles formed from homogeneous solutions in a liquid phase can be easily manipulated, which is particularly interesting. The influence of these factors during the nucleation and growth processes of the particles will affect the size and/or morphology of the final particles (Martins and Trindade, 2012).
Because of its convenient magnetic properties, low toxicity, low cost, high specific surface area and capacity for chemical surface modification, one of the magnetic sorbent that most has attracted the attention of the scientific community is magnetite (Fe_3O_4). For these reasons, it will be one of the materials covered in this work. The most common method for obtaining Fe_3O_4 is the co-precipitation from aqueous Fe^{2+}/Fe^{3+} salt solutions under basic

conditions (using NaOH aqueous solutions) because of its simplicity and efficiency (Carlos et al., 2013). This process is described by the follow chemical equation (Gupta and Gupta, 2005; Martins and Trindade, 2012):

$$Fe^{2+}(aq) + 2Fe^{3+}(aq) + 8OH^{-}(aq) \xrightarrow{(N_2)} Fe_3O_4(s) + 4H_2O(l)$$

Provided that the molar ratio Fe^{3+}/Fe^{2+} is 2:1 and the atmosphere is non-oxidizing (which can be achieved by bubbled nitrogen into the solution to remove oxygen), a complete precipitation of Fe_3O_4 should be expected in an alkaline medium according to thermodynamics of this reaction. Bubbling nitrogen gas not only protects critical oxidation of the magnetite but also reduces the particle size (Gupta and Gupta, 2005). This method is advantageous, mainly due to its simplicity and the possibility of obtaining large amounts of material by environment friends processes (Martins and Trindade, 2012).

Structural characterization Depending on their structure and chemical composition, magnetic nanoparticles can achieve different properties, which can be determined using different methodologies (**Table I**).

Table I - Techniques for nanoparticles characterization.

Technique	Studied characteristic of nanoparticles
Transmission Electron Microscopy (TEM)	Size and shape of particle
Scanning Electron Microscopy (SEM)	Size and morphology of particle
Dynamic Light Scattering (DLS)	Average particle size; overall charge on the nanoparticle
X-ray Diffraction (XRD)	Crystalline structure; particle size
Brunauer-Emmett-Teller (BET) method	Surface area, porosity and mean diameter
Fourier Transform Infrared Spectroscopy (FTIR)	Nature and strength of the bonds
Magnetic Studies	Magnetic properties: saturation magnetization (that represents magnetic intensity of magnetic materials), coercivity and squareness

1.4. Chromium chemistry and toxicity

1.4.1. Chemistry

Chromium (atomic number 24) is a steely-grey, lustrous, hard and brittle metal. It is a naturally occurring element present in the earth's crust crystalline solid (ATSDR, 2012) with atomic weight 51.996, melting point 1907ºC and boiling point 2672ºC. Among the wide range of oxidation states, the most common in the environment are the trivalent(III) and hexavalent(VI) states. These two oxidation states are very different in terms of

physicochemical properties and toxicity. While Cr(III) is an essential nutrient in trace amounts, Cr(VI) is toxic and carcinogenic. Moreover, according to the oxidation state, the solubility of the compounds varies: Cr(III) compounds, such as $Cr(OH)_3$ which precipitate at neutral pH (**Figure 1**), are generally insoluble in water; Cr(VI) is highly soluble in the full pH range (Jin et al., 2016). The ratio between chromium hexavalent, Cr(VI), and trivalent, Cr(III), strongly depends on the solution pH, oxidative properties (redox potential) and kinetics. Hence, depending on the conditions, chromium in water can change from one oxidation state to another (ATSDR, 2012), as represented in **Figure 1**. According to this diagram, there are two predominant forms of Cr(VI) depending on the solution pH: $HCrO_4^-$ is predominant at pH values ranging from 2.0 to 6.5 while CrO_4^{2-} is predominant at pH>6.5. Regarding the presence of Cr(III) in aqueous solution, it exists in four main forms, in which soluble Cr^{3+} complexes predominate at pH values from 0 to 4.0 while at pH between 5.5 and 12.5, Cr(III) precipitates as $Cr(OH)_3$.

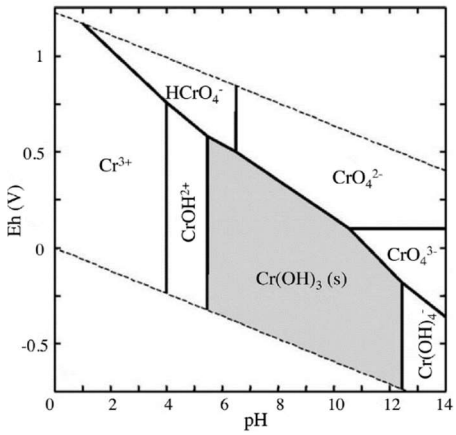

Figure 1 - Eh-pH diagram of Cr-O-H system, in aqueous media, at 25ºC and 1 bar (Jin et al., 2016).

Chromium speciation in aquatic systems may be modified by external factors such as solar energy, complexation in water, redox gradient between bottom water and the upper sediment layer, and interact with other redox sensitive elements such as iron and manganese. **Figure 2** illustrates the transformations and pathway of chromium species in the water column, including the interfaces water-atmosphere and water-sediment (Markiewicz et al., 2015).

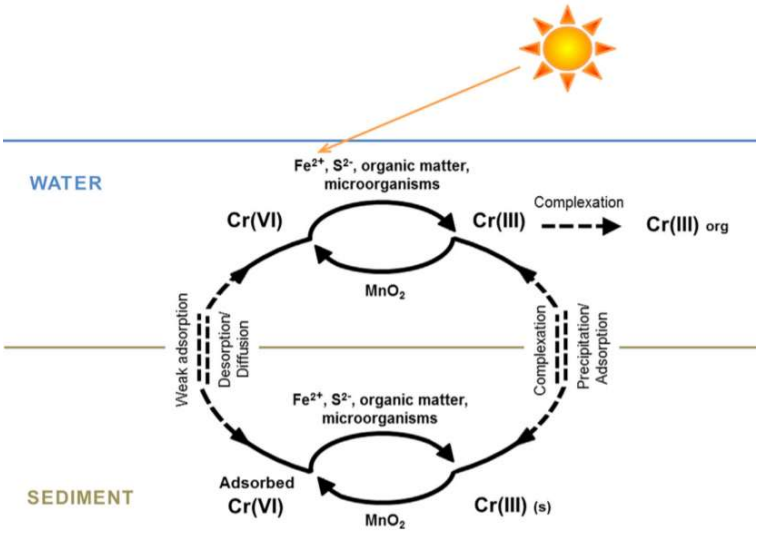

Figure 2 - Pathways of chromium species in the water, including the interfaces with the atmosphere and sediment (Markiewicz et al., 2015).

1.4.2. Toxicity

Exposure of an aquatic organism to water contaminated by chromium may lead to its accumulation because the rate of excretion by the organism is in general lower than the rate of uptake. Chromium tends to be accumulated and have levels amplified along the food chain (Driscoll et al., 2013; Renzoni et al., 1998). This means that organisms at the top of the food chain, such as humans are exposed to higher chromium concentrations. Although chromium (VI) is considered one hundred times more toxic than chromium (III) (Zhou et al., 2017), overall chromium and its compounds have been classified to be human carcinogens by the Institute for the Regulation of Water and Solid Waste (IARC). Chromium causes irritation and ulcers in the stomach and small intestine and it can lead to cancer in several organs (lung, stomach and intestinal tract). Also, it can cause respiratory problems, including irritation of the lining of the nose, runny nose, and breathing problems (such as asthma, cough, shortness of breath and wheezing). Finally, damage on kidney and liver, sperm, and male reproductive system has also been observed (ATSDR, 2012).

In Europe, water quality status is assessed in accordance to Water Framework Directive 2013/39/EU (Council of the European Union and Parlament, 2013). In accordance to this, Environmental Quality Standards (EQS) are implemented, legislating maximum limits for water with different fates, aiming to minimize the bioaccumulation and bioamplification effects and to ensure the protection of water needed for society and ecosystems. A list of priority substances and specific pollutants, including chromium, whose recommended levels

should not be exceeded, was created by Agency for Toxic Substances & Disease Registry (ATSDR) and United States Environmental Protection Agency (EPA). The priority ranking indicated in **Table II** corresponds to this list, which is updated every two years; substances are ordered by degree of danger, considering a combination of its toxicity, occurrence in nature, and its potential for human exposure. The limit concentration in wastewaters is in accordance with European Parliament directives, and the maximum acceptable concentration values in drinking water are recommended by the World Health Organization (WHO).

Table II - Legislated values regarding water contamination with chromium

Chromium species	Rank 2017[i]	Maximum allowed concentration (µg/L)		Concentration in surface water (µg/L)[iii]
		Residual waters	Drinking Water[ii]	
Chromium, hexavalent	17			
Chromium	78		50	10
Chromium, trivalent	351	3000[iv]		

i – According to ATSDR (2017); ii – According to WHO (2011); iii – According to WHO (2003); iv – According to France Guidelines for Metal Finishing Liquid Effluents (Naja and Volesky, 2009).

1.4.3. Natural sources and industrial emissions of chromium

The presence of chromium in aquatic systems is due to natural processes and anthropogenic sources. Soil leaching, weathering of rocks, erosion, and rainwater are major processes favouring the input of chromium to rivers, lakes, estuaries, and ocean (Ray and Shipley, 2015). Development of industries such as electroplating, leather tanning, stainless steel welding, and ferrochrome and chrome pigment production contribute to the increasing levels of chromium to the aquatic environment (ATSDR, 2012; Gong et al., 2016).

Annual emissions data of industrial facilities in EU Member States and in Iceland, Liechtenstein, Norway, Serbia and Switzerland are available at the European Pollutant Release and Transfer Register (E-PRTR). This database collects environmental information of industrial facilities within nine industrial sectors: energy, production and processing of metals, mineral industry, chemical industry, waste and wastewater management, paper and wood production and processing, intensive livestock production and aquaculture, animal and vegetable products from the food and beverage sector, and other activities. Amounts of 91

contaminants released to air, water and land were estimated. Considering the period 2007-2015 it was estimated the annual release of 550 tons of Cr to the European waters (E-PRTR). On the basis of the data reported in 2014 and 2015 it was estimated the weight of various industrial activities on the emission of chromium. The sector "Production and processing of metals" accounts for more than 60% of the chromium emission into the water (**Figure 3**).

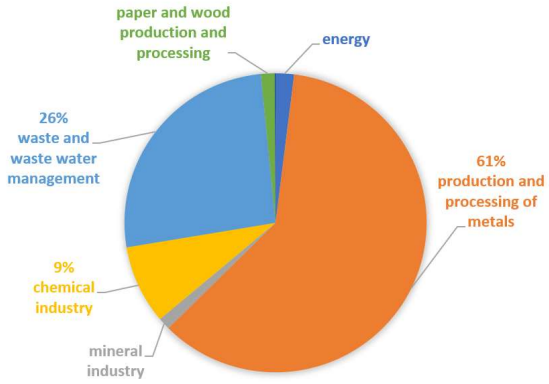

Figure 3 - Proportion of chromium released to European water in 2015 by industrial sectors (E-PRTR).

Chromium has a key role in metal finishing industry modifying the surface of a product to enhance its appearance and reflectivity (such as colour or brightness), wear resistance, corrosion resistance, electrical resistance, chemical resistance, hardness, or to produce surface characteristics essential for subsequent operations (Naja and Volesky, 2009). These processes are applied in several sectors such as telecommunications, aviation, construction, jewellery, transport, among others. More than 650 galvanizing plants are installed in European countries affiliated to the European General Galvanizers Association (Woolley, 2008) being distributed mainly by Germany (160), Italy (90), Spain (72), United Kingdom (62) and France (60).

The second main source of chromium release worldwide responsible for about 20% of chromium emissions is the leather tanning industry where putrescible hide or skin is converted into leather. The permanent stabilization of the skin matrix against biodegradation is possible using basic chromium sulphate (Belay, 2010); so, the exposure is mostly from soluble Cr(III) (ATSDR, 2012). This industry is not so critical in Europe, but has a high impact in Asia, Africa, and South America (Public Partnership for Better Inovation Policies and Instruments in Support of Eco-Innovation: ECOPOL, 2013) (**Figure 4**). For example, leather tannery industry in China is responsible for 20% of chromium discharges into water, total amount from 1990 to 2009 reaching 1.3 x 10^4 tons (Cheng et al., 2014).

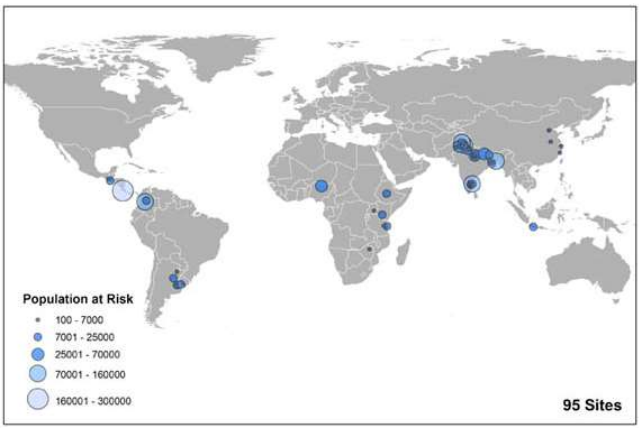

Figure 4 - Worldwide chromium pollution from tannery industry in 2011 (Public Partnership for Better Inovation Policies and Instruments in Support of Eco-Innovation: ECOPOL, 2013).

1.5. Removal of chromium from contaminated waters: a literature review

Due to its toxicity, in the last years, chromium has been removal from waters and wastewaters using the aforementioned techniques. Regarding the chemical precipitation, the studies reported in the literature are only for Cr(III) removal, since it can be precipitated only in the trivalent state (Tünay et al., 2004), either form synthetic or industrial wastewater (Minas et al., 2017; Ramakrishnaiah and B., 2011). Furthermore, there are many studies in the literature about removal of chromium using resins and zeolites for treatment of water and wastewater (Lv et al., 2014; Rengaraj et al., 2001; Santander et al., 2017) by ion exchange. About membrane filtration, the removal of chromium has been study using reverse osmosis (Kocurek et al., 2014; Rad et al., 2009), ultrafiltration (Muthumareeswaran et al., 2017; Vinodhini and Sudha, 2016) nanofiltration (Zargar, 2012) and electrodialysis (Moura et al., 2012) membranes. There are also some studies in the literature about removal of chromium using coagulation / flocculation for treatment of wastewater (Dasgupta et al., 2015; Haydar and Aziz, 2009; Imran et al., 2012). Moreover, there are many studies in the literature related to chromium removal using electrochemical processes, such as Cr(VI) electrocoagulation and electrochemical Cr(VI) reduction in different systems (Duan et al., 2017; Jin et al., 2016).

Like chemical precipitation and ion exchange processes, the sorption has also been widely used for removal of chromium. In the past ten years, several studies have been published on chromium sorption in aqueous phase using nanomaterials. **Table III** lists the nanomaterials and experimental conditions employed through batch (the most common) or fixed-bed

column experiments (as exemplified by the study of Debnath et al. (2010)). **Table III** is a condensed version of the Table presented in the attachments (Chapter 7).

Type of materials. Among the various materials used for chromium removal, nanoparticles are the most common, either using just the core nanoparticle (Debnath et al., 2016; Kaprara et al., 2017; Khan et al., 2016; Mahmoud et al., 2017; Rajput et al., 2016; Sezgin et al., 2016; Srivastava et al., 2016; Valle et al., 2017), with functionalization (Guan et al., 2015; Huang et al., 2017; Lan et al., 2014; Tahergorabi et al., 2016) or supported on substrates (Babaei et al., 2016; Biswal et al., 2013). Other type of materials have been used, such as nanocomposites (Arthy and Phanikumar, 2016; Chooaksorn et al., 2016; Srivastava et al., 2017), nanofibers (Egodawatte et al., 2016) and carbon nanotubes (Lee and Kim, 2016).

Interactions with other elements. Most of the works mentioned in **Table III** describe the chromium sorption experiments using monoelemental systems, i.e. Cr is the only contaminant to be treated. Less than half of the studies tested both monoelemental and multielemental systems. Distilled or ultra-pure water have been considered, which are less complex conditions because no competitive ions or other contaminants are present.

Type of solutions. Only a few studies addressed the treatment of contaminated waters as real samples, such as groundwater, effluents or wastewater (Guan et al., 2015; Kumari et al., 2015; Sezgin et al., 2016; Srivastava et al., 2016; Watts et al., 2015). Chen et al. (2011) have tested natural waters of different complexity (deionized distilled water, tap water, mountain stream water and river water).

Temperature. Most of the removal experiments have been tested at temperature between 20 and 25ºC, presumably to make the process more practical and reduce associated costs. Other studies were performed approximately at 30ºC (Akoz et al., 2012; Arthy and Phanikumar, 2016; Behnajady and Bimeghdar, 2014; Debnath et al., 2010; Guan et al., 2015; Lan et al., 2014; Lee and Kim, 2016; Mao et al., 2012; Paul et al., 2015; Saikia et al., 2011), at 35ºC (Srivastava et al., 2017), and even at 40ºC (Ataabadi et al., 2015; Mohan et al., 2015) mirroring natural situation in warmer countries. Apart from five cases (Dubey et al., 2016; Lee and Kim, 2016; Mohamed et al., 2017; Pang et al., 2011; Valle et al., 2017), efficiency of chromium sorption increases with temperature.

Contact time. In general, contact time between the nanomaterial and the contaminant were less than 2 days, although may be extended, from 3 days (Kumari et al., 2015), to 7 days (Gifford et al., 2016) and 15 days (Watts et al., 2015).

pH. Values of optimal pH in the removal of Cr(III) were between 5 and 7 (Arthy and Phanikumar, 2016; Egodawatte et al., 2016; Guan et al., 2015; Mahmoud et al., 2017; Shahriari et al., 2014; Valle et al., 2017). Removal of Cr(VI) was tested at pH from 2 to 3 (Khan et al., 2016; Lee and Kim, 2016; Luther et al., 2013; Mahmoud et al., 2017; Pang et al., 2011; Rajput et al., 2016; Valle et al., 2017), although some authors have been studied the removal at environmental pH interval, 5-8 (Kaprara et al., 2017; Simeonidis et al., 2015).

Amount of sorbent. It is well documented that, for the same concentration of metal, the rate of chromium sorbed will increase by increasing the amount of sorbent, although the larger the amount of material used, the greater the amount of residues to treat and the cost of process. Several works have tested low doses of sorbent per volume of solution, such as Bisht et al. (2016), Paul et al. (2015), Kaprara et al. (2017), Debnath et al. (2016), Tahergorabi et al. (2016), Khan et al. (2016), Simeonidis et al. (2015), Guo et al. (2013), Mao et al. (2012), Moradi and Baniamerian (2012), Srivastava et al. (2017), Mohamed et al. (2017) and Babaei et al. (2016). In particular Bisht et al. (2016) used 5, 10, 15, 20, 25 and 30 mg/L of EDTA-Fe_3O_4 nanoparticles, Paul et al. (2015) used 10 mg/L and 50 mg/L of TiO_2 nanoparticles and Kaprara et al. (2017) used 25 mg/L of Sn(II) oxy-hydroxides nanoparticles for Cr(VI) removal.

Oxidation state. Cr(VI) species have been the most investigated systems, although some researchers have previously research on Cr(III) species (Arthy and Phanikumar, 2016; Debnath et al., 2016; Egodawatte et al., 2016; Guan et al., 2015; Shahriari et al., 2014; Tahergorabi et al., 2016) and others with both Cr(III) and Cr(VI) (Cantu et al., 2014; Luther et al., 2013; Mahmoud et al., 2017; Parsons et al., 2014; Valle et al., 2017). Only a few studies mention the analytical methodologies to discriminate the quantification of Cr(III) and Cr(VI) during the removal process. Most of the methodologies referred in the works of **Table III** are only able to measure total Cr and so the values reported for uptake capacity or removal efficiency are based on the initial and final concentrations regardless the starting chromium species.

Chromium concentrations. For the removal experiments, a wide range of chromium concentrations has been reported in the literature, more specifically, concentration values between 10 µg/L (Kaprara et al., 2017) and 11 000 000 µg/L (Uygun et al., 2013). The maximum allowed concentration of total chromium in residual waters is 2000 µg/L so the studies that used higher concentrations are not using realistic values. In this way, some

studies (Biswal et al., 2013; Cantu et al., 2014; Chooaksorn et al., 2016; Chowdhury and Yanful, 2010; Gifford et al., 2016; Kaprara et al., 2017; Khan et al., 2016; Luther et al., 2013; Parsons et al., 2014; Simeonidis et al., 2015; Valle et al., 2017) included in their experiments lower concentrations. Among these, Chowdhury and Yanful (2010), Simeonidis et al. (2015) and Gifford et al. (2016) were the only ones that studied concentration equal or <2000 µg/L and Kaprara et al. (2017) studied the removal of 10 µg/L of chromium using Sn(II) oxy-hydroxides nanoparticles.

Best material performance. Lastly, magnetic iron oxide nanoparticles/sugarcane bagasse composite (Arthy and Phanikumar, 2016) and Cr(VI)-imprinted poly(HEMAH) nanoparticles (Uygun et al., 2013) were the materials reported in the literature in the last years as being the ones with the most affinity for Cr(III) and Cr(VI) uptake, achieving a capacity of 518 mg/g and 3830 mg/g, respectively.

Table III - Nanomaterials for Cr removal with respect to the conditions used as reported in the literature in the last 10 years (since 2007).

Reference	Nanomaterial	Type of water	pH	Temperature (ºC)	Amount of sorbent (x10^{-3} mg/L)	Contact time (h)	Initial element concentration (x10^{-3} µg/L)	Cr starting specie	Uptake capacity (mg/g) or removal efficiency (%)	Type of system
(Kaprara et al., 2017)	**Sn(II) oxy-hydroxides NPs** (pH synthesis) $Sn_6O_4(OH)_4$ (pH 2) $Sn_6O_4(OH)_4$ (pH 4) SnO_2 (pH 6) SnO_2 (pH 9) $Sn_3OSO_4(OH)_2$ (pH 2) $Sn_6O_4(OH)_4$ /SnO (pH 4) $Sn_6O_4(OH)_4$ /SnO (pH 6) $Sn_6O_4(OH)_4$ /SnO (pH 9)	Distilled water	6-8	10-30	0.025-0.75	0.016-48	0.010-5.0	Cr(VI)	~31 (30 ºC, $Sn_6O_4(OH)_4$ pH 2)	Mono elemental
	Sn(II) oxy-hydroxides NPs (pH synthesis)	Natural-like water	7.0-7.8	20			0.10	Cr(VI)	19 (pH 7, $Sn_6O_4(OH)_4$ pH 2)	Multi elemental
(Mahmoud et al., 2017)	**Nano-ZrO_2** Nano zirconium oxide **Nano-ZrO_2-glu-CMC** Crosslinking of nanolayer carboxymethyl cellulose (CMC) onto the surface of nano zirconium oxide (Nano-ZrO_2) using glutaraldehyde	Distilled water	1.0-7.0	r.t. [f]	2.5	0.017-1.0	1040-10 400	Cr(III) Cr(VI)	187 (500 mg/L, Nano-ZrO_2-glu-CMC) 73 (500 mg/L, Nano-ZrO_2-glu-CMC)	Mono elemental
			7 2	r.t.	2.5	0.50	5200	Cr(III) Cr(VI)	11-26 Nano-ZrO_2 29-44 Nano-ZrO_2-glu-CMC 4-8 Nano-ZrO_2 14-27 Nano-ZrO_2-glu-CMC (depending on the type of interfering ion)	Multi elemental
(Huang et al., 2017)	**Pd/Fe_3O_4 NPs** Magnetite nanoparticles functionalized with palladium		3	Information not mentioned	5.0	8.0	20	Cr(VI) Total Cr	~60% ~60%	Multi elemental

(Valle et al., 2017)	**$K_2Mn_4O_9$** Rancieite type material		2-6	4-45	2.5	0.083-2.0	0.30-30	Cr(III) Cr(VI)	33% (pH 6)/ 41.8 (45ºC) 23% (pH 2) / 4.22 (4ºC)	Mono elemental
			5 2		2.5	1.0	0.30	Cr(III) Cr(VI)	~4-37% ~0-67% (depending on the type and concentration of interfering ion)	Multi elemental
(Srivastava et al., 2017)	**MNPLB** Lagerstroemia speciosa bark (LB) embedded magnetic nanoparticles	Double distilled water	1.09-7.02	15-40	0.1-0.7	0.17-2.0	50-500	Cr(VI)	739.7 (500 x10^3 µg/L)	Mono elemental
(Lu et al., 2017)	**MNP/MWCNTs** Magnetic iron oxide nanoparticle-multiwalled carbon nanotube composites	Ultrapure water	1.0-9.0	25-45	0.4-2.0	0-24	5.0-50	Cr(VI)	~98% (1000-2000 mg/L) 42.02 (45ºC)	Mono elemental
			2.0		1.0		10	Cr(VI)	~92-95% (depending on the type of interfering ion)	Multi elemental
(Mohamed et al., 2017)	**PAN-CNT/TiO_2-NH_2** Polyacrylonitrile (PAN) and carbon nanotube (CNTs)/titanium dioxide nanoparticles (TiO_2) functionalized with amine groups (TiO_2-NH_2) composite nanofibers		2-9	r.t. (20)	0.1-0.8	0-7	10-300	Cr(VI)	99.7% (6000 mg/L) 861.11 [a]	Mono elemental
(Rajabathar et al., 2017)	**Meso-MnO_2** Mesoporous manganese oxide **AgNPs@meso-MnO_2** silver nanoparticles doped mesoporous manganese oxide **Ag/Graphene-meso-MnO_2** silver nanoparticle graphene deposited mesoporous manganese oxide nanocomposite	Milli-Q water	6	r.t.	6.7	24	50	Cr(VI)	~35%	Mono elemental

(Srivastava et al., 2016)	**$CoFe_2O_4$ NPs** Cobalt ferrite nanoparticles	Distilled water	2-12	25-55	2-12	0-4.0	75-150	Cr(VI)	98.45 % (55ºC, 75 x10^3 µg/L) 16.73 (55ºC)	Mono elemental
		Printing press wastewater	1-12	25-55	10	0-24	1637.5	Cr(VI)	~69%	Multi elemental
(Lee and Kim, 2016)	**MIO-MWCNTs** **MWCNTs** Multi-walled carbon nanotubes **MIO NPs** Magnetic iron oxide nanoparticles		2.6-7.3	5-60	1.0	0.25-4.0	5-100	Cr(VI)	12.61 (100 x10^3 µg/L, MIO-MWCNTs) 80.8% (5 x10^3 µg/L, MIO-MWCNTs)	Mono elemental
(Chooaksorn et al., 2016)	**CN-coated AC** Bituminous activated carbon (AC) coated with chitosan nanoparticles (CN) **CN-AC/DC** CN coated on AC by the dip coating method **CN-AC/WI** CN coated on AC by the wet impregnation method	Deionized water	5.0	Information not mentioned	1.0	0-24	0.10-100	Cr(VI)	77.52 (CN-AC/DC) 61.7% (0.1 x10^3 µg/L, CN-AC/DC)	Mono elemental
(Dubey et al., 2016)	**n-Al_2O_3** γ-alumina nanoparticles modified with cetyl trimethyl ammonium bromide (CTAB)	Distilled water	2.0-10.0	30-60	4-24	0-1.5	5-25	Cr(VI)	94% (5 x10^3 µg/L, pH 2.03, 18 340 mg NPs/L) 18.716 [b] (25 x10^3 µg/L)	Mono elemental
(Gupta et al., 2016)	**CuO NPs** Copper(II) oxide nanoparticles	Double distilled water	2-10	25-45	0.4-5	0-3.0	10-150	Cr(VI)	96.3% (10 x10^3 µg/L) 86.25 (400 mg/L)	Mono elemental
(Bisht et al., 2016)	**IONPs** Magnetic iron oxide nanoparticles **MIONPs** EDTA-modified magnetic iron oxide nanoparticles		2	r.t.	0.0050-0.030	0-18	200-1000	Cr(VI)	99.90% / 499.5 (30 mg/L, MIONPs) 34.06% / 170.33 (30 mg/L, IONPs)	Mono elemental

(Gifford et al., 2016)	**Ti-AX** Titanium dioxide nanoparticles precipitated in anion exchange resins	Synthetic groundwater	8	Information not mentioned	0.60	168	0.10	Cr(VI)	88%	Multi elemental
(Nithya et al., 2016)	**Cs-g-PBA/SG** Chitosan-g-poly(butylacrylate)/ silica gel nanocomposite		3-9	r.t.	10-60	1.0-6.0	62.5-1000	Cr(VI)	98% (62.5-125 x10^3 µg/L) 55.71	Mono elemental
(Sureshkumar et al., 2016)	**Chitosan–Fe_3O_4 nanocomposite strip** Chitosan–magnetite nanocomposite strip	Deionised water	Information not mentioned	Information not mentioned	1 cm x 1 cm 0.010 L	0.17, 0.30, 0.83, 1.2, 1.5, 1.8, 2.2	260	Cr(VI)	~15-92.33%	Mono elemental
(Tahergorabi et al., 2016)	**TF-SCMNPs** Thiol-functionalized mesoporous silica-coated magnetite nanoparticles (**Fe_3O_4 NPs**)	Distilled water	3-10	r.t. (25)	0.080-0.40	0.083-24	8	Cr(III)	42% (pH 10, 400 mg/L) 1.119	Mono elemental
(Khan et al., 2016)	**Fe-Cu binary oxide NPS**	Milli-Q water	1-9	r.t. (25)	0.10-2.5	1.0	1-25	Cr(VI)	~100% (100 mg/L, 1 x10^3 µg/L) 71.43	Mono elemental
(Arthy and Phanikumar, 2016)	**MIN** Magnetic iron oxide nanoparticles **MIN-TW** Magnetic iron oxide nanoparticles/tea waste composite **MIN-SB** Magnetic iron oxide nanoparticles/sugarcane bagasse composite	Deionized water	2-7	30	0.50-1.25	0.083-2.0	50-300	Cr(III)	98.27% (MIN-SB, 1h, 1125 mg/L) 518.134 [d] (MIN-SB, 0.75 h)	Mono elemental
	MIN MIN-TW MIN-SB	Deionized water						Cr(III)	~229-243 ~228-240 ~243-247 (depending on the type of interfering ion)	Multi elemental
(Babaei et al., 2016)	**ST/Mag NPs** Spent tea-supported magnetite nanoparticles	Double-distilled water	2-8	r.t. (20)	0.10-11.0	0.033-4.0	5-300	Cr(VI)	~100% (5 x10^3 µg/L) 30.03	Mono elemental
		Synthetic saline wastewater	2	20	3.0	1.0	10	Cr(VI)	78.3-99.9% 1.09-1.39 (depending on the concentration of interfering ions)	Multi elemental

(Rajput et al., 2016)	**Fe_3O_4 NPs** Magnetic magnetite nanoparticles	Double distilled water	2-10	25-45	1.0-4.0	0-24	2-100	Cr(VI)	~75% (4000 mg/L) 34.9 (45ºC)	Mono elemental
(Egodawatte et al., 2016)	**ESH** Electrospun hematite nanofiber **ESH@MS-60** Electrospun hematite nanofiber/mesoporous silica core/shell **ESH@MS-60-NH_2** Electrospun hematite nanofiber/mesoporous sílica functionalized with amine group		3-6	25	0.25	2.0	5.2-104	Cr(III)	343 (pH 5.4, ESH@MS-60-NH_2)	Mono elemental
(Debnath et al., 2016)	**$CaFe_2O_4$ NPs** Calcium ferrite nanoparticles	Ultrapure deionized water	2-6	r.t.	0.0625-1.0	0.033-1.7	30-250	Cr(III)	340 (62.5 mg/L) 99% (pH 2 / 30 x10^3 µg/L)	Mono elemental
(Sezgin et al., 2016)	**$MnFe_2O_4$ NPs** Manganese ferrite nanoparticles	Real wastewater from galvanotechnic industry	2	r.t.	0.5-6.0	0.17-24	50-250	Total Cr	334.80 (500 mg/L) 71.37% (1500 mg/L)	Multi elemental
(Simeonidis et al., 2015)	**Fe_3O_4 NPs** Magnetite nanoparticles	Distilled water	7	20	0.10-1.0	0.083-24	0.25	Cr(VI)	~2.4 (24 h)	Mono elemental
		Natural-like water	5-8	20	0.10-1.0	0.083-24	0.050-1.0	Cr(VI)	~100% (pH 6.5, 3 h / pH 7.0, 4 h) 4 (pH 5)	Multi elemental
(Martínez et al., 2015)	**Fe_3O_4 NPs** Magnetite nanoparticles		1.5-4.5	10-75	0.50-2.0	0-2.0	0-160	Cr(VI)	~26 (2000 mg/L)	Mono elemental
(Bagheri et al., 2015)	**CS–CA NPs** Chitosan–citric acid nanoparticles **CS NPs** Chitosan nanoparticles	De-ionized water	2-6	25-45	0.50-5.0	0-2.0	10-110	Cr(VI)	94.46% (70 x10^3 µg/L) 38.51 (500 mg/L)	Mono elemental
(Mohan et al., 2015)	**CuO NPs** Cupric oxide nanoparticles	De-ionized double distilled water	2.0-10.0	20-60	0.25-2.5	0-5.8	5-50	Cr(VI)	98.8% 50.0 (250 mg/L)	Mono elemental
(Paul et al., 2015)	**TiO_2 NPs** Titania nanoparticles	Deionized (MilliQ) water	2.0-12.0	28	0.010-0.50	0.083-0.75	5-100	Cr(VI)	85.85 (20 x10^3 µg/L)	Mono elemental

(Watts et al., 2015)	**BnM** Biogenic nano-magnetite	Ultrapure water	12	20	0.75 Anoxic	0-350	Model solution	Cr(VI)	32	Mono elemental
		Contaminated groundwater	11.9	20	0.66 Anoxic 0.66 Oxic	0-200	16.69	Cr(VI)	24 7	Multi elemental
(Guan et al., 2015)	**PAA@VTES@Fe_3O_4 NPs** Magnetite nanoparticles coated with silane coupling agent (VTES) grafted with polyacrylic acid (PAA)	Ultrapure water	2-6	20-40	1.0-6.5	0-24	170	Cr(III)	92.5% (pH 6, 5000-6500 mg/L) 80.6 (40ºC)	Mono elemental
		Tannery effluent	6		5.0	4.0	170	Total Cr	94.0%	Multi elemental
(Ataabadi et al., 2015)	**Fe_3O_4 NPs** Magnetite nanoparticles	Deaerated deionized water	2-10	25-45	1.0-5.0	0-3.0	0-120	Cr(VI)	100% (pH 2, 4000 mg/L, 20 $x10^3$ µg/L, 40ºC)	Mono elemental
							20	Cr(VI)	80-100% (depending on the type and concentration of interfering anion)	Multi elemental
(Kumari et al., 2015)	**Fe_3O_4 nanospheres** Mesoporous magnetite nanospheres	Double distilled water	2-7	25-45	1.0-3.0	1.0-72	5–100	Cr(VI)	44% (1h, 2000 mg/L) 8.90 (45ºC)	Mono elemental
		Groundwater	4	25	2.0	48	10	Cr(VI)	65%	Multi elemental
(Parsons et al., 2014)	**Fe_3O_4 NPs** Magnetite nanoparticles		2-6		2.5	0.083-1.0	0.10-10	Cr(III) Cr(VI)	100% (pH 4, 0.25 h) / 0.555 100% (pH 4, 0.33 h) / 1.705 (depending on the material type)	Mono elemental
					2.5	1.0	0.10	Cr(III) Cr(VI)	~60-100% ~25-100 % (depending on the material type and on the type and concentration of interenfence anion)	Multi elemental
(Cantu et al., 2014)	**Mn_3O_4** Manganese oxide nanomaterial		2-6	4-45	2.5	0.17-4.0	0.30-1000	Cr(III) Cr(VI)	90% (pH 2)/ 54.4 (45ºC) 85% (pH 2) / 5.8 (45ºC)	Mono elemental
(Lan et al., 2014)	**PMMNs** Polyacrylamide modified iron oxide nanoparticles		1-8	30	20	0-2.0	50-1000	Cr(VI)	~99% (pH 3, 100 $x10^3$ µg/L) 35.186	Mono elemental
			3	30		0.67	100	Cr(VI)	~94-98% (depending on the type and concentration of salt)	Multi elemental

(Shahriari et al., 2014)	**Fe_3O_4 NPs** Iron oxide magnetic nanoparticles	Artificial wastewater	3-9	25	250-1500 mg (volume not mentioned)	0.25-1.5	250-1000	Cr(III)	99.9% (pH 9)	Mono elemental
(Behnajady and Bimeghdar, 2014)	**NiO NPs** Mesoporous nickel oxide nanoparticles	Distilled water	4.7-9	30	1.0-7.0	0-0.83	10-50	Cr(VI)	~100% (10 x10^3 µg/L, 7000 mg/L) / ~5 (50 x10^3 µg/L)	Mono elemental
(Uygun et al., 2013)	**Cr(VI)-imprinted poly(HEMAH) NPs** Chromium(VI)-imprinted hydroxyethylmethacrylate (HEMA) polymeric nanoparticles	Milli-Q ultrapure water	2-6	25	Information not mentioned	0-2	1000 -11 000	Cr(VI)	3830.58	Mono elemental
(Guo et al., 2013)	**TiO_2 NPs** Titania nanoparticles		4.0	25	0.10	0-2.5	0-80	Cr(VI)	21.92	Mono elemental
(Biswal et al., 2013)	**Fe_3O_4-loaded seeds** Magnetite nanoparticles loaded natural seeds sabja		2	Information not mentioned	1000 mg (volume not mentioned)	0, 0.25, 0.50, 0.75, 1.0, 1.5, 2.0	1 5 20 30 50	Cr(VI)	~100% 97% ~85% ~80% ~75%	Mono elemental
							50	Cr(VI)	80%	Multi elemental
(Chen et al., 2013)	**Fe_3O_4/CNT NPs** Carbon nanotubes loaded with magnetite nanoparticles		2-12	20-80	1.0	0.083-120	100-1000	Cr(VI)	95% (pH 2) / 60 (pH 2)	Mono elemental
(Luther et al., 2013)	**Fe_3O_4 NPs** Iron(II/III) oxide or magnetite or ferrite nanoparticles **$MnFe_2O_4$ NPs** Magnanese(II) iron (III) oxide or jacobsite or manganese ferrite nanoparticles		2-10	4-50	2.5	1.0	0.30-100	Cr(III) Cr(VI)	100% (Fe_3O_4, pH 6/7) 10.638 100% ($MnFe_2O_4$, pH 2/3) 3.455	Mono elemental
(Mao et al., 2012)	**Magnetic PS-EDTA resin** Magnetic chelating resin with EDTA functionality		2-12	30	0.20-2.0	0.083-10	5-1000	Cr(VI)	100 % (pH 4, 10 h, 1000 mg/L, 5-40 x10^3 µg/L) 250.00	Mono elemental

(Akoz et al., 2012)	Semicarbazone derivatives of calix[4]arene immobilized onto magnetic nanoparticles (Fe_3O_4): **MN-C1**, **MN-C2**, **MN-C3**	Deionized water	1.5-4.5	30	2.5	1.0	5.2-20.8	Cr(VI)	90% (MN-C2, pH 1.5)	Mono elemental
(Moradi and Baniamerian, 2012)	**NC** Nanoporous carbon **Ni-NC** Nickel oxide onto nanoporous carbon **Fe-NC** Iron oxide onto nanoporous carbon	Ultrapure water	2-10	20, 30, 40	0.20	0-6.0	10-100	Cr(VI)	60.8 (Fe-NC, r.t.)	Mono elemental
(Pang et al., 2011)	**PEI-γ-Fe_2O_3@Fe_3O_4 NPs** Polyethylenimine-modified magnetic nanoparticles		2-9	15-35	4.0	0-2.0	50-500	Cr(VI)	98.2% (100 x10^3 µg/L) 83.33 (15ºC)	Mono elemental
			2.2	25	4.0	0.50	100	Cr(VI)	~98-100%	Multi elemental
		Wastewater			2.67	0.50	37.98	Cr(VI)	99.0%	
(Kaya et al., 2011)	**GMDFe** Nanosized ferric oxide loaded glycidyl methacrylatebased polymer		2-10	r.t. (25)	4.0	Equilibrium time	30	Cr(VI)	98% (24 h) 163.47 (pH 2)	Mono elemental
(Li et al., 2011)	**CeO_2 NPs** Monodisperse ceria nanospheres	Simulated wastewater	Information not mentioned	r.t.	1.0	0-2.0	4.8 8	Cr(VI)	94.5% / ~4.5 94.1% / 7.52	Mono elemental
(Chen et al., 2011)	**magMCM-41** Magnetic MCM-41 nanosorbents	Deionized, distilled water	2-7	r.t. (25)	1.0	Information not mentioned	106-156	Cr(VI)	98.8 (pH 2), 83.2 (pH 5)	Mono elemental
		Deionized, distilled water	2-5 5.0				 156	Cr(VI)	67.6 67.6	Multi elemental
		Tap water	5.2				114	Cr(VI)	46.8	
		Mountain stream water	5.4 2, 5, 8				122	Cr(VI)	31.2 97% (pH 2), 97% (pH 5), 86% (pH 8)	
		River water	5.5				106	Cr(VI)	41.6	

(Sayin and Yilmaz, 2011)	**BHCB-MN** 5,11,17,23-tetra-tert-butyl-25,27-di(benzhydrazidylmethoxy)-26,28-dihydroxy-calix[4]arene immobilized silica-based magnetic nanoparticles	Deionized water	1.5 2.5 3.5 4.5	25	2.5	1	5.2	Cr(VI)	66% ~64% 11% ~0%	Mono elemental
(Saikia et al., 2011)	**$Cu_2CO_3(OH)_2$ NPs** Malachite nanoparticles	Milli-Q water	4-9	10-40	5.0-20	1-16	20-500	Cr(VI)	82.2 75% (pH 5, 50 x10^3 µg/L)	Mono elemental
			5				50	Cr(VI)	70%	Multi elemental
(Debnath et al., 2010)	**NHTO** Nanoparticles of hydrous titanium(IV) oxide	Distilled water	2.0	30	1000-3000 mg (packed column)	0.013-0.026	8.0-32.0	Cr(VI)	12.94 [e] (32.0 x10^3 µg/L)	Mono elemental
		Industrial effluent wastewater	2.06	30	4000	0.026	15.67	Cr(VI)	~100%	Multi elemental
(Liu et al., 2010)	**α-Fe_2O_3 NPs** Hematite nanoparticles	Dilute simulated landfill leachate	3-8	20-35	0.50-3.0	0-24	20-200	Cr(VI)	~90% (pH 3)	Mono elemental
			6.7				20	Cr(VI)	~50%	Multi elemental
(Chowdhury and Yanful, 2010)	**Fe_3O_4-γ-Fe2O3 NPs** Magnetite-maghemite nanoparticles	De-ionized water	2-14	r.t.	0.40	0.17-4	1-2	Cr(VI)	96% (pH 2, 1 x10^3 µg/L) 4.45 (pH 2, 2 x10^3 µg/L)	Mono elemental
			4		0.40			Cr(VI)	35-90%	Multi elemental
(Hu et al., 2007)	Magnetic NPs: $MnFe_2O_4$ $MgFe_2O_4$ $ZnFe_2O_4$ $CuFe_2O_4$ $NiFe_2O_4$ $CoFe_2O_4$	Milli-Q water	2.0-9.3	22.5	5.0	0-1.0	20-100	Cr(VI)	100% ($MnFe_2O_4$, 0.083 h)	Mono elemental

[a]Nonlinear Pseudo-second-order model. [b]Pseudo-second-order model. [c]Langmuir type 4 capacity. [d]Langmuir type 1 capacity. [e]Thomas model column capacity. [f]Room temperature.

Note that,
the conditions that are shaded correspond to the best uptake capacity or removal efficiency obtained;
in general, when the type of water is not referred, the authors may have used distilled or milli-Q water;

in the column correspondent to “Cr starting specie”, total chromium concentration was quantified in the works that refer it; in the other works no mention is made regarding the specie or if it is total concentration;
in the column correspondent to “Uptake capacity (mg/g) or removal efficiency (%)”, when the value does not present units, it is the uptake capacity; otherwise, it is the removal efficiency;
the value presented in parentheses in the column “Uptake capacity (mg/g) or removal efficiency (%)” corresponds to the condition that gave rise to the value of uptake capacity or removal efficiency presented;
the uptake capacity values which do not presented a subscript were obtained either experimentally or by Langmuir model;
sometimes, the authors refer to experimental conditions of experiments whose results they do not present;
from column “Type of water” until “Cr starting specie”, the conditions mentioned are the same for the below lines

1.1. Hypothesis of work and objectives

According to the reported data on chromium removal from waters (**Table III**), the overall aim of this research work will be to contribute to study low cost and efficient materials for the recovery of waters contaminated with chromium, with a view to future application in the treatment of industrial effluents. So, general objective of this work is to study the remediation of water contaminated with chromium, that is a priority substance, using magnetic nanoparticles based on ferrites, and to apply these materials in real wastewaters for removal of chromium.

The specific objectives are:

- To evaluate the effect of amount of sorbent used in the Cr removal studies in order to reduce it and consequently to decrease the amount of residues to treat and the cost of the process.
- To study the influence of the pH of the solution on Cr removal efficiency, which is intended to be adjusted to similar pH found in real industrial effluents.
- To evaluate the effect of the ionic strength of the solution and the effect of dissolved organic matter on Cr removal efficiency once real effluents have other ions.

To achieve these objectives, the following tasks are planned:

- Synthesis of different types of ferrites, namely magnetite, manganese ferrite and cobalt ferrite (respectively, Fe_3O_4, $MnFe_2O_4$ and $CoFe_2O_4$) NPs, which will be used for chromium sorption. Despite ferrites are more expensive than magnetite, transition metal variation allows the variation of the magnetic properties. Accordingly, it is possible to reduce the material cost if, with a much smaller amount of sorbent, higher efficiency rates are achieved than those when using magnetite.
- Characterization of the nanoparticles prepared by several techniques, such as XRD, FTIR, TEM, Chemical Analysis, BET Method, Magnetic Studies and Isoelectric Point.
- Evaluation of the influence of experimental parameters (amount of sorbent, pH, presence of interfering ions, dissolved organic matter) in the chromium removal from aqueous solutions using ferrite nanoparticles. To perform the quantification of chromium an ICP-OES (Inductively Coupled Plasma-Optical Emission Spectometry) will be used. This technique only allows us to measure total chromium
- Modelling of kinetic data to predict the performance of the different material, using common mathematical methods (such as pseudo 1^{st} order, pseudo 2^{nd} order, and Elovich).

Chapter 2

Materials and methods

2.1. Washing of the material used

All the material used in the performed test was thoroughly washed before and after use, to avoid possible contaminations. Thus, the washing procedure of the material starts with an abundant washing with water (tap water and distilled water), followed by placement in HNO3 25% (v/v) for 24 hours. After this period, the material was washed again several times with distilled water.

The volumetric flasks, in which the ion solutions were prepared, were also washed with the matrix used in the sorption experiments before the preparation of the solutions. Chromium samples were stored in polystyrene tubes (10 mL). Prior use all tubes were acid-washed with HNO_3 25% for 24 hours and then rinsed with abundant water (tap water and distilled water). All material is dried at room temperature, protected from the air.

2.2. Reagents

Chemicals were readily available from commercial sources and were used as received without further purification: Ammonium hydroxide solution (NH_3 in H_2O, 25%, Riedel-de-Häen), Chromium(III) (Cr^{3+} in HNO_3, 1000 mg/L, Inorganic Ventures), Cobalt(II) chloride hexahydrate ($CoCl_2.6H_2O$, 98%, Panreac), Ethanol (C_2H_5OH, >99%, Panreac), Humic acid sodium salt (technical grad, Sigma-Aldrich), Iron(II) sulfate heptahydrate ($FeSO_4.7H_2O$, >99%, Merk), Manganese(II) sulfate monohydrate ($MnSO_4.H_2O$, >99%, Riedel-de-Häen), Nitric acid (HNO_3, puriss. p.a., 65%, Merck), Potassium hydroxide (KOH, >98%, Pronolab), Potassium nitrate (KNO_3, >99%, Merk), Sodium hydroxide (NaOH, >98%, Pronolab).

2.3. Chemical synthesis of spinel type nanoparticles

Magnetic NPs used in this study were synthesised according with the following procedure:

Fe_3O_4 nanoparticles

Magnetic iron oxide NPs with an average size of 50 nm were synthesized by oxidative hydrolysis of iron(II) sulphate in alkaline conditions, according to the procedure described in Oliveira-Silva et al. (2014), as follows. Ultra-pure water was first deoxygenated with N_2 under vigorous stirring during 2 hours. Then, 1.90 g (34 mmol) of KOH and 1.52 g (15 mmol) of KNO_3 were added to 25 mL of deoxygenated water using a 250 mL round flask. This mixture was heated at 60ºC, under N_2, and mechanically stirred at 500 rpm. After total

dissolution, 25 mL of an aqueous solution of $FeSO_4.7H_2O$ (4.75 g, 17 mmol) was added drop-by-drop to the mixture and mechanical stirring was increased to 700 rpm. The resulting solution presented a dark-green colour after complete addition of the Fe(II) salt. The solution reacted for 30 minutes. After reaction, the round flask was transferred to a hot oil bath at 90ºC, under N_2 but without stirring, during 4 hours. Finally, the resulting black powder was washed several times with deoxygenated water and ethanol. After washing, particles were dried by evaporating the solvent in an oven at 40ºC.

$MnFe_2O_4$ nanoparticles

The experiment above was repeated but adding simultaneously 10 mL of aqueous $MnSO_4.H_2O$ (6 mmol) and 15 ml of aqueous $FeSO_4.7H_2O$ (11 mmol).

$CoFe_2O_4$ nanoparticles

The experiment above was repeated but adding simultaneously 10 mL of aqueous $CoCl_2.6H_2O$ (6 mmol) and 15 mL of aqueous $FeSO_4.7H_2O$ (11 mmol).

2.4. Characterization of the materials

In order to confirm the identity of the materials involved in this work and to determine some of its characteristics, a large number of characterization techniques were used. The results and the respective discussion can be found in the Chapter 3.

2.4.1. General characterization methods

X-Ray Diffraction (XRD) data for all materials were obtained at ambient temperature on an Empyrean PANalytical diffractometer (Cu $K_{\alpha 1,2}$ X-radiation, λ_1 = 1.54060 Å; λ_2 = 1.54443 Å). The registration of the diffraction patterns was performed with a step size of 0.026 degrees, in continuous mode, in the $15 \leq 2\theta \leq 100^o$ range.

Fourier Transform Infrared (FT-IR) spectra (in the range 4000-350 1/cm) were recorded by directly placing of the samples on the diamond crystal unit of Reflectance Total Attenuated (ATR), using a Bruker Tensor 27 spectrophotometer after 256 scans with resolution of 4 1/cm.

STEM/TEM (Scanning Transmission Electron Microscopy / Transmission Electron Microscopy) images were acquired using an Electron Microscope Hitachi, SU-70 working

at 20 kV. Samples were prepared by direct deposition of a drop of NPs dispersed in ethanol, evaporating at room temperature over a grid of cupper coated with a carbon film.

Brunauer-Emmet-Teller (BET) surface area analyses were performed on an automated surface area analyser (Micromeritics Gemini 2380) by means of nitrogen adsorption-desorption.

Regarding the study of magnetic properties, measurements of hysteretic cycle were performed using magnetometer VSM at room temperature (~ 293K). The magnetization was normalized to the total mass of the sample.

Isoelectric point of nanoparticles was determined by zeta potential measurements, using a Zetasizer Nano ZS (Malvern Instruments). A solution of nanoparticles was prepared in ultra-pure water. The pH of the solution was adjusted for different pH (between 2 and 10) using NaOH or HNO_3 solutions. The temperature was fixed at 25ºC, and three replicate measurements of zeta potential were performed for each sample.

Chromium analysis were performed by Inductively Coupled Plasma-Optical Emission Spectometry (ICP-OES), on a Horiba Jobin Yvon Activa M spectrometer (radial configuration) equipped with a Burgener MiraMist nebulizer (sample flow of 1 mL/min), peristaltic sample delivery pump with three canals, argon flow (nebulizer: 0.02 L/min; auxiliary gas: 0.2 L/min; plasma: 12 L/min), nebulizer chamber, CCD (coupled charging device) for detection, and algorithm background correction for quantification. The operating mode of this technique is shown in more detail below.

Iron, manganese, cobalt and chromium content in the materials were also determined by ICP-OES. Briefly, about 20 mg of sample were accurately weighted into an acid-washed Teflon reactor; then 3 mL of HNO_3 (70%) were added, and reactors were placed on a CEM - MDS-81D microwave digestion system (equipped with 12 pressurized vessels) at a ramp temperature up to 140ºC for 5 min, then up to 175°C for 3 min, and finally at 175°C for 4 min 30 s. A second digestion cycle was carried out after addition of 3 mL of HCL (37%) for complete digestion of the materials. After digestion, samples were diluted with ultra-pure water and then analyzed by ICP-OES.

2.5. Removal of chromium from waters

The ability of the synthesized NPs to remove Cr(III) from aqueous solution was evaluated by performing sorption experiments of batch (discontinuous) type. In these experiments, the

effect of amount of sorbent used, the influence of the pH of the solution, the effect of increasing the ionic strength of the solution and the influence of organic matter in the removal of chromium were evaluated.

Effect of amount of sorbent

The removal tests using different amounts of magnetic NPs were performed to monoelementary aqueous solutions with a concentration of 2000 μg/L of chromium(III). Round bottom flasks of 1000 mL were used, fully closed, to prevent possible losses of solvent, in accordance with the experimental setup shown in **Figure 5**. The solution of chromium was freshly prepared by dilution of the standard commercial solution (1000 mg/L) in ultra-pure water. The NPs were weighed on analytical balances and the solutions were prepared in volumetric flasks with adequate capacity so that the ion concentration and NPs amount in prepared solutions are exactly known. When preparing the solutions micropipettes were used to perform various measurements and to transfer volumes. For the measuring of NPs mass, an analytical balance accurate to the microgram was used. The tests were realised at room temperature, under mechanical stirring, by putting a known mass of NPs (10, 50, 100 and 200 mg) in contact with the aqueous solution, at pH *ca.* 6.

Effect of pH

The effect of pH on the sorption process was studied for an initial Cr(III) concentration of 2000 μg/L and the selected values were 4, 6, 8 and 10. The pH adjustments were performed using nitric acid or sodium hydroxide solutions, before the addition of the pre-weighed sorbent. The tests were realised in ultra-pure water using 50 and 100 mg/L of $CoFe_2O_4$ NPs.

Effect of ionic strength

The effect of ionic strength on the sorption of Cr(III) was evaluated using solutions of chromium prepared in ultra-pure water, mineral water and saline water (salinity of 15 g/L). Composition of minaral water used for these experiments is presented in the next Table. This information was taken from the bottle label. Saline water was obtained by diluting filtered seawater with ultra-pure water.

Table IV – Analytical composition of mineral water used for these tests.

pH	Cations concentration (mg/L)	Anions concentration (mg/L)
5.8-7.0	Na^+ = 4.4 (± 1.1) Ca^{2+} = 2.7 (± 1.6)	HCO_3^- = 16.5 (± 8.0) Cl^- = 3.2 (± 0.9)

The tests were performed using 50 and 100 mg/L of $CoFe_2O_4$ NPs in aqueous solutions with a concentration of 2000 µg/L of chromium(III), at pH 4, 6 and 10.

Effect of organic matter

The effect of humic substances on the sorption of Cr(III) was evaluated using sodium humic salt solutions with concentrations of 5 and 10 mg/L at pH 4, 6 and 10, and for initial Cr(III) concentration of 2000 µg/L. The tests were realised either in mineral water or saline water (salinity of 15 g/L), using 100 mg/L of $CoFe_2O_4$ NPs.

For all the different studies, the moment when we proceeded to the mixture of NPs and aqueous solution was recorded as the start time (t_0), which served as the reference for carrying out the subsequent collections. After addition of NPs, it was used an ultrasonic bath (~60 seconds) to obtain a better dispersion of the particles in the solution. Over the aqueous chromium solution contact time with the NPs, aliquots (5-10 mL) of sample were being collected using Pasteur pipettes, in fixed and increasing times. These aliquots were under the influence of a magnet for approximately 15-30 minutes (to ensure that all NPs were removed). After separation of NPs, the aliquots were immediately acidified (pH < 2) with 25 µL of concentrated HNO_3 (65% v/v) and stored at 4°C until analysed by ICP-OES.

Figure 5 - Experimental set used in removal tests of Cr(III), using magnetic NPs (Figueira, 2010).

2.6. Samples quantification by ICP-OES

The technique of ICP-OES has been widely used to quantify elements in samples due to their multi-elemental capacity as well as the very low range of detection limits.

The preparation of the samples is one of the most important points since it constitutes the biggest source of error of the analytical quantification. When analysing samples by ICP, it is sometimes necessary to solubilize the samples. For this purpose, solid samples such as NPs are initially digested (the most common solid sample preparation method).

The next step is to introduce the liquid sample in the equipment, which is suctioned by a very thin capillary tube. This sample is transported to the nebulizer (which functions as a spray with a flow of 1.0 mL/min) and is transformed into very small droplets. Argon (torch gas with a flow of 12 L/min) takes the sample from the nebulizer to the plasma, which is ionized argon (this ionization is achieved through an alternating electric current). In plasma, the temperature is so high that the solvent evaporates and all bonds between the molecules are broken down to obtain atoms in the gaseous state (Skoog et al., 2002).

Since the temperature is so high the electrons go to the excited state and when they return to the ground state they release energy, whose wavelength is characteristic for each element; the concentration of the elements is proportional to the intensity of the emission analytical signal.

The principal components of ICP-OES are represented in Figure 6.

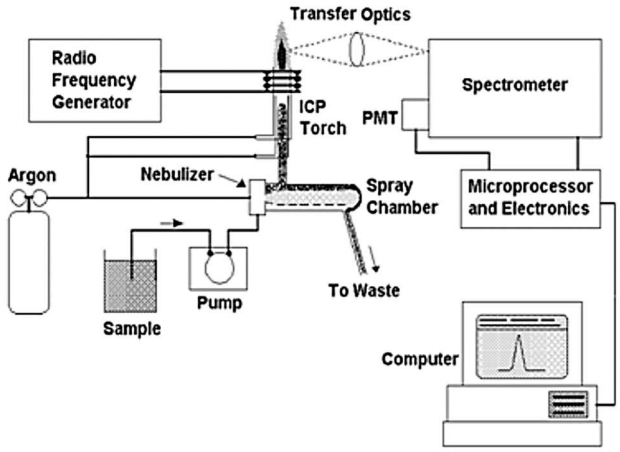

Figure 6 – Scheme of ICP-OES principal components (Boss and Fredeen, 1997).

Quality control

To ensure that the results obtained in the analysis are reliable and have the required quality, quality control is carried out in parallel with the analysis of the samples.

Before starting the analysis of the samples, a calibration curve is made for which at least 5 standards of different concentrations, prepared from a mono-elemental solution is used; the curve is only accepted if a correlation coefficient of more than 0.9995 and an error of less than 10% in each standard is obtained. The intensity of the analytical signal of the sample is compared to that curve in order to determine the concentration.

In addition, a blank, a certified reference material, a check standard (prepared by dilution from an independent standard stock solution and whose concentration coincides with that of one of the calibration curve standards), a replica of all samples (in order to verify the drift of the equipment), a duplicate in each set of ten samples (which allows to verify the repeatability of the quantification process) and a recovery test in each set of ten samples (to evaluate the matrix interference) are also analysed.

For the chromium quantification, the calibration curve was prepared using standards with concentrations between 4 and 2000 µg/L. It was assumed that the value of lower concentration standard (4 µg/L) is the quantification limit and that the detection limit value is one third of the quantification limit (1.3 µg/L). The blank concentration was always under the detection limit. In the case of replica, duplicate and check standard a maximum error of 10% was accepted. Regarding the certified reference material, it was used a reference material obtained from a water interlaboratory comparison test of RELACRE entity, carried out in October 2017, and the range of accepting values varied between 85% and 115%. The recovery test range of accepting varied between 90 and 110%. All the results presented in this work fulfilled these quality criteria.

Chapter 3

Results

3.1. Materials characterization

The NPs synthesised were characterized by several techniques as follows.

3.1.1. X-ray diffraction

X-ray diffraction analysis were used to confirm the crystalline phase of obtained NPs. By comparison with databases, it is observed that the spectra of X-ray diffraction obtained (**Figure 7**) confirm the existence of the cores Fe_3O_4, $MnFe_2O_4$ and $CoFe_2O_4$ in NPs synthesized.

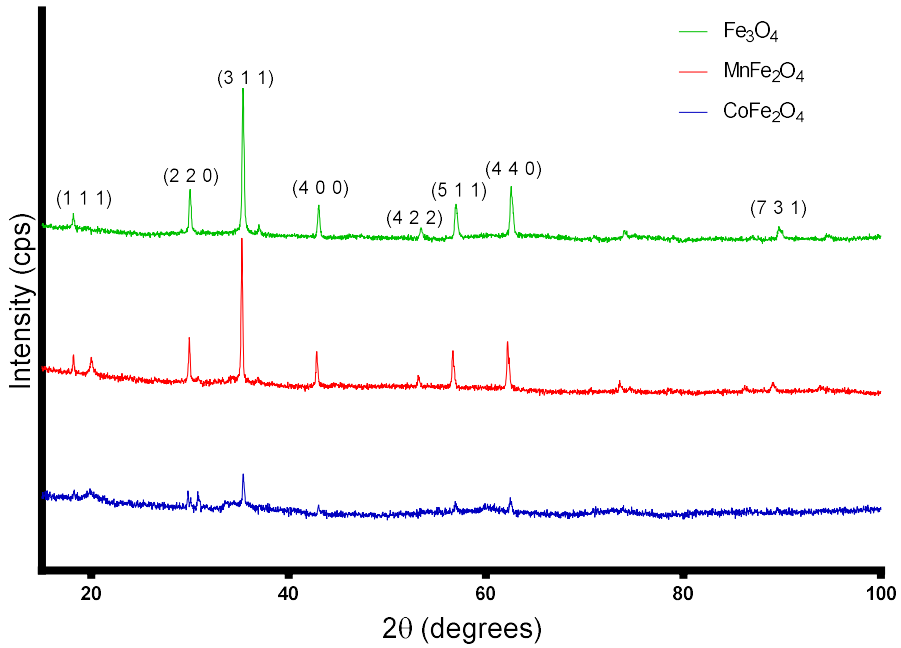

Figure 7 - XDR pattern of Fe_3O_4, $MnFe_2O_4$, $CoFe_2O_4$ NPs and the corresponding crystal planes.

In the previous diffractogram, the peaks corresponding to the crystalline planes (1 1 1), (2 2 0), (3 1 1), (4 0 0), (4 2 2), (5 1 1), (4 4 0) and (7 3 1) characteristic at 2θ equal to 18.3, 30.1, 35.5, 43.1, 53.5, 57.0, 62.6 and 89.7 are indexed.

The crystalline phase of the nanoparticles resulting from the Cr(III) removal ($CoFe_2O_4$@Cr) was also identified through XRD (**Figure 8**).

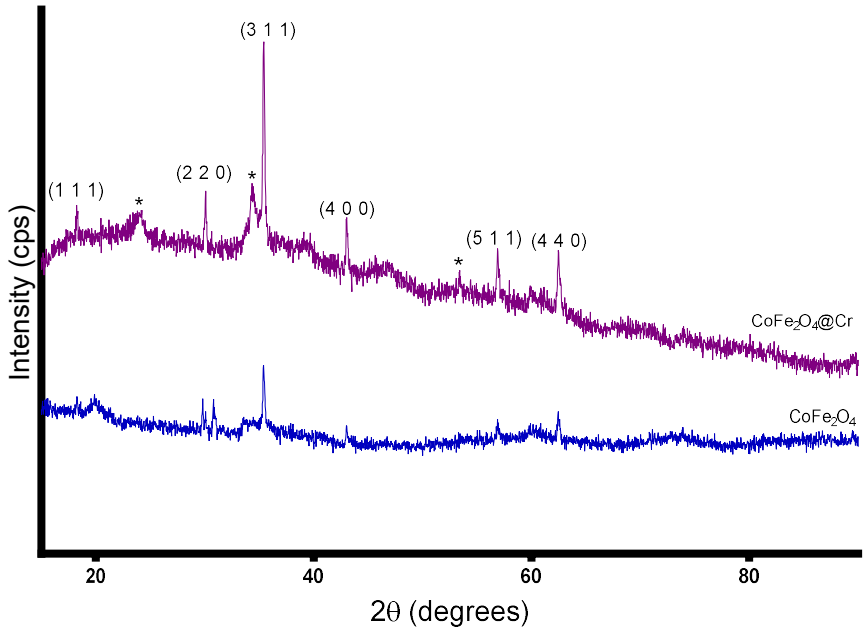

*Figure 8 - XDR pattern of $CoFe_2O_4$ and $CoFe_2O_4$@Cr NPs and the corresponding crystal planes. The peaks marked with * correspond to the crystalline planes of the $CoFe_2O_4$ NPs.*

In the diffractogram of **Figure 8**, in addition to the peaks already observed and corresponding to the crystalline phases of the planes present in $CoFe_2O_4$ nanoparticles, other three peaks provably relative to the presence of chromium are presented.

3.1.2. Fourier-transform infrared spectroscopy (FTIR)

The FTIR spectra of Fe_3O_4, $MnFe_2O_4$ and $CoFe_2O_4$ NPs were also registered and are presented below (**Figure 9**).

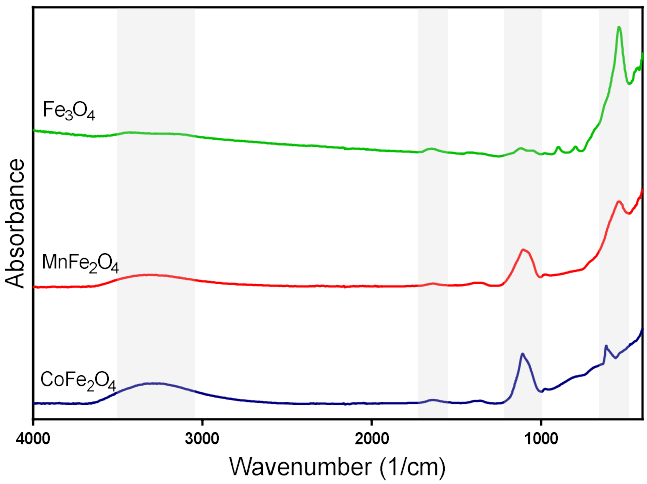

Figure 9 - FTIR-ATR spectra of Fe_3O_4, $MnFe_2O_4$ and $CoFe_2O_4$ NPs.

These spectra were obtained using a spectrophotometer IR Fourier transform and the ability to use the technique of attenuated total reflectance (FTIR-ATR), which allowed the direct analysis of various solids without being necessary the preparation of KBr pellets.
Based on a vibration frequencies table of chemical groups (Socrates, 2004) and in the information relating to the characterization of materials presented in Tavares et al. (2013), Figueira et al. (2011), Mahmoodi (2013), Zhang et al. (2014), Zhao et al. (2015), correspondence between the bands present in the FTIR-ATR spectra obtained and the types of vibrations that may have originated these bands was taken. The results of this analysis are summarized in **Table V**.

Table V - Summary of some of the bands obtained in the FTIR-ATR spectra of the synthesised NPs, and possible correspondence with the vibrations of particular chemical groups.

		Vibrational mode			
		ν(Metal-O)	ν(Metal-OH) or ν(Metal-OH_2)	δ(H-O-H)	ν(O-H)
Position (1/cm) and the intensity of bands in FTIR-ATR spectrum	Fe_3O_4	540 (vs)	1116 (vw)	1651 (vw)	3419 (vw)
	$MnFe_2O_4$	542 (m)	1104 (s)	1636 (vw)	3292 (w)
	$CoFe_2O_4$	615 (m)	1108 (s)	1642 (vw)	3292 (m)

Intensity of bands: vs - very strong; s – strong; m – medium; w – weak; vw – very weak
ν: streching vibration → it implies variations in the length of chemical bonds; δ: bending vibration → it implies spatial changes of the atoms that constitute the molecule, without there being any variation in the length of chemical bonds.

The peak at 600–500 1/cm is due to the metal–oxygen bond. The broad band in the region of 3100-3600 1/cm and a weak band in the region of 1630 1/cm may be attributed to the presence of humidity in the samples (molecular water adsorbed to the surface or incorporated into the crystalline lattice). The peak at around 1100 1/cm is due to metal-OH and metal-OH_2 bounds (Bellusci et al., 2009), which reflect the sorption of water on the oxide.

To evaluate the stability of these kind of NPs, FTIR spectra of material synthesised in 2016 were acquired at that time and again in 2018. The FTIR spectra of Fe_3O_4 NPs showing the time evolution is presented in the next Figure.

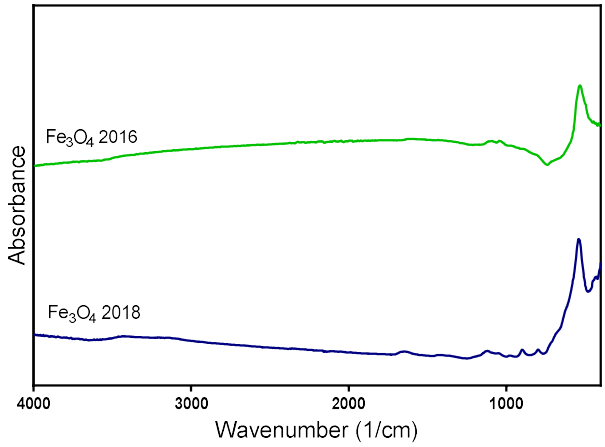

Figure 10 - FTIR-ATR spectra of Fe_3O_4 NPs, acquired in 2016 and 2018.

As it can be observed, there is no significant differences in the NPs structure after 2 years. This can be also observed for $MnFe_2O_4$ and $CoFe_2O_4$ NPs, whose spectra are presented in the attachments (Chapter 7).

After three specific removal tests, using 200 mg/L of NPs to remove Cr(III) in ultra-pure water, the NPs used were recovery and analysed by this technique in order to observe the effect of chromium bounded to the NPs. The spectra obtained are presented below (**Figure 11**).

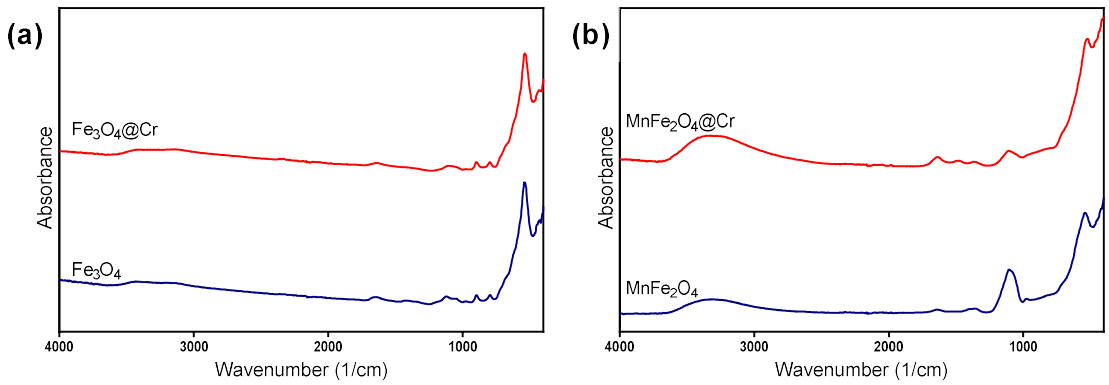

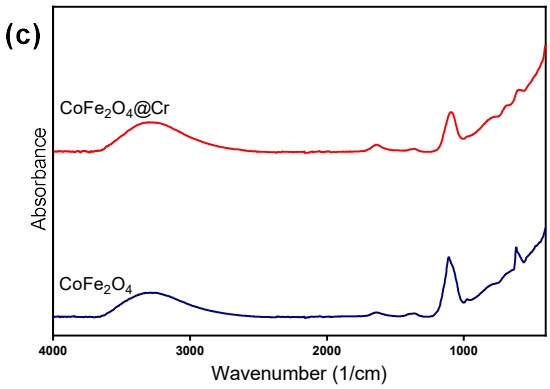

Figure 11 - FTIR-ATR spectrum of Fe_3O_4@Cr, $MnFe_2O_4$@Cr and $CoFe_2O_4$@Cr NPs resulting from removal tests using 200 mg/L of NPs to sorption of Cr(III) in ultra-pure water.

There are no significant changes in the spectra between Fe_3O_4 and Fe_3O_4@Cr NPs; on the contrary, the comparison between the spectra of manganese and cobalt ferrites shown slightly changes in the intensity of bands.

3.1.3. Electron microscopy

The electron microscopy involves the use of a beam of electrons instead of light (optical microscope), which allows obtaining images of samples with extremely reduced dimensions (as nanomaterials) with suitable resolution.

Images of the analysis by electron microscopy of the ferrite NPs used in this work (with exception of manganese ferrite NPs), are presented in **Figures 12 and 13**.

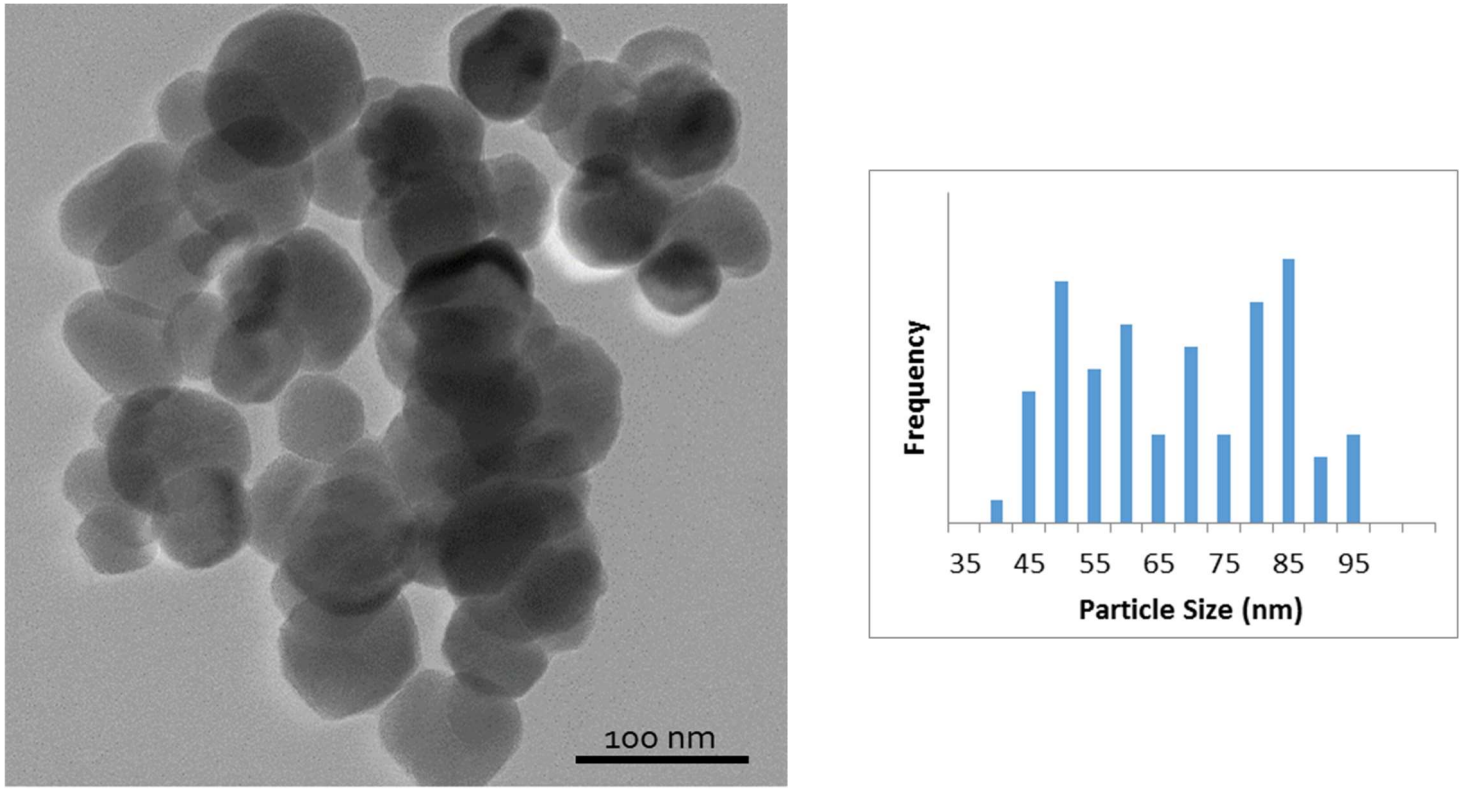

Figure 12 - Images of Fe_3O_4 NPs obtained by electron microscopy (TEM): core (left) and the histogram of the core sizes distribution (right).

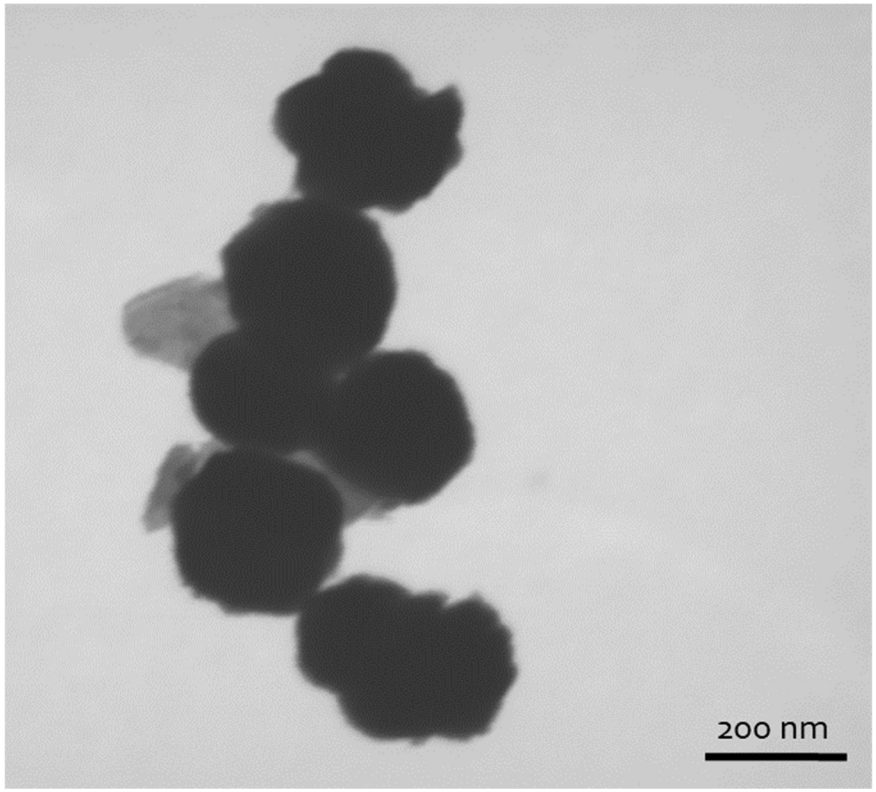

Figure 13 - TEM images of $CoFe_2O_4$ NPs obtained by electron microscopy (STEM): core (left) and the histogram of the core sizes distribution (right).

According to these results, it is possible to observe the NPs shape, which is spherical. Also, it is possible to estimate the particle size.

In the case of magnetite, several measurements of particle size were made (using Image J software), and then the histogram was constructed. Regarding to results obtained, magnetite appears to have a bimodal distribution with a first population with an average size of 50 nm and a second around 80-85 nm.

In the case of cobalt ferrite, a mean particle size of 60 nm for cobalt ferrite was estimated. As it can be observed, the obtained nanoparticle sample has a relatively narrow distribution of sizes, so this synthesis is quite adequate for the formation of monodisperse cobalt ferrite nanoparticles.

Finally, for manganese ferrite, it was not possible to acquired electron microscopy picture, but a distribution with a population with an average size superior to the other NPs would be expected, according to BET surface area results, which are presented below.

3.1.4. Chemical analysis of NPs

The NPs were digested with acid and then the ratio between the cations (Mn/Fe and Co/Fe) was determined by ICP-OES. The results indicate that the composition of the manganese ferrite synthesized is $Mn_{1.00}Fe_{2.17}O_4$ while $Co_{1.00}Fe_{1.98}O_4$ is the composition of the cobalt ferrite synthesized.

3.1.5. BET surface area

Table VI shows BET surface area, porosity volume and pore diameter of the NPs used in this work.

Table VI - Values of BET surface area (S_{BET}), porosity volume (V_p) and pore diameter (D_p) of the different types of NPs used in this work.

Samples	S_{BET} (m^2/g)	V_p (cm^3/g)	D_p (nm)
Fe_3O_4	31.3	0.08	9.9
$MnFe_2O_4$	22.3	0.04	7.6
$CoFe_2O_4$	33.3	0.07	9.2

Based on these results, it seems that manganese ferrite NPs are bigger than the other NPs since the surface area of these nanomaterials may increases with decreasing particle size. This could be confirmed through STEM images; however the images were not acquired for all the NPs used.

3.1.6. Magnetic properties

Figure 14 shows the results of magnetic measurements performed on neat ferrite NPs. All samples show magnetic hysteresis as expected for ferromagnetic materials. It is important to note that the magnetization value for magnetite NPs is within the reported values for this material (Girginova et al., 2010; Oliveira-Silva et al., 2014). For the Mn containing samples, as compared to the Fe and Co counterparts, the saturation magnetization (maximum value of magnetization observed) is very low (inferior to 10 emu/g). Note that a high magnetic susceptibility is a key factor for the response of these nanoparticles in the application of an external magnetic field.

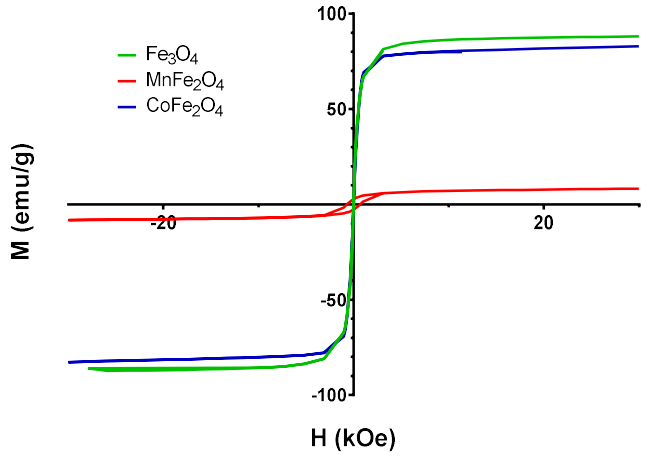

Figure 14 -Magnetization curve of the NPs used in this work in function of the magnetic field.

In **Figure 15** is not visible a magnetic cycle with hysteresis for Fe_3O_4 and $CoFe_2O_4$ NPs. However, when the image is magnified, the curves show that there is a certain hysteresis, as follows:

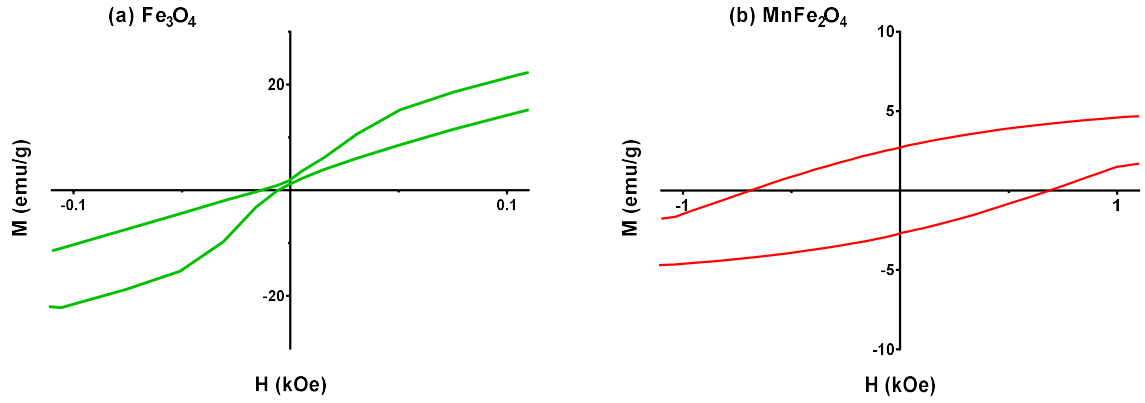

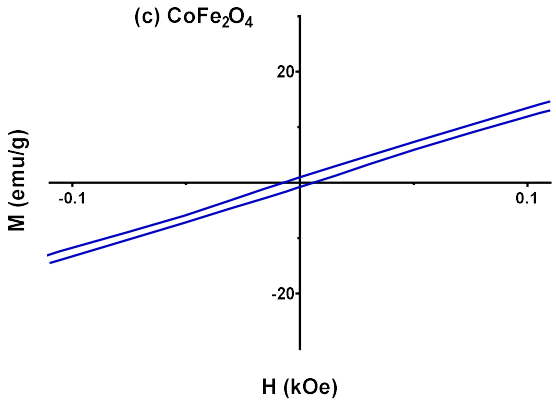

Figure 15 - Magnification of the magnetization curve of the Fe_3O_4, $MnFe_2O_4$, $CoFe_2O_4$ NPs.

Based on **Figure 15**, it is possible to realise that $CoFe_2O_4$ NPs can be reused since, due to their low coercivity, they are easily demagnetized.

3.1.7. Isoelectric point

The isoelectric point (or point of zero charge), is the pH value at which the zeta potential, which is equivalent to the net charge of the nanoparticle including bound ions, is zero.

Figure 16 displays zeta potentials as a function of solution pH for Fe_3O_4, $MnFe_2O_4$ and $CoFe_2O_4$ NPs. With an increase in solution pH, the zeta potential of NPs decreased.

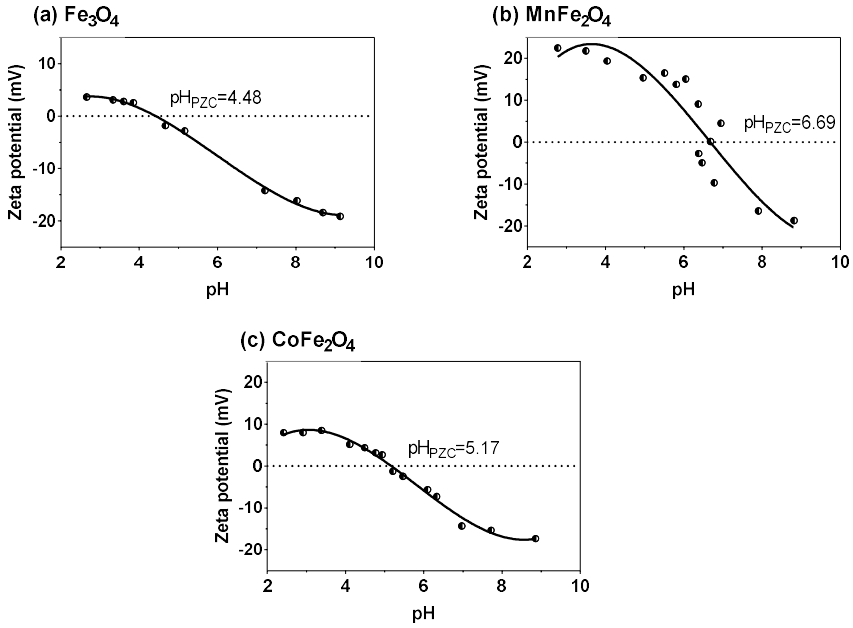

Figure 16 - Zeta potentials as a function of solution pH for (a) Fe_3O_4, (b) $MnFe_2O_4$ and (c) $CoFe_2O_4$ NPs.

At pH 4.48, 6.69 and 5.17, the net charge of Fe_3O_4, $MnFe_2O_4$, $CoFe_2O_4$ NPs is zero, which is the point of zero charge (PZC) of these NPs. Below pH_{PZC}, the surface of NPs attracted protons and therefore was positively charged; on the contrary, by increasing the solution pH over to pH_{PZC}, NPs released the protons into the solution and the surface became negatively charged. In this way, depending on the solution pH, the charged surface will affect the sorption of chromium due to the electrostatic attraction or repulsion. Also, according to Suh et al. (2015), at certain conditions, the principal mechanism favourable to sorption of Cr(III) ions onto metal oxide surfaces of NPs is chemical affinity instead of electrostatic attraction.

3.2. Removal of chromium from waters

Chromium concentrations in solution after the previously defined times of contact with NPs were measured. The equilibrium was reached after 48 hours for all the systems.

3.2.1. Effect of amount of sorbent

There are some studies which demonstrate a reduction in concentration of Cr(III) and Cr(VI) in synthetic water and real wastewater using Fe_3O_4 NPs (Arthy and Phanikumar, 2016; Ataabadi et al., 2015; Bisht et al., 2016; Kumari et al., 2015; Lee and Kim, 2016; Luther et al., 2013; Martínez et al., 2015; Parsons et al., 2014; Rajput et al., 2016; Shahriari et al., 2014; Simeonidis et al., 2015); however, either the amount of sorbent used is too high or chromium concentrations are unrealistic. Regarding the $MnFe_2O_4$ and $CoFe_2O_4$ NPs, its use may be interesting from the point of view of magnetic properties because with the change of transition metal comparing to magnetite, the magnetic properties are also changed, which may have influence the removal process; moreover, the few studies using these materials (Hu et al., 2007; Luther et al., 2013; Sezgin et al., 2016; Srivastava et al., 2016) test also an high amount of NPs.

Therefore, a set of preliminary removal tests of Cr(III) from ultra-pure water per action of different amounts of Fe_3O_4, $MnFe_2O_4$ and $CoFe_2O_4$ NPs was carried out to evaluate the sorption capacity of the different materials and the contact time necessary to reach the equilibrium. These tests were performed at room temperature with adjustment of pH at *ca.* 6, and were made to obtain a first knowledge regarding the behaviour of NPs in the removal of this ion. The amount of NPs used were 10, 50, 100 and 200 mg, for a chromium concentration of 2000 µg/L (which is the maximum allowed concentration in residual waters discharge in Portugal (Ministério do Ambiente, 1998)).

The results obtained for the removal of Cr(III) using NPs of Fe_3O_4, $MnFe_2O_4$ and $CoFe_2O_4$ indicate that removal was high efficient when using $MnFe_2O_4$ and $CoFe_2O_4$ NPs (**Figure 17**).

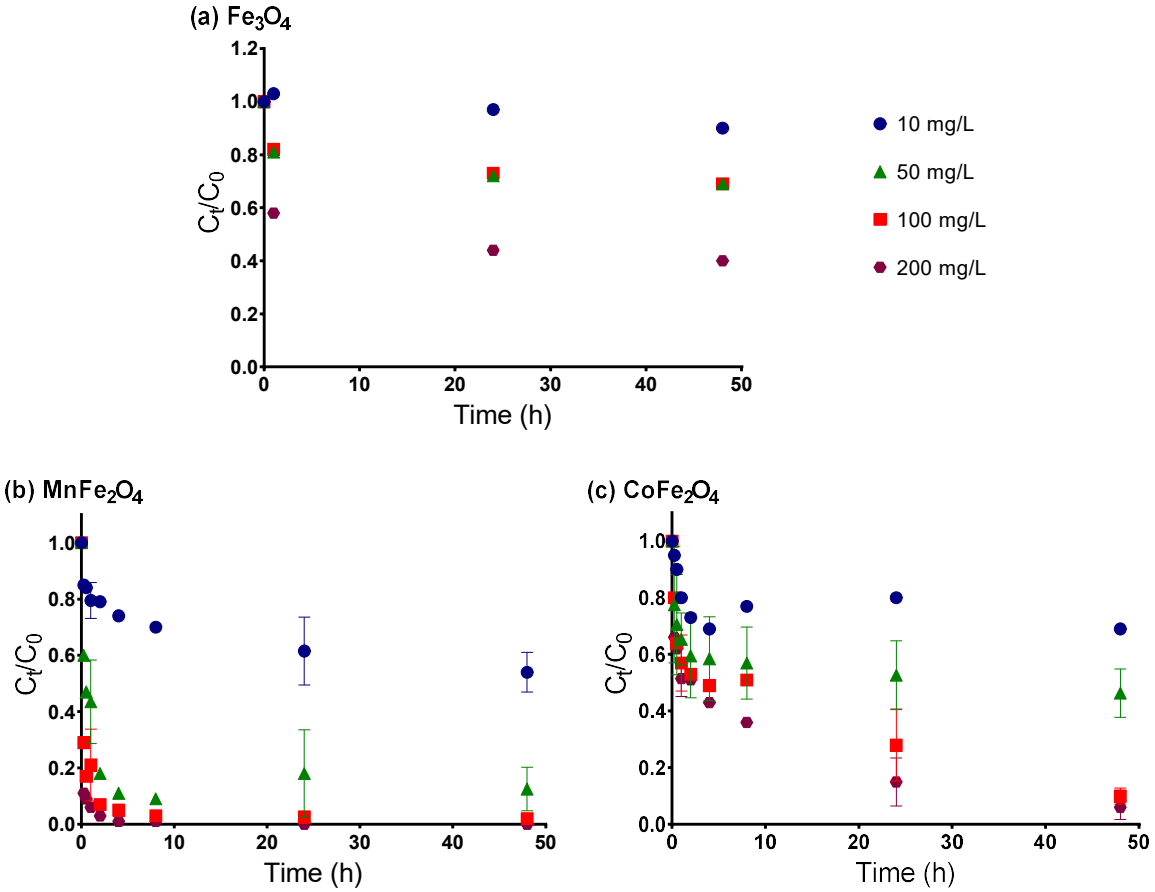

Figure 17 - Profile of variation of the normalized concentration of Cr(III) in aqueous solution, in function of contact time with different amounts of magnetic NPs. Note that some of the values of manganese and cobalt ferrites are average values.

The analysis of these results shows that, under the conditions used, there were no significant changes in the concentration of Cr(III) when the amount of Fe_3O_4 NPs used was increased from 10 mg to 50 mg and then to 100 mg/L, observing a removal of only 10 to 31% of Cr(III) in solution; however using 200 mg/L of NPs it is possible to remove more than 50% of Cr(III) in solution. On the contrary, the cores of manganese ferrite and cobalt ferrite removed more than 50% of Cr(III) in solution using 50 mg/L of NPs (which means that is necessary four times less amount of material to obtain the same result as with magnetite nanoparticles). Moreover, with 100 mg/L of NPs the manganese ferrite removed about 98% and the cobalt

ferrite removed 90%. Finally, using 200 mg/L of NPs, manganese ferrite removed all Cr(III) in solution and cobalt ferrite removed 94% of Cr(III).

Despite the high efficiency of manganese ferrite NPs – being the only ones able to remove the required amount of Cr(III) to obtain water considered sufficiently "clean" for human consumption (50 µg/L) –, the synthesis and consequently the results obtained using these NPs are not easily reproductible when compared to those obtained with $CoFe_2O_4$ NPs (thus, duplicates are not real). So, for the study of the other experimental conditions (see next sections), despite of being more expensive, the $CoFe_2O_4$ NPs were the ones chosen.

3.2.1. Effect of pH

Taking into account the results obtained in the effect of sorbent amount tests, we proceeded to the study of pH effect. Clearly there is an improvement in the removal with increased mass NPs, but not justified to use 200 mg/L of material. Thus, these tests comparing the different values of pH were performed using 50 and 100 mg/L of NPs and the selected pH values were 4, 6 and 10. At this stage, full kinetics of removal of Cr(III) was performed. Furthermore, only were used NPs of $CoFe_2O_4$, since they are not the most effective, but they are the ones with most reproductible percentages of sorption.

The results obtained for the removal of Cr(III) using $CoFe_2O_4$ NPs at different pH (4, 6 and 10) indicate that in all experiments performed in this phase, it exists removal of Cr(III) in solution. Also, removal was more efficient at pH of 10 of NPs (**Figure 18**).

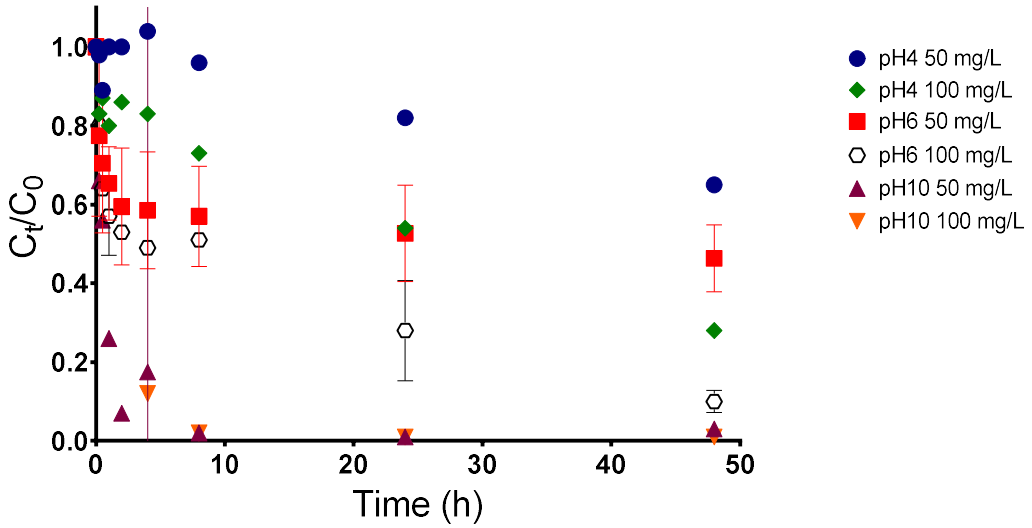

Figure 18 - Profile of variation of the normalized concentration of Cr(III) in aqueous solution (ultra-pure water) at different pH (4, 6 and 10), in function of contact time with magnetic $CoFe_2O_4$ NPs (using 50 and 100 mg/L). Note that some of the values obtained for the removal at pH 6 and pH 10 using 50 mg/L of NPs are average values.

An additional test at pH 8 and using 50 mg/L of $CoFe_2O_4$ NPs were carried out, obtaining 92% of chromium removal. So, it was found that chromium removal at pH 10 was the most rapid and effective, followed by removal at pH 8.

3.2.1. Effect of ionic strength

In order to test the efficiency of the nanoparticles in real samples, some tests were carried out by contacting the nanoparticles with solutions of increasing complexity. The experimental conditions for these tests were the same as in the pH tests to compare the removal efficiency in matrices with different complexity.

The variation of the normalized concentration of Cr(III) in solution in function of contact time is shown in **Figure 19**.

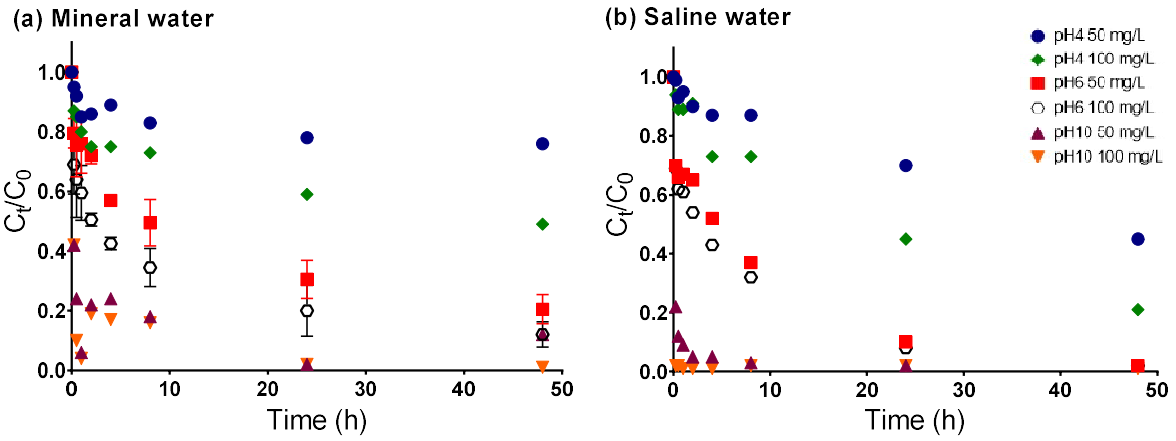

Figure 19 - Profile of variation of the normalized concentration of Cr(III) in aqueous solution (mineral and saline water). at different pH (4, 6 and 10), in function of contact time with magnetic $CoFe_2O_4$ NPs (using 50 and 100 mg/L). The values obtained for the removal in mineral water at pH 6 using 50 and 100 mg/L of NPs are average values.

The majoritary elements (Na, Mg, K, Ca, Mn, Fe and Cu) contents of mineral water samples were analysed before and after the removal studies. There were no significant changes in the concentration of these elements, except for an increase in Fe and K concentration in the samples in which NPs were added, due to the presence of trace amounts of NPs in solution. As can be seen from the Figure, the removal of the Cr(III) present in solution was almost complete and quite fast at pH 10, for both matrices. In the case of saline water experiments, after 1 hour the removal percentage was greater than 90%; these results allow us to conclude that even using a much more complex matrix, such as saline water, the removal of Cr(III) by

$CoFe_2O_4$ NPs is efficient. However, this efficiency tends to decrease when the removal occurs in mineral water when compared to the other matrices.

Moreover, comparing the Cr(III) sorption kinetics to the nanoparticles in the three matrices (ultra-pure, mineral and saline water – **Figures 18 and 19**), Cr(III) removal in saline water was slightly faster despite the higher amount of ions present in this matrix, which could somehow interfere with the nanoparticles in the removal of Cr(III).

3.2.1. Effect of organic matter

The influence of interfering substances - dissolved organic matter - in the removal of Cr(III) was evaluated. As already mentioned, these experiments were carried out in the matrices previously tested (mineral and saline water), at different values of pH (4, 6 and 10), to which humic salt solutions with concentrations of 5 and 10 mg/L were added. For comparison, the same amount of $CoFe_2O_4$ NPs was used in all the tests (100 mg/L).

The variation of the normalized concentration of Cr(III) in solution in function of contact time is shown in **Figure 20**.

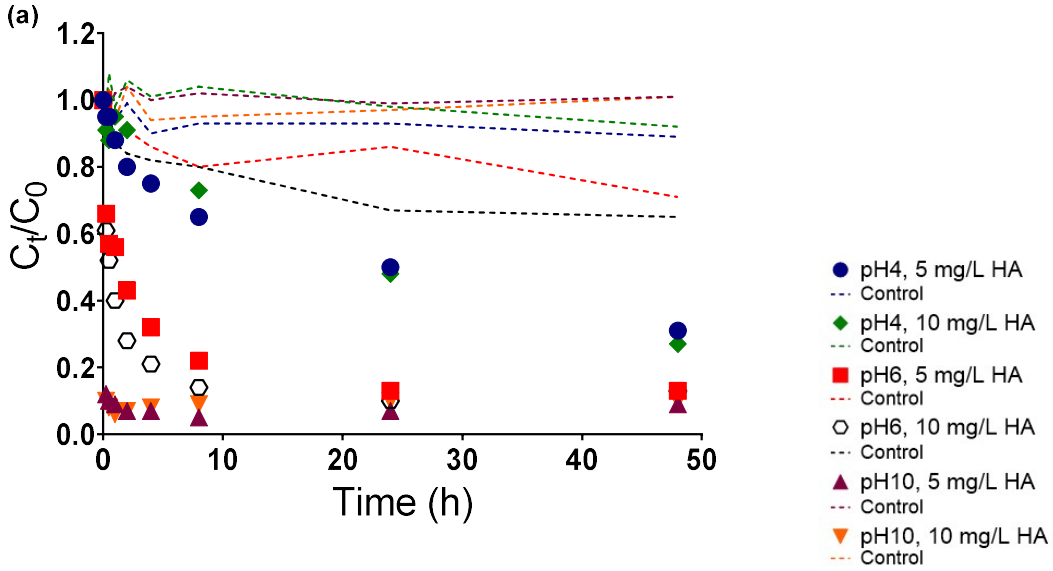

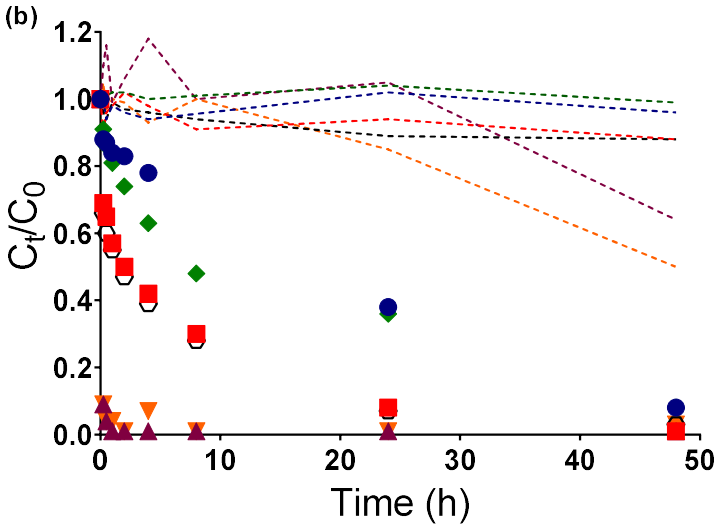

Figure 20 - Profile of variation of the normalized concentration of Cr(III) in aqueous solution (mineral and saline water with 5 and 10 mg/L of dissolved humic acids – HA) at different pH (4, 6 and 10), in function of contact time with magnetic $CoFe_2O_4$ NPs (using 100 mg/L).

Humic acids have been reported in literature for the removal of Cr(III). In this way, the variation of the normalized concentration of control – that is a mono-elemental aqueous solution of Cr(III) to which no NPs were added – was also represented in **Figure 20**. As can be seen, there is a decrease in control concentration over time; that is, Cr (III) is not removed exclusively by the NPs and some of this removal is due to the presence of humic acids (HA). To facilitate the analysis of the influence of humic acids in the chromium removal, a Table summarizing the Cr(III) removal percentage after 48 hours for the two matrices and for the different concentrations of humic acids is presented above.

Table VII – Removal percentage of Cr(III) after 48 hours for different values of pH, in mineral and saline water, in function of humic acids concentration.

	Mineral water			Saline water		
	0 mg/L humic acids	5 mg/L humic acids	10 mg/L humic acids	0 mg/L humic acids	5 mg/L humic acids	10 mg/L humic acids
pH 4	51%	65%	71%	79%	91%	92%
pH 6	88%	84%	82%	98%	99%	97%
pH 10	99%	91%	90%	99%	99%	95%

At pH 4, both in mineral water and saline water, as the HA concentration increases, the percentage of Cr(III) removal also increases. Also, there is no competition between Cr(III) and HA.

At the higher pH values (6 and 10), the percentage of removal tends to decrease slightly with the presence of humic acids, being the effect most pronounced in mineral water. It is also found that as HA concentration increases, the competition between HA and Cr(III) becomes more evident, with a slight loss of efficacy in the removal of this ion.

Chapter 4

Discussion

4.1. Removal of chromium from waters

The study of several parameters, such as the amount of sorbent, pH, ionic strength of the solution and the presence of organic matter, for the removal of Cr(III) using $CoFe_2O_4$ NPs allowed a broad understanding of the behaviour of this material in different conditions.

4.1.1. Chromium sorbed in the NPs

All the NPs were characterized after removal tests by FTIR-ATR to confirm the bond of Cr(III) to the NPs. It was observed that on the contrary to Fe_3O_4@Cr NPs, the comparison between the spectra of $MnFe_2O_4$@Cr and $CoFe_2O_4$@Cr NPs shows slightly changes in the intensity of bands and deviations of *ca.* 20 1/cm in the band of metal–oxygen bond. This difference between materials can be explained by the fact that Fe_3O_4 NPs just removed about 60% and in the case of other ferrites the sorption percentage was superior to 95%; in the other hand, these difference can be associated to the binding mechanism between Cr(III) and the NPs. So, in the case of manganese and cobalt ferrites, the deviation of metal–oxygen bond band may suggests the bond of Cr(III) to the oxygen atoms of NPs, being that in this case it seems to occur a partial substitution of Fe(III) ions by Cr(III) ions. This is in accordance to Luther et al. (2013) published work, in which exchange mechanism is referred as the mechanism for the binding. In the case of interaction between Fe_3O_4 NPs and Cr(III) ions, since there is no evident change in the spinel structure, Cr(III) may precipitate as an insoluble hydroxide on particle surface (Simeonidis et al., 2015).

Besides this analysis, $CoFe_2O_4$@Cr NPs were also analysed by X-ray diffraction and the results corroborate the hypothesis of iron sites substitution in cobalt ferrite's structure by Cr(III) ions, participating in mixed oxides. In XRD diffractogram of **Figure 8**, in addition to the presence of new peaks, disappearance (or attenuation) of others was detected and this change in relation to the diffractogram of the starting materials (prior to contact with Cr (III) in the removal studies) may be consistent with changes in the structure of the initial spinel; there are also deviations in two of the most intense peaks of the spinel – the peaks corresponding to the crystalline planes (2 2 0).and (3 1 1) appeared at 2θ equal to 29.81 and 35.41, and after the binding of Cr(III) to cobalt ferrite they appear 30.08 and 35.43, respectively.

4.1.2. Effect of amount of sorbent

For all mass values used, a decrease in the Cr(III) concentration in the liquid fraction occurs over time. It is also verified that as the mass of NPs increases, the residual concentration of Cr(III) in solution tends to decrease, so the removal efficiency increases. This can be explained by the fact that the smaller the amount of material used, the lower the number of sites available for sorption of Cr(III). However, the amount of Cr(III) removed per milligram of nanoparticle increases with the decrease of the nanoparticle mass used, which means that the sorption capacity significantly increased.

Removal percentage with manganese ferrite (**Figure 21**) was higher than removal percentage with magnetite and cobalt ferrite for all amounts of material (manganese ferrite was 36-67% and 6-34% more efficient, respectively). This observation could be explained by the point of zero charge of these particles, which could have influence on the interactions between the NPs and the Cr(III) ions. At pH > PZC the surface is negatively charged while at pH < PZC it develops positive charge (by protonation of oxygen atoms). In this way, for the pH values used in these tests (*ca.* 6), the surface of manganese ferrite is positively charged while the other NPs surface is negatively charged. On the other hand, $Cr(OH)_3$ is the predominant form of Cr(III) in solution at pH 6. So, the different PZC values of the NPs is not the explanation for the differences in the removal.

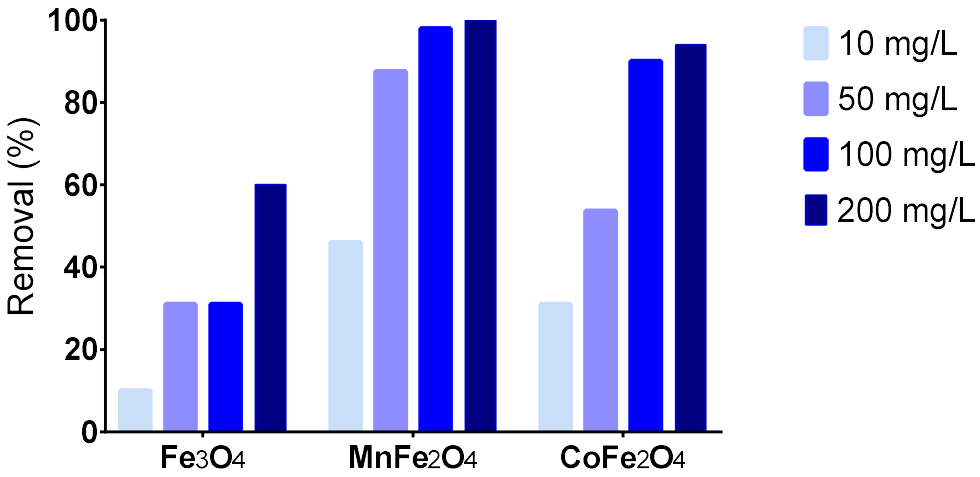

Figure 21 - Profile of variation of the removal percentage of Cr(III) in aqueous solution, according to the different amounts of magnetic NPs (Fe_3O_4, $MnFe_2O_4$, $CoFe_2O_4$) tested.

Thus, another approach must be taken. Then, the results obtained for Cr(III) removal with manganese ferrite may be due to good affinity of this element with manganese, related with exchange of electrons, as reported in the literature for other elements as As(III) (Parsons et al., 2009); the explanation for the different efficiency of removal with the three materials tested may be due to the possible different electron transfers from either the Fe, Mn or Co ions (Parsons et al., 2009).

4.1.3. -Effect of pH

The removal of chromium using $CoFe_2O_4$ NPs is influenced by the relative amount of certain species of this ion in solution (speciation), so the pH is one of the most important parameters affecting the metal sorption onto sorbents.

Redox potential of removal tests at different values of pH was measured in order to know which the chromium specie in contact with cobalt ferrite NPs was. According to the results obtained, $CrOH^{2+}$ was the specie in solution at pH 4 while $Cr(OH)_3$ was the specie in solution at pH 6 and 10 (**Figure 22**).

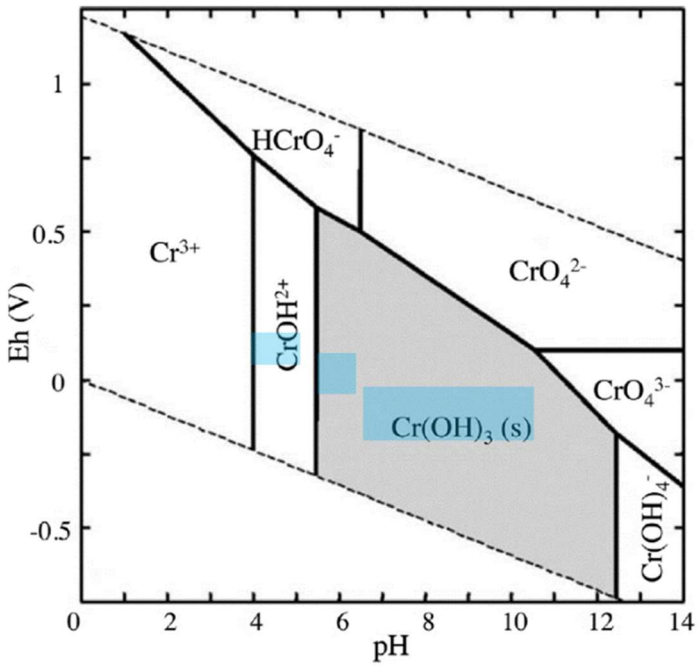

Figure 22 - Eh-pH diagram of Cr-O-H system, in aqueous media, at 25ºC and 1 bar (Jin et al., 2016). The experimental conditions to which the removal tests were carried out are shaded.

As noted previously, the removal is increasingly efficient as the pH (4, 6 and 10) of the solution is increased. At pH 4, besides the predominance of a specie different than that present at pH 6 and 10, at low pH the hydrogen ions are strongly competing sorbates (Rocha et al., 2014), which can explained the low removal percentages (35% and 72%) since they compete with Cr(III) for the active sites in the material. Comparing the results obtained at pH 6 and 10, at pH 10 the sorbent material will be surrounded by hydroxyl groups, producing a negative surface charge and as a result, the sorption of cationic species – Cr(III) in this case – will be favourable.

4.1.4. Effect of ionic strength

The ionic strength of the solution is another parameter which may influence the sorption process, since the ions present compete with Cr(III) for the binding to NPs.

Cobalt ferrite NPs are clearly efficient for the removal of Cr(III) from more complex matrices as presented above, suggesting that they are very promising materials to be applied in wastewater and industrial effluents treatment.

Despite the slightly decrease of removal efficiency in mineral water when compared to the results obtained from ultra-pure water, the values of removal efficiency obtained at pH 6 and 10 were satisfactory, ranged between 80 and 99% (**Figure 23**); At pH 4, besides the competition between Cr(III) and hydrogen ions, there are other ions in mineral water competing for the limited number of binding sites.

Contrary to what happened in the mineral water matrix, the removal of Cr (III) from saline water was more efficient than the removal of ultra-pure water, with higher removal percentages achieved (**Figure 23**). According to the literature (Rocha et al., 2014), the formation of chloro complexes with some metals can occur in the presence of inorganic ligands like chloride (which is present in saline water). Depending on the affinity of chloro complexes to the sorbent surface, the sorption can be positive or negatively affected. In this way, an enhance in the Cr(III) removal from saline water can occur if the chloro complexes have a higher affinity to the $CoFe_2O_4$ NPs surface than the $Cr(OH)_3$ (dominant Cr species at pH 6 and 10); then, a higher number of these complexes will cause an increase in the removal efficiency.

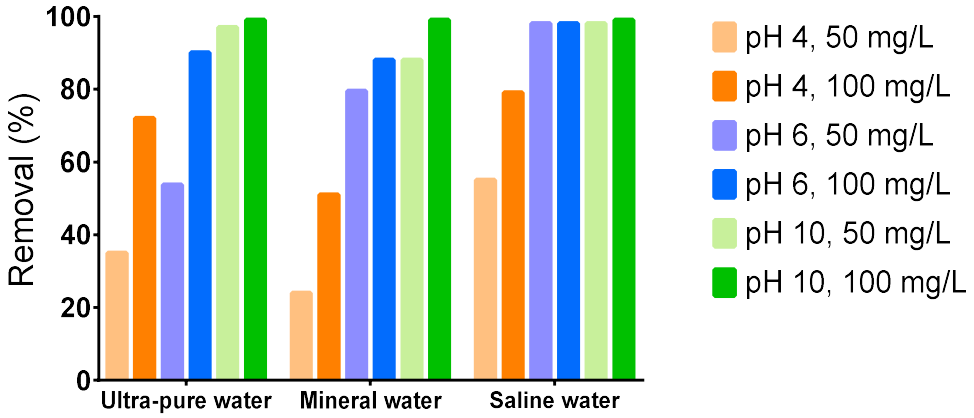

Figure 23 - Profile of variation of the removal percentage of Cr(III) in aqueous solution using $CoFe_2O_4$ NPs, according to the solution pH and the amounts of material used, for the matrices tested.

4.1.5. Effect of organic matter

In the removal of Cr(III) in the presence of dissolved organic matter (humic acids were used in the studies carried out in this work) two aspects must be taken into account.

On the one hand, experiments without NPs (designated as control) demonstrate a decrease in the concentration of Cr(III) with time, which is predictable, since humic acids have been used as sorbents for Cr(III) removal (Santosa et al., 2008). As shown in **Figure 24**, higher the concentration of humic acids in solution, the greater its influence on the removal (for pH 6 and 10).

On the other hand, dissolved humic acids act as a strong complexing agent (Rocha et al., 2014) and this is the reason for the decrease in the removal efficiency (at pH 6 and 10) as the concentration of humic acids increases. Note that to occur complexation, it is necessary a minimum concentration of each specie involved in the reaction. In the presence of humic acids, a fraction of Cr(III) in solution becomes unavailable due to the formation of stable complexes between humic acids and Cr(III), resulting in a decrease in the uptake of this metal by the NPs. Even so, considering only the Cr(III) not complexed with humic acids, the values of removal efficiency obtained were superior or equal to 80 and 90% at pH 6 and 10, respectively (**Figure 24**). Regarding the kinetic profile of the removal of Cr(III) by cobalt ferrite NPs at pH 4, it is positively affected by the presence of dissolved humic acids; these results show that the Cr–humic acids complexes formed have a higher affinity to the

$CoFe_2O_4$ NPs surface than the $Cr(OH)^{2+}$ and the influence of humic acids in the Cr(III) removal decreases with decreases with the increase of its concentration (**Figure 24**).

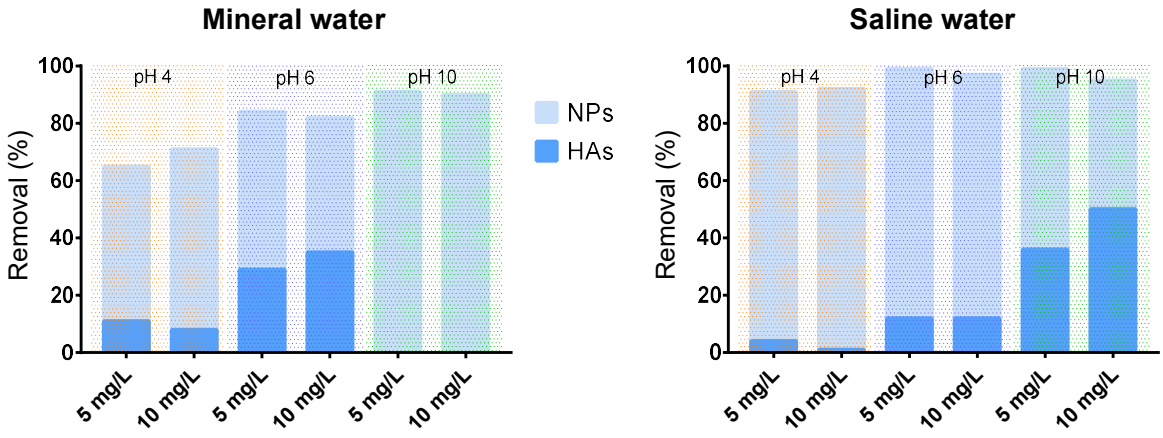

Figure 24 - Profile of variation of the removal percentage of Cr(III) in aqueous solution (mineral and saline water, both with dissolved organic matter) using $CoFe_2O_4$ NPs (100 mg/L), according to the solution pH (4, 6 and 10) and the amounts of material (50 and 100 mg/L) used, showing in influence (in %) of different humic acids (HAs) concentration in the removal of Cr(III)).

4.1.1. Kinetic studies

This section presents the graphical adjustment of the kinetic models of pseudo 1st order, pseudo 2nd order and Elovich to the experimental data (only for the best results – tests with removal percentages superior to 95%) in order to determine which model from among those used best describes the removal process of Cr(III) by the ferrite NPs with core of cobalt.

All kinetic models used have the same number of parameters (two), implying that they have the same number of degrees of freedom; thus, the parameter R^2 corresponds to a valid criterion for making a comparison of the adequacy of the various models used in adjusting the experimental results.

Regarding the removal of Cr(III) by 100 mg/L of $CoFe_2O_4$ NPs at pH 10 in saline water (either in the presence or not of dissolved organic matter) (**Figure 25 d and f**), adjustment of the kinetic models considered to the experimental data seems to indicate that with any model, the results obtained are adequately modelled (see **Table VIII**). However, it is necessary a careful interpretation because the removal kinetics in these two cases is so fast that the steady state is achieved in a very short time. A correct application of such models

requires a relatively large set of points in the area of the graphic q_t vs t wherein the chromium concentration effectively decreases (increases q_t).

For cases in which the existence of chromium removal with high efficiency (>95%) by the $CoFe_2O_4$ NPs was verified, the graphics q_t vs. t and the respective adjustments of kinetic models are described below. Note that the legend used in the first graph applies to the remaining graphs presented in this page and in the next one.

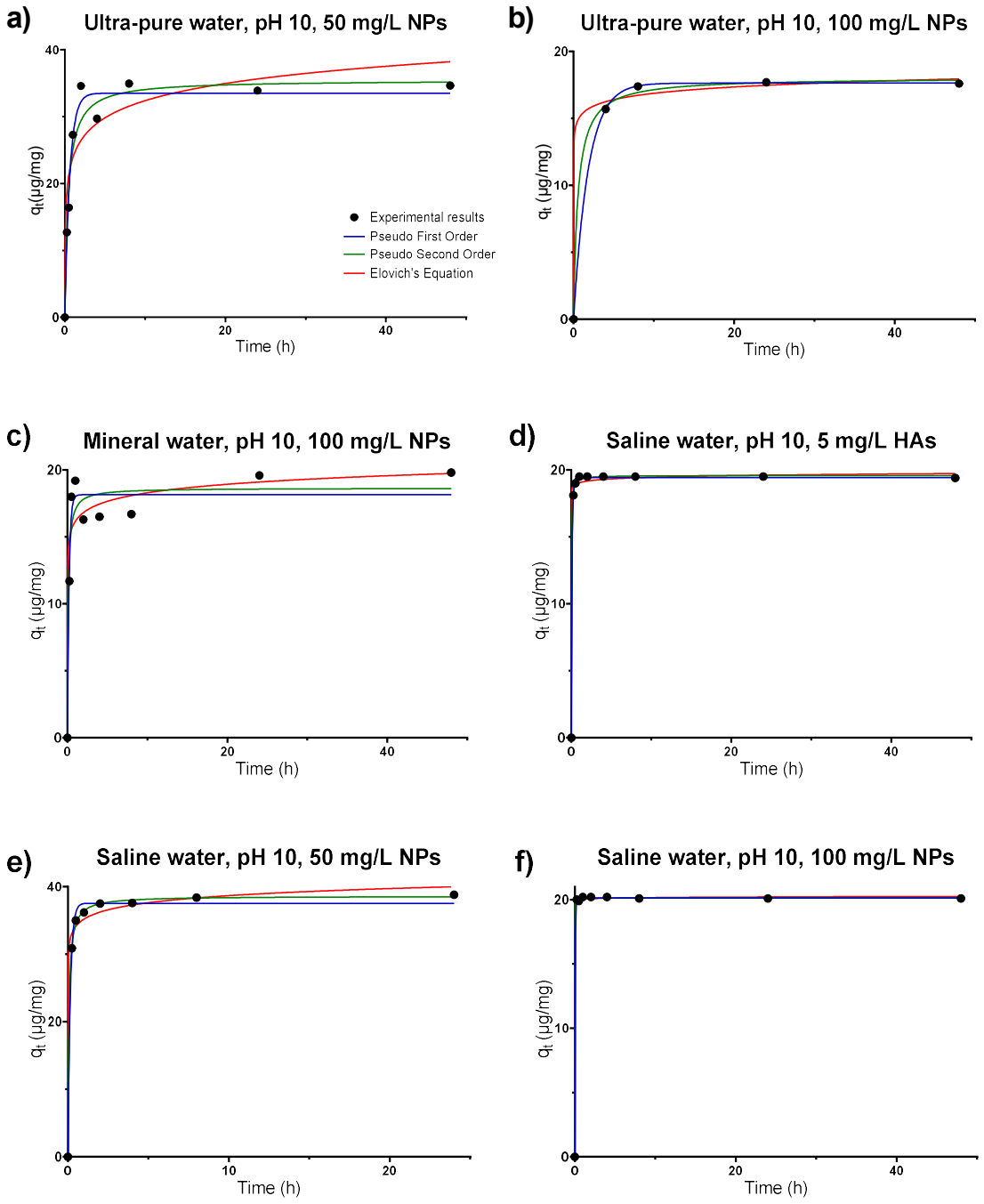

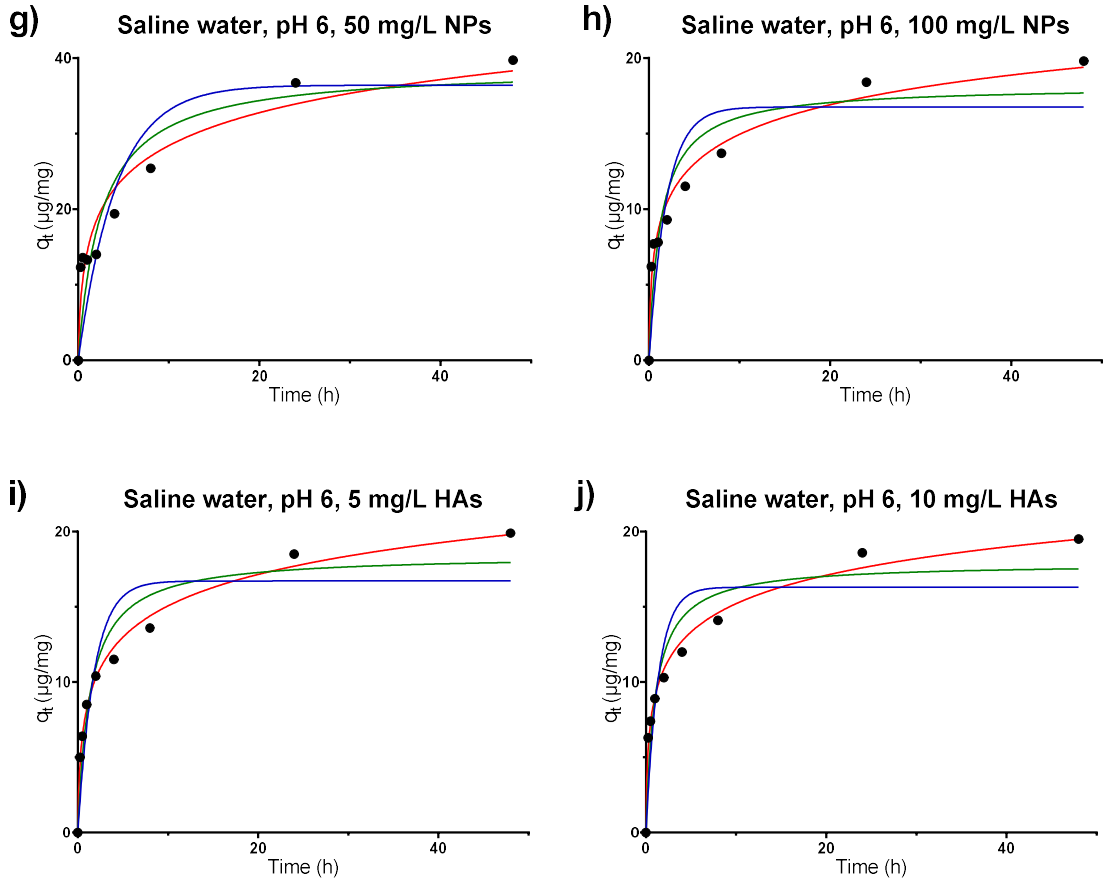

Figure 25 - Adjustment of the kinetic models of pseudo 1st order, pseudo 2nd order and Elovich to the results obtained in Cr(III) removal test with efficiency superior to 95%, by the $CoFe_2O_4$ NPs.

In the cases corresponding to a removal at pH 6 (**Figure 25 g-j**), a simple visual inspection of graphs depicted shows that the kinetic model Elovich corresponds to a best adjust of the experimental results. Regarding the removal at pH 10, this observation is not so simple. In this case, it is necessary to use the parameter R^2 to determine which is the model that corresponds to a more efficient adjustment. The values obtained for the parameters of the kinetic models used in this study are presented in the **Table VIII**. Given the table data presented there, it is observed that the model that best adjusts the removal of Cr(III) at pH 10 from saline water (**Figure 25 e-f**) is the pseudo 2nd order model, while from the other matrices (**Figure 25 a-d**) the results were better fit by the pseudo 1st order model. However, the R^2 value obtained in the removal of Cr(III) from ultra-pure water at pH 10 (using 50 mg/L of NPs), from mineral water at pH 10 (using 100 mg/L of NPs) and from saline water at pH 6 (using 50 mg/L of NPs) (**Figure 25 a, c and g**. respectively) is not very high,

indicating that probably no kinetic models used adjusts efficiently the experimental results. On the other hand, the high value of R^2 in the removal of Cr(III) from ultra-pure water at pH 10 (using 100 mg/L of NPs) (**Figure 25 b**) can be due to the lack of points in the area of the graphic wherein the q_t increases.

The sorption of metals to magnetic NPs is a complex process and involves several mechanisms, such as adsorption on the NPs surface and pores, ion-exchange, surface precipitation and complexation and chelation (Rocha et al., 2014). Regarding the experimental results better adjusted by pseudo 1st order model, chemical sorption is the mechanism associated to the sorption process (Ho and Mckay, 1998) and the surface of the material is considered homogeneous, so only one binding mechanism should occur; for the studies whose sorption kinetics follows pseudo 2nd order model, the sorption is controlled by the chemisorption process involving valency forces (sharing or exchange of electrons between the sorbent and sorbate) or ionic forces (ion exchange) (Ho, 2006), being that more than one binding mechanism may occur. Contrary to the models of pseudo 1st order and pseudo 2nd order, which involve certain mechanistic assumptions allowing to obtain some conclusions regarding the type of mechanism involved in adsorption processes that they model, the Elovich equation is semi-empirical and there is no a consensus regarding its nature. Thus, the mechanism associated with the sorption processes involved in the tests at pH 6 can not be well identified, but it is usually associated to chemisorption.

Table VIII - Values obtained in the adjustment of experimental results to the pseudo 1st order, pseudo 2nd order and Elovich's models, using the software GraphPad Prism 7.

Amount of $CoFe_2O_4$ NPs	Matrix	pH	Concentration of humic acids	q_e exp (μg/mg)	Degrees of Freedom	Pseudo first order model				Pseudo second order model				Elovich's model			
						Parameters		Adjustment		Parameters		Adjustment		Parameters		Adjustment	
						k_1	q_e (μg/mg)	R^2	$s_{y/x}$	k_2	q_e (μg/mg)	R^2	$s_{y/x}$	α	β	R^2	$s_{y/x}$
50 mg/L	Ultra-pure water	pH 10	0 mg/L	34.7	11	1.6	33.5	0.9343	3.603	0.068	35.5	0.9299	3.722	2.307E+03	0.2697	0.8686	5.097
100 mg/L	Ultra-pure water	pH 10	0 mg/L	17.6	3	0.55	17.6	1.000	0.04428	0.10	18.1	0.9985	0.3389	3.524E+09	1.461	0.9961	0.5574
100 mg/L	Mineral water	pH 10	0 mg/L	19.8	7	4.8	18.2	0.9434	1.591	0.57	18.6	0.9230	1.855	3.957E+07	1.087	0.9079	2.028
50 mg/L	Saline water	pH 6	0 mg/L	39.7	7	0.24	36.4	0.7828	6.287	0.010	38.8	0.8502	5.221	5.512E+01	0.1576	0.9388	3.336
100 mg/L	Saline water	pH 6	0 mg/L	19.8	7	0.52	16.8	0.7860	3.056	0.043	18.2	0.8851	2.239	5.477E+01	0.3525	0.9786	0.9656
50 mg/L	Saline water	pH 10	0 mg/L	38.8	6	6.6	37.6	0.9953	0.9699	0.43	38.6	0.9994	0.3328	1.951E+10	0.6612	0.9919	1.271
100 mg/L	Saline water	pH 10	0 mg/L	20.1	7	21	20.1	0.9998	0.09877	21	20.2	0.9999	0.08530	3.422E+160	18.59	0.9997	0.1175
100 mg/L	Saline water	pH 6	5 mg/L	19.9	7	0.56	16.7	0.8473	2.660	0.040	18.5	0.9315	1.781	4.327E+01	0.3298	0.9933	0.5560
100 mg/L	Saline water	pH 6	10 mg/L	19.5	7	0.73	16.3	0.8153	2.819	0.054	17.9	0.9116	1.950	7.122E+01	0.3660	0.9908	0.6278
100 mg/L	Saline water	pH 10	5 mg/L	19.4	7	11	19.4	0.9996	0.1404	2.7	19.6	0.9995	0.1469	1.826E+46	5.683	0.9970	0.3751

Chapter 5

Final Remarks

5.1. Conclusions

The increase of population and contamination affect the extension of water reservoirs with quality for human consumption. So, there is a need to reduce consumption and to find solutions to recuperate the quality of waters, crucial to ensure the survival and maintenance of the quality of life of living beings and essential to the ecosystems that sustain them.

Chromium is among the most toxic trace elements, according to EPA; also, it is on the list of priority substances (ATSDR, 2017). Published literature in the last decade shows that nanomaterials exhibit high adsorption capacity for chromium species though most studies have focus on mono-elemental spiked ultra-pure water. Despite their effectiveness and relative low-cost, the practical uses of nanomaterials for decreasing chromium concentrations in simple aquatic matrices, requires further research. The viability and success of nanomaterials as sorbents depends on crucial factors that need to be evaluated, such as: the effect of natural and artificial chelators commonly present in contaminated waters; effect of interferences, such as trace elements competing with chromium sorption; reduction of the mass of sorbent per water volume or recovery processes that minimizes wastes which ultimately might result in the discharge of nanoparticles to the environment.

In this work, it was possible to synthesize nanoparticles of magnetite, manganese ferrite and cobalt ferrite. NPs were well characterized and their sorption capacity for Cr(III) was investigated, being that cobalt ferrite NPs were intensively studied. Considering the results presented, it can be concluded that both manganese and cobalt ferrite nanoparticles are efficient for Cr(III) removal; with magnetite NPs it would be necessary to use high amounts of material to obtain the same results as with less amount of manganese and cobalt ferrites. For all the studied experimental conditions, $CoFe_2O_4$ NPs proved to be a very efficient material in the removal of Cr(III) from water, except at low pH (pH 4) and/or using less amount of material (10 mg/L). In the study of the influence of pH on the removal process, it was verified a more favourable (and faster) sorption of chromium as the pH of the solution increases, yielding removal percentages between 35 and 97% when using 50 mg/L of NPs and percentages between 72 and 99% when using twice that amount of material. The efficiency of cobalt ferrite NPs for Cr(III) removal was tested in more complex matrices (mineral and saline water), which allowed to evaluate the effect of ionic strength on the ability of these nanomaterials to remove chromium from water; in general, removal is less efficient in mineral water compared to removal in ultra-pure water, but efficiency increases

in saline water. Relative to the effect of dissolved organic matter in mineral and saline water, this effect is also not significant in terms of competition with Cr(III), decreasing less than 10% maximum removal efficiency at pH 6 and 10 and improving removal at pH 4 (leading to an increase in efficiency of up to 20%).

Regarding sorption kinetics of Cr(III), the model that best adjusted the experimental data was the pseudo 1st order model (for tests at pH 10 in ultra-pure, mineral and saline water with dissolved organic matter), the pseudo 2nd order model (for tests at pH 10 in saline water), and the model Elovich (for tests at pH 6).

Finally, cobalt ferrite NPs are an excellent option for water treatment due to the ease and reproducibility of synthesis, rapid removal of waters by magnetic separation, combined with the fact that this material causes low amounts of solid waste, and the possibility of being reused reducing its cost.

5.1. Suggestions for future work

Associated with the rapid growth of nanotechnology in recent years, concerns about the environmental impact of nanomaterials have grown. In this context, some studies (Giakisikli and Anthemidis, 2013) report the possibility of reusing these materials in certain applications, such as preconcentration methods. Thus, as a suggestion for future work, it could be interesting to evaluate the viability and cost benefit balance of the recycling of NPs as an alternative to its simple release to the environment. In the particular case of NPs used in this work, it could be interesting to explore the reuse of CoFe2O4 NPs since, due to their low coercivity, they are easily demagnetized.

Regarding the removal studies, it would be important to evaluate the influence of other contaminants, such as drugs/pharmaceuticals in chromium removal from waters, since some compounds are frequently detected in natural waters and can influence the performance of chromium removal. The size of the NPs can also be a parameter to consider in the future, analysing the pros and cons of changing the dimensions of the NPs in the removal process efficiency and the subsequent separation of the NPs. Moreover, before the application of cobalt ferrites nanoparticles in the total chromium removal from real wastewaters, it would be necessary to study in the laboratory their behaviour in such conditions.

In addition to the kinetic studies, a sorption process may be further characterized by balance studies. These studies are carried out at controlled temperatures (hence, the respective

associated mathematical models are often referred to as isothermal) and involved studying qe vs Ce, being useful to determine the maximum sorption capacity of a particular sorbent for a given adsorbate. Another suggestion for future work will be to proceed to balance studies of these sorption processes.

Chapter 6

References

Akoz E, Erdemir S, Yilmaz M. Immobilization of novel the semicarbazone derivatives of calix[40]arene onto magnetite nanoparticles for removal of Cr(VI) ion. J Incl Phenom Macrocycl Chem 2012;73:449–58.

Arami H, Khandhar A, Liggitt D, Krishnan KM. In vivo delivery, pharmacokinetics, biodistribution and toxicity of iron oxide nanoparticles. Chem Soc Rev 2015;44:8576–607.

Arthy M, Phanikumar BR. Efficacy of Iron-Based Nanoparticles and Nanobiocomposites in Removal of Cr3+. J Hazardous, Toxic, Radioact Waste 2016;20:28.

Ataabadi M, Hoodaji M, Tahmourespour A, Kalbasi M, Abdouss M. Optimization of factors affecting hexavalent chromium removal from simulated electroplating wastewater by synthesized magnetite nanoparticles. Environ Monit Assess 2015;187:4165–75.

ATSDR. Priority List of Hazardous Substances 2017. http://www.atsdr.cdc.gov/spl/ (accessed December 2, 2017).

ATSDR. Toxicological Profile for Chromium. Agency Toxic Subst Dis Regist 2012.

Babaei AA, Ahmadi M, Goudarzi G, Jaafarzadeh N, Baboli Z. Adsorption of chromium(VI) from saline wastewater using spent tea-supported magnetite nanoparticle. Desalin Water Treat 2016;57:12244–56.

Babel S, Kurniawan TA. Low-cost adsorbents for heavy metals uptake from contaminated water: a review. J Hazard Mater 2003;97:219–43.

Bagheri M, Younesi H, Hajati S, Mehdi S. Application of chitosan-citric acid nanoparticles for removal of chromium(VI). Int J Biol Macromol 2015;80:431–44.

Batool S, Akib S, Ahmad M, Balkhair KS, Ashraf MA. Study of modern nano enhanced techniques for removal of dyes and metals. J Nanomater 2014;2014:20.

Behnajady MA, Bimeghdar S. Synthesis of mesoporous NiO nanoparticles and their application in the adsorption of Cr(VI). Chem Eng J 2014;239:105–13.

Belay AA. Impacts of Chromium from Tannery Effluent and Evaluation of Alternative Treatment Options. J Environ Prot (Irvine, Calif) 2010;1:53–8.

Bellusci M, La Barbera A, Seralessandri L, Padella F, Piozzi A, Varsanoa F. Preparation of albumin-ferrite superparamagnetic nanoparticles using reverse micelles. Polym Int 2009;58:1142–7.

Bisht G, Neupane S, Makaju R. Supercritical CO2 Assisted Synthesis of EDTA-Fe3O4 Nanocomposite with High Adsorption Capacity for Hexavalent Chromium. J Nanomater 2016;2016:10.

Biswal M, Bhardwaj K, Singh PK, Singh P, Yadav P, Prabhune A, et al. Nanoparticle-loaded multifunctional natural seed gel-bits for efficient water purification. RSC Adv 2013;3:2288–95.

Boss CB, Fredeen KJ. Concepts, Instrumentation, and Techniques in Inductively Coupled Plasma Optical Emission Spectrometry. 2ª ed. Perkin Elmer; 1997.

Cantu Y, Remes A, Reyna A, Martinez D, Villarreal J, Ramos H, et al. Thermodynamics, kinetics, and activation energy studies of the sorption of chromium(III) and chromium(VI) to a Mn3O4 nanomaterial. Chem Eng J 2014;254:374–83.

Carlos L, Einschlag FSG, González MC, Mártire DO. Applications of Magnetite Nanoparticles for Heavy Metal Removal from Wastewater. In: Einschlag PFSG, editor. Waste Water - Treat. Technol. Recent Anal. Dev., InTech; 2013, p. 63–77.

Chen R, Chai L, Li Q, Shi Y, Wang Y, Mohammad A. Preparation and characterization of magnetic Fe3O4/CNT nanoparticles by RPO method to enhance the efficient removal of Cr(VI). Environ Sci Pollut Res 2013;20:7175–85.

Chen X, Lam KF, Yeung KL. Selective removal of chromium from different aqueous systems using magnetic MCM-41 nanosorbents. Chem Eng J 2011;172:728–34.

Cheng H, Zhou T, Li Q, Lu L, Lin C. Anthropogenic chromium emissions in China from 1990 to 2009. PLoS One 2014;9:87753–61.

Chooaksorn W, Nitisoravut R, Polprasert C, Babel S, Laohhasurayotin K, Kangwansupamonkon W. Enhancement of Cr(VI) Ion Removal Using Nanochitosan Coated on Bituminous Activated Carbon. Water Environ Res 2016;88:2150–8.

Chowdhury SR, Yanful EK. Arsenic and chromium removal by mixed magnetite e maghemite nanoparticles and the effect of phosphate on removal. J Environ Manage 2010;91:2238–47.

Council of the European Union, Parlament E. Directive 2013/39/EU of the European Parliament and of the Council of 12 August 2013 amending Directives 2000/60/EC and 2008/105/EC as regards priority substances in the field of water policy. Off J Eur Union 2013.

Dasgupta J, Mondal D, Chakraborty S, Sikder J, Curcio S, Arafat HA. Nanofiltration based water reclamation from tannery effluent following coagulation pretreatment. Ecotoxicol Environ Saf 2015;121:22–30.

Debnath A, Majumder M, Pal M, Das NS, Chattopadhyay KK, Saha B, et al. Enhanced Adsorption of Hexavalent Chromium onto Magnetic Calcium Ferrite Nanoparticles: Kinetic, Isotherm, and Neural Network Modeling. J Dispers Sci Technol 2016;37:1806–18.

Debnath S, Biswas K, Ghosh UC. Removal of Ni(II) and Cr(VI) with Titanium(IV) Oxide Nanoparticle Agglomerates in Fixed-Bed Columns. Ind Eng Chem Res 2010;49:2031–9.

Demir V, Ates M, Arslan Z, Camas M, Celik F, Bogatu C, et al. Influence of alpha and gamma-iron oxide nanoparticles on marine microalgae species. Bull Environ Contam Toxicol 2015;95:752–7.

Driscoll CT, Mason RP, Chan HM, Jacob DJ, Pirrone N. Mercury as a global pollutant: Sources, pathways, and effects. Environ Sci Technol 2013;47:4967–83.

Duan W, Chen G, Chen C, Sanghvi R, Iddya A, Walker S, et al. Electrochemical removal of hexavalent chromium using electrically conducting carbon nanotube/polymer composite ultrafiltration membranes. J Memb Sci 2017;531:160–71.

Dubey S, Upadhyay SN, Sharma YC. Optimization of removal of Cr by γ-alumina nano-adsorbent using response surface methodology. Ecol Eng 2016;97:272–83.

Egodawatte S, Greenstein KE, Vance I, Rivera E, Myung N V, Parkin GF, et al. Electrospun hematite nanofiber/mesoporous silica core/shell nanomaterials as an efficient adsorbent for heavy metals. RSC Adv 2016;6:90516–25.

Fernandes T, Soares S, Trindade T, Daniel-da-Silva A. Magnetic Hybrid Nanosorbents for the Uptake of Paraquat from Water. Nanomaterials 2017;7:68.

Figueira P, Lopes CB, Daniel-da-Silva AL, Pereira E, Duarte AC, Trindade T. Removal of mercury (II) by dithiocarbamate surface functionalized magnetite particles: Application to synthetic and natural spiked waters. Water Res 2011;45:5773–84.

Figueira PAM. Nanomagnetes para remoção de iões metálicos de águas residuais. Universidade de Aveiro, 2010.

Francisquini E, Schoenmaker J, Souza JA. Nanopartículas Magnéticas e suas Aplicações. Química Supramol. e Nanotecnologia. 1st ed., 2014, p. 269–88.

Fu F, Wang Q. Removal of heavy metal ions from wastewaters: A review. J Environ Manage 2011;92:407–18.

García A, Espinosa R, Delgado L, Casals E, González E, Puntes V, et al. Acute toxicity of cerium oxide, titanium oxide and iron oxide nanoparticles using standardized tests. Desalination 2011;269:136–41.

Giakisikli G, Anthemidis AN. Magnetic materials as sorbents for metal/metalloid preconcentration and/or separation . A review. Anal Chim Acta 2013;789:1–16.

Gifford M, Chester M, Hristovski K, Westerhoff P. Reducing remediation impacts of metal

(hydr)oxide nanoparticle embedded anion exchange resins using anticipatory life cycle assessment. Environ Sci Nano 2016;3:1351–60.

Girginova PI, Daniel-da-Silva AL, Lopes CB, Figueira P, Otero M, Amaral VS, et al. Silica coated magnetite particles for magnetic removal of Hg2+ from water. J Colloid Interface Sci 2010;345:234–40.

Gode F. Removal of Chromium Ions from Aqueous Solutions by Adsorption Method. Hazard. Mater. Wastewater Treat. Remov. Anal., 2007, p. 275–308.

Gong Y, Tang J, Zhao D. Application of iron sulfide particles for groundwater and soil remediation: A review. Water Res 2016;89:309–20.

Guan X, Chang J, Fan H. A magnetically-separable Fe3O4 surface grafted with polyacrylic acid for chromium(III) removal from tannery effluents. RSC Adv 2015;5:50126–36.

Guo J, Cai X, Li Y, Zhai R, Zhou S, Na P. The preparation and characterization of a three-dimensional titanium dioxide nanostructure with high surface hydroxyl group density and high performance in water treatment. Chem Eng J 2013;221:342–52.

Gupta AK, Gupta M. Synthesis and surface engineering of iron oxide nanoparticles for biomedical applications. Biomaterials 2005;26:3995–4021.

Gupta VK, Chandra R, Tyagi I, Verma M. Removal of hexavalent chromium ions using CuO nanoparticles for water purification applications. J Colloid Interface Sci 2016;478:54–62.

Haydar S, Aziz JA. Coagulation-flocculation studies of tannery wastewater using combination of alum with cationic and anionic polymers. J Hazard Mater 2009;168:1035–40.

Ho YS. Review of second-order models for adsorption systems. J Hazard Mater B 2006;136:681–9.

Ho YS, Mckay G. Sorption of dyes from aqueous solution by peat. Chem Eng J 1998;70:115–24.

Hu J, Lo IMC, Chen G. Comparative study of various magnetic nanoparticles for Cr(VI) removal. Sep Purif Technol 2007;56:249–56.

Hua M, Zhang S, Pan B, Zhang W, Lv L, Zhang Q. Heavy metal removal from water/wastewater by nanosized metal oxides: A review. J Hazard Mater 2012;211–212:317–31.

Huang B, Qi C, Yang Z, Guo Q, Chen W, Zeng G. Pd/Fe3O4 nanocatalysts for highly effective and simultaneous removal of humic acids and Cr(VI) by electro-Fenton with H2O2

in situ electro-generated on the catalyst surface. J Catal 2017;352:337–50.

Hull MS, Vikesland PJ, Schultz IR. Uptake and retention of metallic nanoparticles in the Mediterranean mussel (Mytilus galloprovincialis). Aquat Toxicol 2013;140–141:89–97.

Imran Q, Hanif MA, Riaz MS, Noureen S, Ansari TM, Bhatti HN. Coagulation/flocculation of tannery wastewater using immobilized chemical coagulants. J Appl Res Technol 2012;10:79–86.

ISO. International Organization for Standardization 2012. https://www.iso.org/obp/ui/#iso:std:iso:ts:80004:-2:ed-1:v1:en (accessed June 16, 2016).

Jin W, Du H, Zheng S, Zhang Y. Electrochemical processes for the environmental remediation of toxic Cr(VI): A review. Electrochim Acta 2016;191:1044–55.

Kaprara E, Tziarou N, Kalaitzidou K, Simeonidis K, Balcells L. The use of Sn(II) oxy-hydroxides for the effective removal of Cr(VI) from water: Optimization of synthesis parameters. Sci Total Environ 2017;605–606:190–8.

Kaya IGB, Duranoglu D, Beker U, Senkal BF. Development of Polymeric and Polymer-Based Hybrid Adsorbents for Chromium Removal from Aqueous Solution. Clean - Soil, Air, Water 2011;39:980–8.

Khan HA, Shanker R. Toxicity of Nanomaterials. Biomed Res Int 2015;2015:2.

Khan SU, Zaidi R, Hassan SZ., Farooqi I. H., Azam A. Application of Fe-Cu binary oxide nanoparticles for the removal of hexavalent chromium from aqueous solution. Water Sci Technol 2016;74:165–75.

Kitzes J, Wackernagel M, Loh J, Peller A, Goldfinger S, Cheng D, et al. Shrink and share: humanity's present and future Ecological Footprint. Philos Trans R Soc Lond B Biol Sci 2008;363:467–75.

Kocurek P, Kolomazník K, Bařinová M. Chromium Removal from Wastewater by Reverse Osmosis. WSEAS Trans Environ Dev 2014;10:358–65.

Kumari M, Jr. CUP, Mohan D. Heavy metals [chromium (VI) and lead (II)] removal from water using mesoporous magnetite (Fe3O4) nanospheres. J Colloid Interface Sci 2015;442:120–32.

Kurniawan TA, Chan GYS, Lo W-H, Babel S. Physico-chemical treatment techniques for wastewater laden with heavy metals. Chem Eng J 2006;118:83–98.

Lan G, Hong X, Fan Q, Luo B, Shi P, Chen X. Removal of Hexavalent Chromium in Wastewater by Polyacrylamide Modified Iron Oxide Nanoparticle. J Appl Polym Sci

2014;131:40945–55.

Lee C, Kim S. Cr(VI) Adsorption to Magnetic Iron Oxide Nanoparticle-Multi-Walled Carbon Nanotube Adsorbents. Water Environ Res 2016;88:2111–20.

Li J, Kalam A, Al-shihri AS, Su Q, Zhong G, Du G. Monodisperse ceria nanospheres: Synthesis, characterization, optical properties, and applications in wastewater treatment. Mater Chem Phys 2011;130:1066–71.

Lin C-J. The chemical transformations of chromium in natural waters - A model study. Water Air Soil Pollut 2002;139:137–58.

Liu TY, Zhao L, Tan X, Liu SJ, Li JJ, Qi Y, et al. Effects of physicochemical factors on Cr(VI) removal from leachate by zero-valent iron and a-Fe2O3 nanoparticles. Water Sci Technol 2010;61:2759–68.

Lopes CB, Figueira P, Tavares DS, Lin Z, Daniel-da-Silva AL, Duarte AC, et al. Core-shell magnetite-silica dithiocarbamate-derivatised particles achieve the Water Framework Directive quality criteria for mercury in surface waters. Environ Sci Pollut Res 2013;20:5963–74.

Lu W, Li J, Sheng Y, Zhang X, You J, Chen L. One-pot synthesis of magnetic iron oxide nanoparticle-multiwalled carbon nanotube composites for enhanced removal of Cr(VI) from aqueous solution. J Colloid Interface Sci 2017;505:1134–46.

Luther S, Brogfeld N, Kim J, Parsons JG. Study of the thermodynamics of chromium(III) and chromium(VI) binding to iron (II/III) oxide or magnetite or ferrite and magnanese(II) iron (III) oxide or jacobsite or manganese ferrite nanoparticles. J Colloid Interface Sci 2013;400:97–103.

Lv G, Li Z, Jiang WT, Ackley C, Fenske N, Demarco N. Removal of Cr(VI) from water using Fe(II)-modified natural zeolite. Chem Eng Res Des 2014;92:384–90.

Madaeni SS. The application of membrane technology for water disinfection. Water Res 1999;33:301–8.

Mahmoodi NM. Manganese ferrite nanoparticle: Synthesis, characterization, and photocatalytic dye degradation ability. Desalin Water Treat 2013;3994:1–7.

Mahmoud ME, Abdou AEH, Sobhy ME. Engineered nano-zirconium oxide-crosslinked-nanolayer of carboxymethyl cellulose for speciation and adsorptive removal of Cr(III) and Cr(VI). Powder Technol 2017;321:444–53.

Mahmoudi M, Simchi A, Imani M, Shokrgozar MA, Milani AS, Häfeli UO, et al. A new approach for the in vitro identification of the cytotoxicity of superparamagnetic iron oxide

nanoparticles. Colloids Surfaces B Biointerfaces 2010;75:300–9.

Mao N, Yang L, Zhao G, Li X, Li Y. Adsorption performance and mechanism of Cr(VI) using magnetic PS-EDTA resin from micro-polluted waters. Chem Eng J 2012;200–202:480–90.

Markiewicz B, Komorowicz I, Sajnóg A, Belter M, Barałkiewicz D. Chromium and its speciation in water samples by HPLC/ICP-MS - technique establishing metrological traceability: A review since 2000. Talanta 2015;132:814–28.

Martínez LJ, Muñoz-Bonilla A, Mazario E, Recio FJ, Palomares FJ, Herrasti P. Adsorption of chromium(VI) onto electrochemically obtained magnetite nanoparticles. Int J Environ Sci Technol 2015;12:4017–24.

Martins MA, Trindade T. Os nanomateriais e a descoberta de novos mundos na bancada do químico. Quim Nova 2012;35:1434–46.

Mazur LP. Brown marine macroalgae as a natural cation exchanger for toxic metal ions separation and recovery from water. Universidade do Porto, 2017.

Minas F, Chandravanshi BS, Leta S. Chemical precipitation method for chromium removal and its recovery from tannery wastewater in Ethiopia. Chem Int 2017;3:291–305.

Ministério do Ambiente. Decreto-Lei n.º 236/98 de 1 de Agosto. Diário Da República 1998;176:3676–722.

Mohamed A, Nasser WS, Osman TA, Toprak MS, Muhammed M, Uheida A. Removal of chromium (VI) from aqueous solutions using surface modified composite nanofibers. J Colloid Interface Sci 2017;505:682–91.

Mohan S, Singh Y, Verma DK, Hasan SH. Synthesis of CuO nanoparticles through green route using Citrus limon juice and its application as nanosorbent for Cr(VI) remediation : Process optimization with RSM and ANN-GA based model. Process Saf Environ Prot 2015;96:156–66.

Mokadem Z, Saïdi-Besbes S, Agusti G, Elaissari A, Derdour A. Magnetic nanoadsorbents for metal remediation. J Colloid Sci Biotechnol 2016;5:11–133.

Moradi SE, Baniamerian MJ. Metal-oxide-modified nanostructured carbon application as novel adsorbents for chromate ion removal from water. Int J Mater Res 2012;103:743–8.

Moura RCA, Bertuol DA, Ferreira CA, Amado FDR. Study of chromium removal by the electrodialysis of tannery and metal-finishing effluents. Int J Chem Eng 2012;2012:7.

Muthumareeswaran MR, Alhoshan M, Agarwal GP. Ultrafiltration membrane for effective

removal of chromium ions from potable water. Sci Rep 2017;7:41423–34.

Naja GM, Volesky B. Toxicity and Sources of Pb, Cd, Hg, Cr, As, and Radionuclides in the Environment. Heavy Met. Environ. 1st ed., 2009, p. 13–62.

Navarro E, Baun A, Behra R, Hartmann NB, Filser J, Miao AJ, et al. Environmental behavior and ecotoxicity of engineered nanoparticles to algae, plants, and fungi. Ecotoxicology 2008;17:372–86.

Nithya R, Gomathi T, Sudha PN, Venkatesan J, Anil S, Kim S. Removal of Cr(VI) from aqueous solution using chitosan-g-poly(butyl acrylate)/silica gel nanocomposite. Int J Biol Macromol 2016;87:545–54.

NPI. Emission estimation technique manual for galvanizing. NPI - Natl Pollut Invent 2012.

Oliveira-Silva R, Pinto da Costa J, Vitorino R, Daniel-da-Silva AL. Magnetic chelating nanoprobes for enrichment and selective recovery of metalloproteases from human saliva. J Mater Chem B 2014;3:238–49.

Pang Y, Zeng G, Tang L, Zhang Y, Liu Y, Lei X. Preparation and application of stability enhanced magnetic nanoparticles for rapid removal of Cr(VI). Chem Eng J 2011;175:222–7.

Parlament E, Council of the European Union. Directive 2010/75/UE of the European Parliament and of the Council of 24 November 2010 on industrial emissions (integrated pollution prevention and control). Off J Eur Union 2010.

Parsons JG, Hernandez J, Gonzalez CM, Gardea-torresdey JL. Sorption of Cr(III) and Cr(VI) to high and low pressure synthetic nano-magnetite (Fe3O4) particles. Chem Eng J 2014;254:171–80.

Parsons JG, Lopez ML, Peralta-Videa JR, Gardea-Torresdey JL. Determination of arsenic(III) and arsenic(V) binding to microwave assisted hydrothermal synthetically prepared Fe3O4, Mn3O4, and MnFe2O4 nanoadsorbents. Microchem J 2009;91:100–6.

Paul ML, Samuel J, Roy R, Chandrasekaran N. Studies on Cr(VI) removal from aqueous solutions by nanotitania under visible light and dark conditions. Bull Mater Sci 2015;38:393–400.

Public Partnership for Better Inovation Policies and Instruments in Support of Eco-Innovation: ECOPOL. Leather - Tanning with Chromium 2013. https://ecopolproject.blogspot.de/2013/10/leather-tanning-with-chromium.html (accessed February 1, 2018).

Qiu H, Lv L, Pan B, Zhang QQ, Zhang W, Zhang QQ. Critical review in adsorption kinetic

models. J Zhejiang Univ Sci A 2009;10:716–24.

Quina FH. Nanotecnologia e o Meio Ambiente: Perspectivas e Riscos. Quim Nov 2004;27:1028–9.

Rad SAM, Mirbagheri SA, Mohammadi T. Using Reverse Osmosis Membrane for Chromium Removal from Aqueous Solution. World Acad Sci Eng Technol 2009;57:348–52.

Rajabathar JR, Shukla AK, Ali A, Al-Lohedan HA. Silver nanoparticle/r-graphene oxide deposited mesoporous-manganese oxide nanocomposite for pollutant removal and supercapacitor applications. Int J Hydrogen Energy 2017;42:15679–88.

Rajput S, Pittman CU, Mohan D. Magnetic magnetite (Fe3O4) nanoparticle synthesis and applications for lead (Pb2+) and chromium (Cr6+) removal from water. J Colloid Interface Sci 2016;468:334–46.

Ramakrishnaiah CR, B. P. Hexavalent Chromium Removal by Chemical Precipitation Method: A Comparative Study. Int J Environ Res Dev 2011;1:41–9.

Ray PZ, Shipley HJ. Inorganic nano-adsorbents for the removal of heavy metals and arsenic: a review. RSC Adv 2015;5:29885–907.

Rengaraj S, Yeon K-H, Moon S-H. Removal of chromium from water and wastewater by ion exchange resins. J Hazard Mater 2001;87:273–87.

Renzoni A, Zino F, Franchi E. Mercury Levels along the Food Chain and Risk for Exposed Populations. Environ Res 1998;77:68–72.

Rocha LS, Lopes CB, Henriques B, Tavares DS, Borges JA, Duarte AC, et al. Competitive effects on mercury removal by an agricultural waste: application to synthetic and natural spiked waters. Environ Technol 2014;35:661–73.

Saikia J, Saha B, Das G. Efficient removal of chromate and arsenate from individual and mixed system by malachite nanoparticles. J Hazard Mater 2011;186:575–82.

Salgueiro AM, Daniel-da-Silva AL, Girão A V., Pinheiro PC, Trindade T. Unusual dye adsorption behavior of κ-carrageenan coated superparamagnetic nanoparticles. Chem Eng J 2013;229:276–84.

Santander P, Morales D, Rivas BL, Kabay N, Yilmaz I, Kuşku Ö, et al. Removal of Cr(VI) from aqueous solution by a highly efficient chelating resin. Polym Bull 2017;74:2033–44.

Santosa SJ, Siswanta D, Sudiono S, Utarianingrum R. Chitin-humic acid hybrid as adsorbent for Cr(III) in effluent of tannery wastewater treatment. Appl Surf Sci 2008;254:7846–50.

Sayin S, Yilmaz M. Synthesis of a new calixarene derivative and its immobilization onto magnetic nanoparticle surfaces for excellent extractants toward Cr(VI), As(V), and U(VI). J Chem Eng Data 2011;56:2020–9.

Sezgin N, Yalçın A, Köseoğlu Y. MnFe2O4 nano spinels as potential sorbent for adsorption of chromium from industrial wastewater. Desalin Water Treat 2016;57:16495–506.

Shahriari T, Bidhendi GN, Mehrdadi N, Torabian A. Effective parameters for the adsorption of chromium(III) onto iron oxide magnetic nanoparticle. Int J Environ Sci Technol 2014;11:349–56.

Simeonidis K, Kaprara E, Samaras T, Angelakeris M, Pliatsikas N, Vourlias G. Optimizing magnetic nanoparticles for drinking water technology : The case of Cr(VI). Sci Total Environ 2015;535:61–8.

Skoog DA, Holler FJ, Nieman TA. Princípios de Análise Instrumental. 5ª Edição. 2002.

Smita S, Gupta SK, Bartonova A, Dusinska M, Gutleb AC, Rahman Q. Nanoparticles in the environment: assessment using the causal diagram approach. Environ Heal 2012;11:11.

Socrates G. Infrared and Raman characteristic group frequencies. Third. 2004.

Srivastava S, Agrawal SB, Mondal MK. Synthesis, characterization and application of Lagerstroemia speciosa embedded magnetic nanoparticle for Cr(VI) adsorption from aqueous solution. J Environ Sci 2017;55:283–93.

Srivastava V, Kohout T, Sillanpää M. Potential of cobalt ferrite nanoparticles (CoFe2O4) for remediation of hexavalent chromium from synthetic and printing press wastewater. J Environ Chem Eng 2016;4:2922–32.

Suh YJ, Chae JW, Jang HD, Cho K. Role of chemical hardness in the adsorption of hexavalent chromium species onto metal oxide nanoparticles. Chem Eng J 2015;273:401–5.

Sundaravadivel M, Vigneswaran S, Visvanathan C. Waste minimization in metal finishing industries. Wastewater Recycl Reuse, Reclam 2004;1:317–36.

Sureshkumar V, Daniel SCGK, Ruckmani K, Sivakumar M. Fabrication of chitosan – magnetite nanocomposite strip for chromium removal. Appl Nanosci 2016;6:277–85.

Tahergorabi M, Esrafili A, Kermani M, Shirzad-Siboni M. Application of thiol-functionalized mesoporous silica-coated magnetite nanoparticles for the adsorption of heavy metals. Desalin Water Treat 2016;57:19834–45.

Tavares DS, Daniel-Da-Silva AL, Lopes CB, Silva NJO, Amaral VS, Rocha J, et al. Efficient sorbents based on magnetite coated with siliceous hybrid shells for removal of mercury ions.

J Mater Chem A 2013;1:8134–8143.

Tavares DS, Lopes CB, Daniel-da-Silva AL, Duarte AC, Trindade T, Pereira E. The role of operational parameters on the uptake of mercury by dithiocarbamate functionalized particles. Chem Eng J 2014;254:559–70.

Thekkudan VN, Vaidyanathan VK, Ponnusamy SK, Charles C, Sundar S, Vishnu D, et al. Review on nanoadsorbents: a solution for heavy metal removal from wastewater. IET Nanobiotechnology 2016;11:213–24.

Trindade T, Thomas PJ. Defining and using very small crystals. In: Reedijk J, Poeppelmeier K, editors. Compr. Inorg. Chem. II. Vol.4, Oxford: Elsevier; 2013, p. 343–69.

Tünay O, Kabdaşli I, Hung Y-T. Treatment of Metal Finishing Wastes. Handb. Ind. Hazard. Wastes Treat. 2nd ed., 2004, p. 203–74.

Uygun M, Feyzioğlu E, Özçalışkan E, Caka M, Ergen A, Akgöl S, et al. New generation ion-imprinted nanocarrier for removal of Cr(VI) from wastewater. J Nanoparticle Res 2013;15:1833–43.

Valle JP, Gonzalez B, Schulz J, Salinas D, Romero U, Gonzalez DF, et al. Sorption of Cr(III) and Cr(VI) to K2Mn4O9 nanomaterial a study of the effect of pH, time, temperature and interferences. Microchem J 2017;133:614–21.

Verdonschot PFM, Spears BM, Feld CK, Brucet S, Keizer-Vlek H, Borja A, et al. A comparative review of recovery processes in rivers, lakes, estuarine and coastal waters. Hydrobiologia 2013;704:453–74.

Vinodhini PA, Sudha PN. Removal of heavy metal chromium from tannery effluent using ultrafiltration membrane. Text Cloth Sustain 2016;2:15.

Wang X, Guo Y, Yang L, Han M, Zhao J, Cheng X. Nanomaterials as Sorbents to Remove Heavy Metal Ions in Wastewater Treatment. J Environ Anal Toxicol 2012;2:154–8.

Watts MP, Coker VS, Parry SA, Pattrick RAD, Thomas RAP, Kalin R, et al. Biogenic nano-magnetite and nano-zero valent iron treatment of alkaline Cr(VI) leachate and chromite ore processing residue. Appl Geochemistry 2015;54:27–42.

WHO. Guidelines for Drinking-water Quality. World Heal Organ 2011.

WHO. Chromium in Drinking-water. World Heal Organ 2003.

Xu P, Zeng GM, Huang DL, Feng CL, Hu S, Zhao MH, et al. Use of iron oxide nanomaterials in wastewater treatment: A review. Sci Total Environ 2012;424:1–10.

Zargar FH. Separation of Hexavalent Chromium from Water Using Nanofiltration. Int. Conf. Trade, Tour. Manag., 2012, p. 134–8.

Zhang H, Mcdowell RG, Martin LR, Qiang Y. Selective extraction of heavy and light lanthanides from aqueous solution by advanced magnetic nanosorbents. ACS Appl Mater Interfaces 2016;8:9523–31.

Zhang Y, Yan T, Yan L, Guo X, Cui L, Wei Q, et al. Preparation of novel cobalt ferrite/chitosan grafted with graphene composite as effective adsorbents for mercury ions. J Mol Liq 2014;198:381–7.

Zhao F, Zou Y, Lv X, Liang H, Jia Q, Ning W. Synthesis of CoFe2O4 – Zeolite Materials and Application to the Adsorption of Gallium and Indium. J Chem Eng Data 2015;60:1338–44.

Zhou W, Yin B-C, Ye B-C. Highly sensitive surface-enhanced Raman scattering detection of hexavalent chromium based on hollow sea urchin-like TiO2@Ag nanoparticle substrate. Biosens Bioelectron 2017;87:187–94.

Zhu X, Tian S, Cai Z. Toxicity Assessment of Iron Oxide Nanoparticles in Zebrafish (Danio rerio) Early Life Stages. PLoS One 2012;7:46286–91.

Chapter 7

Attachments

FTIR-ATR

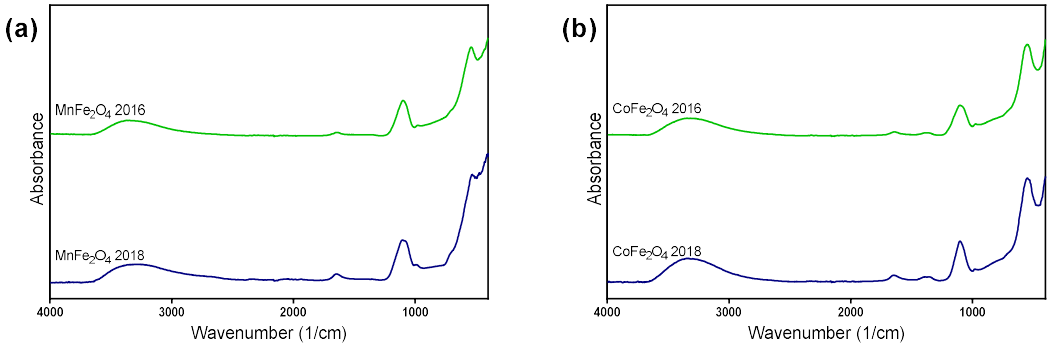

Figure 26 - FTIR-ATR spectra of (a) $MnFe_2O_4$ and (b) $CoFe_2O_4$ NPs, acquired in 2016 and 2018.

Table IX - Nanomaterials for Cr removal with respect to the conditions used as reported in the literature in the last 10 years (since 2007).

Reference	Nanomaterial	Type of water	pH	Temperature (ºC)	Amount of sorbent (x10^{-3} mg/L)	Contact time (h)	Initial element concentration (x10^{-3} µg/L)	Cr starting specie	Uptake capacity (mg/g) or removal efficiency (%)	Type of system
(Kaprara et al., 2017)	**S n(II) oxy-hydroxides NPs** (pH synthesis)	Distilled water	6-8	10-30	0.025-0.75	0.016-48	0.010-5.0	Cr(VI)	~31 (30ºC, $Sn_6O_4(OH)_4$ pH 2)	Mono elemental
	$Sn_6O_4(OH)_4$ (pH 2) $Sn_6O_4(OH)_4$ /SnO (pH 4)		6, 7, 8 6, 7, 8	20	0.025-0.75	24	0.25-5.0		29.359 (pH 6), 23.440 (pH 7), 21.359 (pH 8) 10.354 (pH 6), 8.112 (pH 7), 6.990 (pH 8)	
	$Sn_6O_4(OH)_4$ (pH 2) $Sn_6O_4(OH)_4$ (pH 4) SnO_2 (pH 6) SnO_2 (pH 9) $Sn_3OSO_4(OH)_2$ (pH 2) $Sn_6O_4(OH)_4$ /SnO (pH 4) $Sn_6O_4(OH)_4$ /SnO (pH 6) $Sn_6O_4(OH)_4$ /SnO (pH 9)		7	20			0.010		19 10 <0.5 <0.5 6.1 5.2 5.2-6.1 5.2-6.1	
	$Sn_6O_4(OH)_4$ (pH 2)		7	10, 20, 30	0.20	0.016-48	5.0		~19 (10ºC), 27 (20ºC), 31 (30ºC)	
	Sn(II) oxy-hydroxides NPs (pH synthesis)	Natural-like water	7.0-7.8	20			0.10	Cr(VI)	19 (pH 7, $Sn_6O_4(OH)_4$ pH 2)	Multi elemental
	$Sn_6O_4(OH)_4$ (pH 2) $Sn_6O_4(OH)_4$ (pH 4) $Sn_6O_4(OH)_4$ /SnO (pH 4) $Sn_6O_4(OH)_4$ /SnO (pH 9)		7.0 7.8 7.0 7.0 7.0	20			0.010		19 18.5 7.0 4.0 4.8	

(Mahmoud et al., 2017)	**Nano-ZrO_2** Nano zirconium oxide **Nano-ZrO_2-glu-CMC** Crosslinking of nanolayer carboxymethyl cellulose (CMC) onto the surface of nano zirconium oxide (Nano-ZrO_2) using glutaraldehyde	Distilled water	1.0-7.0	r.t. [f]	2.5	0.017-1.0	1040-10 400	Cr(III) Cr(VI)	187 (500 mg/L, Nano-ZrO_2-glu-CMC) 73 (500 mg/L, Nano-ZrO_2-glu-CMC)	Mono elemental
			1.0-7.0	r.t.	2.5	0.50	5200	Cr(III) Cr(VI)	3-26 Nano-ZrO_2 (pH 7) 44-58 Nano-ZrO_2-glu-CMC (pH 7) 2-6 Nano-ZrO_2 (pH 1-2) 19-35 Nano-ZrO_2-glu-CMC (pH 1-2)	
				r.t.	2.5	0.017, 0.083, 0.17, 0.25, 0.33, 0.42, 0.50, 0.67, 0.83, 1.0	5200	Cr(III) Cr(VI)	26 Nano-ZrO_2 (1 h) 62 Nano-ZrO_2-glu-CMC (1 h) 6 Nano-ZrO_2 (1 h) 37 Nano-ZrO_2-glu-CMC (1 h)	
				r.t.	0.50, 1.0, 1.5, 2.0, 2.5, 3.0, 4.0, 5.0, 7.5, 10	0.50	5200	Cr(III) Cr(VI)	94 Nano-ZrO_2 (500 mg/L) 187 Nano-ZrO_2-glu-CMC (500 mg/L) 10 Nano-ZrO_2 (500 mg/L) 73 Nano-ZrO_2-glu-CMC (500 mg/L)	
			7 2	r.t.	2.5	0.50	1040, 2080, 3120, 4160, 5200, 6240, 7279, 8319, 9349, 10 400	Cr(III) Cr(VI)	62 Nano-ZrO_2 (10 400 x10^3 µg/L) 89 Nano-ZrO_2-glu-CMC (10 400 x10^3 µg/L) 18 Nano-ZrO_2 (10 400 x10^3 µg/L) 54 Nano-ZrO_2-glu-CMC (10 400 x10^3 µg/L)	
			7 2	r.t.	2.5	0.50	5200	Cr(III) Cr(VI)	11-26 Nano-ZrO_2 29-44 Nano-ZrO_2-glu-CMC 4-8 Nano-ZrO_2 14-27 Nano-ZrO_2-glu-CMC (depending on the type of interfering ion)	Multi elemental

(Huang et al., 2017)	**Pd/Fe_3O_4 NPs** Magnetite nanoparticles functionalized with palladium		3	Information not mentioned	5.0	8.0	20	Cr(VI) Total Cr	~60% ~60%	Multi elemental
(Valle et al., 2017)	**$K_2Mn_4O_9$** Rancieite type material		2-6	4-45	2.5	0.083-2.0	0.30-30	Cr(III) Cr(VI)	33% (pH 6)/ 41.8 (45ºC) 23% (pH 2) / 4.22 (4ºC)	Mono elemental
			2, 3, 4, 5, 6	r. t.	2.5	1.0	0.30	Cr(III) Cr(VI)	~5-33% (pH 6) ~3-23% (pH 2)	
			5 2	4, 25, 45	2.5	0.083, 0.17, 0.25, 0.50, 1.0, 1.5, 2.0	30	Cr(III) Cr(VI)	21.7 (4ºC), 36.5 (25ºC), 41.8 (45ºC) 4.22 (4ºC), 4.08 (25ºC), 3.25 (45ºC)	
			5 2		2.5	1.0	0.30	Cr(III) Cr(VI)	~4-37% ~0-67% (depending on the type and concentration of interfering ion)	Multi elemental
(Srivastava et al., 2017)	**MNPLB** Lagerstroemia speciosa bark (LB) embedded magnetic nanoparticles	Double distilled water	1.09-7.02	15-40	0.1-0.7	0.17-2.0	50-500	Cr(VI)	739.7 (500 x10^3 µg/L)	Mono elemental
			2.05	35	0.4	0.17, 0.50, 0.83, 1.2, 1.5, 1.83, 2.0	100		234.3 (0.17h), 237.2 (0.50h), 239.7 (0.83h), 243.1 (1.2h), 249.7 (1.5h), 249.7 (1.83h), 249.8 (2.0h)	
			2.05	35	0.4	1.5	50, 100, 200, 250, 300, 500		124.9 (50 x10^3 µg/L), 249.7 (100 x10^3 µg/L), 350.4 (200 x10^3 µg/L), 384.5 (250 x10^3 µg/L), 444.0 (300 x10^3 µg/L), 739.7 (500 x10^3 µg/L)	
			2.05	35	0.1, 0.2, 0.3, 0.4, 0.5, 0.6, 0.7	1.5	100		675.2 (100 mg/L), 394.7 (200 mg/L), 315.2 (300 mg/L), 249.7 (400 mg/L), 199.9 (500 mg/L), 166.6 (600 mg/L), 142.8 (700 mg/L)	
			1.09, 2.05, 3.0, 4.02, 5.04, 6.07, 7.02	35	0.4	1.5	100		249.7 (pH 1.09), 249.7 (pH 2.05), 242.3 (pH 3.0), 235.5 (pH 4.02), 234.6 (pH 5.04), 231.6 (pH 6.07), 225.5 (pH 7.02)	

			2.05	15, 20, 25, 30, 35, 40	0.4	1.5	100		197.4 (15ºC), 208.0 (20ºC), 239.9 (25ºC), 246.3 (30ºC), 249.7 (35ºC), 249.7 (40ºC)	
(Lu et al., 2017)	**MNP/MWCNTs** Magnetic iron oxide nanoparticle-multiwalled carbon nanotube composites	Ultrapure water	1.0-9.0	25-45	0.4-2.0	0-24	5.0-50	Cr(VI)	~98% (1000-2000 mg/L) 42.02 (45ºC)	Mono elemental
			1, 2, 3, 4, 5, 6, 7, 8, 9	25	1.0	4.0	5.0		~15-95% (pH 2)	
			2.0	25	0.4, 0.6, 0.8, 1.0, 1.2, 1.6, 2.0	4.0	5.0		~61-98% (1000-2000 mg/L)	
			2.0	25, 35, 45	1.0	24	5.0, 10, 20, 30, 40, 50		22.22 (25ºC), 39.68 (35ºC), 42.02 (45ºC) (depending on the material type)	
			2.0	25	1.0	0.083-6.0	5.0, 10, 15		4.964 (5 x10^3 µg/L), 9.457 (10 x10^3 µg/L), 13.43 (15 x10^3 µg/L) (depending on the material type)	
			2.0		1.0		10	Cr(VI)	~92-95% (depending on the type of interfering ion)	Multi elemental
(Mohamed et al., 2017)	**PAN-CNT/TiO_2-NH_2** Polyacrylonitrile (PAN) and carbon nanotube (CNTs)/titanium dioxide nanoparticles (TiO_2) functionalized with amine groups (TiO_2-NH_2) composite nanofibers		2-9	r.t. (20)	0.1-0.8	0-7	10-300	Cr(VI)	99.7% (6000 mg/L) 861.11 [a]	Mono elemental
			2, 3, 4, 5, 7, 9	20	0.5		10		~65-99% (pH 2)	
			2	20, 40, 60	0.5		10-300		732 (20ºC), 704.7 (40ºC), 584.8 (60ºC)	
			2	20		0-7	10 20 30 50 80 100 200 300		26.67 [a] 53.88 [a] 78.95 [a] 137.30 [a] 217.47 [a] 276.47 [a] 550.87 [a] 861.11 [a]	
			2		0.1, 0.2, 0.4, 0.6, 0.8	0.67	100		55.2-99.7% (6000 mg/L)	

(Rajabathar et al., 2017)	**Meso-MnO_2** Mesoporous manganese oxide **AgNPs@meso-MnO_2** silver nanoparticles doped mesoporous manganese oxide **Ag/Graphene-meso-MnO_2** silver nanoparticle graphene deposited mesoporous manganese oxide nanocomposite	Milli-Q water	6	r.t.	6.7	24	50	Cr(VI)	~35% 98% / 460 68% / 140	Mono elemental
(Srivastava et al., 2016)	**$CoFe_2O_4$ NPs** Cobalt ferrite nanoparticles	Distilled water	2-12	25-55	2-12	0-4.0	75-150	Cr(VI)	98.45 % (55ºC, 75 x10^3 µg/L) 16.73 (55ºC)	Mono elemental
				25	10	0-4.0	75, 100, 125, 150		65.50-91.76% (75 x10^3 µg/L)	
					2, 4, 6, 8, 10, 12				~62-93% (12 x10^3 mg/L)	
			2, 4, 6, 8, 10, 12	25	10		75		50.0-94.14% (pH 2)	
				25, 40, 55	10	2.0	75 100 125 150		91.76-98.45% (55ºC) 84.57-93.45% (55ºC) 75.20-85.94% (55ºC) 65.50-74.91% (55ºC)	
			6	25, 40, 55	10	2.0			10.53 (25ºC), 10.98 (40ºC), 16.73 (55ºC)	
		Printing press wastewater	1-12	25-55	10	0-24	1637.5	Cr(VI)	~69%	Multi elemental
			0.98	25	10	0-24	1637.5		~69 %	
			1, 2, 4, 5, 10, 12	25	10		1637.5		~36-89% (pH 10/12)	
			2	25, 40, 55	10	2.0	1637.5		46.44-64.56% (55ºC)	

(Lee and Kim, 2016)	**MIO-MWCNTs** **MWCNTs** Multi-walled carbon nanotubes **MIO NPs** Magnetic iron oxide nanoparticles		2.6-7.3	5-60	1.0	0.25-4.0	5-100	Cr(VI)	12.61 (100 x10^3 µg/L, MIO-MWCNTs) 80.8% (5 x10^3 µg/L, MIO-MWCNTs)	Mono elemental
		MIO-MWCNTs MWCNTs MIO NPs	3	30	1.0	0.25, 0.50, 0.75, 1.0, 2.0, 3.0, 4.0	10		4.54 – 5.93 (4 h) 4.80 (4 h) 5.27 (4 h)	
		MIO-MWCNTs	3	30	1.0	4.0	5-100		12.6-80.8% (5 x10^3 µg/L) 4.04-12.61 (100 x10^3 µg/L)	
		MIO-MWCNTs	3	5, 15, 30, 45, 60	1.0	0.25, 0.50, 0.75, 1.0, 2.0, 3.0, 4.0	10		5.47-6.64 (5ºC)	
		MIO-MWCNTs	2.6-7.3	30	1.0		10		2.13-5.70 (pH 3)	
					1.0		5-100		11.256	
(Chooaksorn et al., 2016)	**CN-coated AC** Bituminous activated carbon (AC) coated with chitosan nanoparticles (CN) **CN-AC/DC** CN coated on AC by the dip coating method **CN-AC/WI** CN coated on AC by the wet impregnation method	Deionized water	5.0	Information not mentioned	1.0	0-24	0.10-100	Cr(VI)	77.52 (CN-AC/DC) 61.7% (0.1 x10^3 µg/L, CN-AC/DC)	Mono elemental
			5.0		1.0	0-24	0.10-100		61.35 CN NPs 57.47 CN-AC/WI 77.52 CN-AC/DC 38.5-61.7% CN-AC/DC (0.1 x10^3 µg/L)	
			5.0		1.0	0-24	10		4.66 CN-AC/WI 4.84 CN-AC/DC	
(Dubey et al., 2016)	**n-Al_2O_3** γ-alumina nanoparticles modified with cetyl trimethyl ammonium bromide (CTAB)	Distilled water	2.0-10.0	30-60	4-24	0-1.5	5-25	Cr(VI)	94% (5 x10^3 µg/L, pH 2.03, 18 340 mg NPs/L) 18.716 [b] (25 x10^3 µg/L)	Mono elemental
			2, 4, 6, 8, 10						~46-94% (pH 2)	
			2			0-1.5	5 10 15		4.707 8.415 12.155 [b]	

							20 25		15.933 [b] 18.716 [b] ~40-94% (5 x10^3 µg/L, 1h)	
			2		4, 8, 12, 16, 20, 24				~52-94% (20 000-24 000 mg/L)	
			2	20 30 40 60			5, 10, 15, 20, 25		~64-94% (5 x10^3 µg/L) / 0.8952 ~54-87% (5 x10^3 µg/L) / 0.8204 ~50-70% (5 x10^3 µg/L) / 1.0149 ~40-63% (5 x10^3 µg/L) / 0.7469	
			2.03		18.34		5		94%	
(Gupta et al., 2016)	**CuO NPs** Copper(II) oxide nanoparticles	Double distilled water	2-10	25-45	0.4-5	0-3.0	10-150	Cr(VI)	96.3% (10 x10^3 µg/L) 86.25 (400 mg/L)	Mono elemental
			2, 3 4, 5, 6, 7, 8, 9, 10	r.t.	1.0	3.0	20		33.05-65.5% (pH 3) 13.1 (pH 3)	
			3	r.t.	0.40, 0.80; 1.2, 1.6, 2.0, 3.0, 4.0, 5.0		20		34.5-92.8% (5000 mg/L) 18.56-86.25 (400 mg/L)	
			3	r.t.	1.6	0-3.0	20		~82% (1h)	
			3	r.t.	1.6	3.0	10, 20, 30, 50, 70, 100, 150		16.33-96.3% (10 x10^3 µg/L)	
			3	25 35 45	1.6	3.0	20		83% / 15.625 17.636 94% / 18.518	
(Bisht et al., 2016)	**IONPs** Magnetic iron oxide nanoparticles **MIONPs** EDTA-modified magnetic iron oxide nanoparticles		2	r.t.	0.0050-0.030	0-18	200-1000	Cr(VI)	99.90% / 499.5 (30 mg/L, MIONPs) 34.06% / 170.33 (30 mg/L, IONPs)	Mono elemental
			2	r.t.	0.0050, 0.010, 0.015, 0.020, 0.025, 0.030	3.0			320.17-499.5 (30 mg/L) MIONPs 86.88-170.33 (30 mg/L) IONPs	

						18			64.03% (5 mg/L), 77.67% (10 mg/L), 89.16% (15 mg/L), 93.77% (20 mg/L), 96.65% (25 mg/L), 99.90% (30 mg/L) MIONPs 17.37% (5 mg/L),19.15% (10 mg/L), 22.41% (15 mg/L), 25% (20 mg/L), 29.05% (25 mg/L), 34.06% (30 mg/L) IONPs	
			2	25	0.010	0.33, 0.66, 1.0, 1.3, 1.7, 2.0, 2.3, 2.7, 3.0, 18	1000		163.97 (3h), 452.26 (18h) MIONPs 147.95 (3h), 170.33 (18h) IONPs	
			2	25		3.0	200, 400, 600, 800, 1000		82.80-367.67 MIONPs (1000 x10^3 µg/L) 37.55-106.33 IONPs (1000 x10^3 µg/L)	
(Gifford et al., 2016)	**Ti-AX** Titanium dioxide nanoparticles precipitated in anion exchange resins	Synthetic groundwater	8	Information not mentioned	0.60	168	0.10	Cr(VI)	88%	Multi elemental
(Nithya et al., 2016)	**Cs-g-PBA/SG** Chitosan-g-poly(butylacrylate)/ silica gel nanocomposite		3-9	r.t.	10-60	1.0-6.0	62.5-1000	Cr(VI)	98% (62.5-125 x10^3 µg/L) 55.71	Mono elemental
			3, 4, 5, 6, 7, 8, 9		10	1.0	100		~94.1-97.4% (pH 7)	
					10, 20, 30, 40, 50, 60				~97.4-97.73% (60 000 mg/L)	
			7	25	10	1.0-6.0	100		~96.7-98 (5-6h)	
			7	r.t.	10	1.0	62.5, 125, 250, 500, 750, 1000		54-98% (62.5-125 x10^3 µg/L) 55.71	
(Sureshkumar et al., 2016)	**Chitosan–Fe_3O_4 nanocomposite strip** Chitosan–magnetite nanocomposite strip	Deionised water	Information not mentioned	Information not mentioned	1 cm x 1 cm 0.010 L	0.17, 0.30, 0.83, 1.2, 1.5, 1.8, 2.2	260	Cr(VI)	~15-92.33%	Mono elemental

X

(Tahergorabi et al., 2016)	**TF-SCMNPs** Thiol-functionalized mesoporous silica-coated magnetite nanoparticles (**Fe_3O_4 NPs**)	Distilled water	3-10	r.t. (25)	0.080-0.40	0.083-24	8	Cr(III)	42% (pH 10, 400 mg/L) 1.119	Mono elemental
			3, 5, 7, 10	r.t.	0.40	0.083, 0.17, 0.25, 0.33	8		2.5-42% (pH 10, 0.33 h)	
			10		0.080, 0.16, 0.24, 0.32, 0.40	0.33	8		1.375-42% (400 mg/L)	
			10		0.40 TF-SCMNP 0.40 Fe_3O_4	0.33	8		42% 13.875%	
			10		0.080-0.40	24	8		1.119	
(Khan et al., 2016)	**Fe-Cu binary oxide NPS**	Milli-Q water	1-9	r.t. (25)	0.10-2.5	1.0	1-25	Cr(VI)	~100% (100 mg/L, 1 x10^3 µg/L) 71.43	Mono elemental
			3	25	0.10 0.50 1.0 2.5	1.0	1, 5, 10, 25		~10-50% (1 x10^3 µg/L) 81.3% (1 x10^3 µg/L) 76.54% (5 x10^3 µg/L) 71.43% (10 x10^3 µg/L) 73.76% (25 x10^3 µg/L) ~92-98% (1 x10^3 µg/L) ~99-100% (1 x10^3 µg/L)	
			3	25	0.10, 0.50, 1.0, 2.5	1.0	5		27.9% (100 mg/L), 76.54% (500 mg/L), 97.48% (1000 mg/L), 99.86% (2000 mg/L)	
			1, 3, 5, 7, 9	25	0.50	1.0	5		41.25% (pH 1), 76.54% (pH 3), 71.5% (pH 5), 53.28% (pH 7), 26.82% (pH 9)	
			3	25	0.10	0-10	1.15		~40% (4 h)	
			3	25	1.0				71.43	

(Arthy and Phanikumar, 2016)	**MIN** Magnetic iron oxide nanoparticles **MIN-TW** Magnetic iron oxide nanoparticles/tea waste composite **MIN-SB** Magnetic iron oxide nanoparticles/sugarcane bagasse composite	Deionized water	2-7	30	0.50-1.25	0.083-2.0	50-300	Cr(III)	98.27% (MIN-SB, 1h, 1125 mg/L) 518.134 [d] (MIN-SB, 0.75 h)	Mono elemental
	MIN MIN-TW MIN-SB		2, 3, 4, 5, 6	30	1.0	0.75	50		83.86% / 45.93 (pH 6) 78.46% / 39.23 (pH 6) 94.23% / 47.11 (pH 6)	
	MIN MIN-TW MIN-SB		6	30	1.0	0.75	50, 100, 200, 250		90.90% / 227.25 (250×10^3 µg/L) 89.82% / 224.558 (250×10^3 µg/L) 96.74% / 241.87 (250×10^3 µg/L)	
	MIN MIN-TW MIN-SB		6	30	1.0	0.083-2.0	250		93.03% / 232.59 (0.92 h) 92.83% / 232.08 (1 h) 98.27% / 245.68 (1 h)	
	MIN MIN-TW MIN-SB		6	30	0.50, 0.75, 1.0, 1.125	0.92 1.0 1.0	250		93.03 % (1125 mg/L) 232.59 (500 mg/L) 92.83% (1125 mg/L) 232.08 (500 mg/L) 98.27% (1125 mg/L) 245.68 (500 mg/L)	
	MIN MIN-TW MIN-SB					0.82 0.84 0.75			502.779 [c] 466.773 [c] 518.134 [d]	
	MIN MIN-TW MIN-SB			30, 35, 45					323.59 (30ºC), 242.92 (35ºC), 246.89 (45ºC) 232.08 (30ºC), 241.99 (35ºC), 245.52 (45ºC) 245.06 (30ºC), 247.16 (35ºC), 248.99 (45ºC)	
	MIN MIN-TW MIN-SB	Deionized water						Cr(III)	~229-243 ~228-240 ~243-247 (depending on the type of interfering ion)	Multi elemental

(Babaei et al., 2016)	**ST/Mag NPs** Spent tea-supported magnetite nanoparticles	Double-distilled water	2-8	r.t. (20)	0.10-11.0	0.033-4.0	5-300	Cr(VI)	~100% (5 x10^3 µg/L) 30.03	Mono elemental
			2, 3, 4, 5, 6, 7, 8	20	5.0	2.0	10		~65-92.8% (pH 2)	
			2	20	0.10-11.0	2.0	10		10.1-99.7% (6000 mg/L)	
			2	20	6.0	0.033-4.0	10 100		1.44 / 99.7% (1h) 13.92 / 81.8% (1h)	
			2	20	6.0	2.0	5-300		30.03 ~55-100% (5 x10^3 µg/L)	
		Synthetic saline wastewater	2	20	3.0	1.0	10	Cr(VI)	78.3-99.9% 1.09-1.39 (depending on the concentration of interfering ions)	Multi elemental
(Rajput et al., 2016)	**Fe_3O_4 NPs** Magnetic magnetite nanoparticles	Double distilled water	2-10	25-45	1.0-4.0	0-24	2-100	Cr(VI)	~75% (4000 mg/L) 34.9 (45ºC)	Mono elemental
			2, 4, 6, 8, 10	25	1.0		20		10-58.4% (pH 2)	
			2	25	1.0 2.0 4.0	0-24	50		30% / 14.01 57% / 16.13 [b] ~75% / 8.70 [b]	
			2	25	2.0	0-24	25 50 100		9.90 [b] 8.85 [b] 17.24 [b]	
			2	25, 35, 45	2.0	0-24	2-100		20.2 (25ºC), 26.8 (35ºC), 34.9 (45ºC)	
(Egodawatte et al., 2016)			3-6	25	0.25	2.0	5.2-104	Cr(III)	343 (pH 5.4, ESH@MS-60-NH_2)	Mono elemental
	ESH Electrospun hematite nanofiber		5.4	25		2.0			208	
	ESH@MS-60 Electrospun hematite nanofiber/mesoporous silica core/shell		5.4	25		2.0			178	

	ESH@MS-60-NH_2 Electrospun hematite nanofiber/mesoporous sílica functionalized with amine group		5.4	25		2.0			343	
(Debnath et al., 2016)	**$CaFe_2O_4$ NPs** Calcium ferrite nanoparticles	Ultrapure deionized water	2-6	r.t.	0.0625-1.0	0.033-1.7	30-250	Cr(III)	340 (62.5 mg/L) 99% (pH 2 / 30 x10^3 µg/L)	Mono elemental
			2, 3, 4, 5, 6		1.0	0.67	50		5.80-49.50 (pH 2) 11.5-99% (pH 2)	
					1.0		30-250		29-122 (250 x10^3 µg/L) ~49-99% (30 x10^3 µg/L)	
			2		1.0	0.033-1.67	30, 50, 70, 100, 125		~30-115 (125 x10^3 µg/L)	
			2		0.0625, 0.125, 0.25, 0.50, 0.75, 1.0	0.67	50		~340 (62.5 mg/L) > 95% (1000 mg/L)	
			2		1.0	0.67	30-250		124.11	
(Sezgin et al., 2016)	**$MnFe_2O_4$ NPs** Manganese ferrite nanoparticles	Real wastewater from galvanotechnic industry	2	r.t.	0.5-6.0	0.17-24	50-250	Total Cr	334.80 (500 mg/L) 71.37% (1500 mg/L)	Multi elemental
			2		0.50, 1.0, 1.5, 2.0, 3.0, 6.0	24			34.68-334.80 (500 mg/L) ~50-71.37% (1500 mg/L)	
			2		1.5	0.17-24			~80 / ~60% (2 h)	
			2		1.5	24	50, 100, 150, 250		~10-40 (250 x10^3 µg/L) ~25-30% (50 x10^3 µg/L)	
					1.5	2.0			89.18 / 59.35%	
(Simeonidis et al., 2015)	**Fe_3O_4 NPs** Magnetite nanoparticles	Distilled water	7	20	0.10-1.0	0.083-24	0.25	Cr(VI)	~2.4 (24 h)	Mono elemental

		Natural-like water	5-8	20	0.10-1.0	0.083-24	0.050-1.0	Cr(VI)	~100% (pH 6.5, 3 h / pH 7.0, 4 h) 4 (pH 5)	Multi elemental
			7			0.083-24	0.25		~1.1 (24 h)	
			5-8		0.10	24	0.050-1.0		1-4 (pH 5)	
			6.5 7.0 7.5		1.0	0.50-5.8	0.10		~100% (3 h) ~100% (4 h) ~95% (5 h)	
(Martínez et al., 2015)	**Fe_3O_4 NPs** Magnetite nanoparticles		1.5-4.5	10-75	0.50-2.0	0-2.0	0-160	Cr(VI)	~26 (2000 mg/L)	Mono elemental
			3.5	20	2.0	0-2.0	80		~12 (2 h)	
			1.5, 2.5, 3.5, 4.5	20	2.0	0.50	80		~5.5-13.5 (pH 1.5)	
			3.5	10, 20, 45, 75	2.0	0.50	80		~9-25 (75ºC)	
			3.5	20	2.0	0.50	0, 5, 10, 20, 40, 80, 160		~3-12 (160 x10^3 µg/L)	
			3.5	20	0.50, 1.0, 2.0	0.50	80		~10.5-12 (500 mg/L) ~7.5-26 (2000 mg/L)	
(Bagheri et al., 2015)	**CS–CA NPs** Chitosan–citric acid nanoparticles	De-ionized water	2-6	25-45	0.50-5.0	0-2.0	10-110	Cr(VI)	94.46% (70 x10^3 µg/L) 38.51 (500 mg/L)	Mono elemental
	CS NPs Chitosan nanoparticles		4	25	2.0	0, 0.17, 0.33, 0.66, 1.0, 1.83, 2.0	25		61.75% CS-CA (1-2 h) 83.54% CS (1-2 h)	
	CS–CA NPs		2, 3, 4, 5, 6	25	3.0	1.0	50		52.89-86.83% (pH 3) ~9-14 (pH 3)	
			4	25	0.50, 1.0, 1.5, 2.0, 2.5, 3.0, 3.5	1.0	50		38.51-83.33% (3000-3500 mg/L) 3.88-38.51 (500 mg/L)	
			3	25	3.0	1.0	10, 30, 50,70, 90, 110		53.42-94.46% (70 x10^3 µg/L) 22.4 (70 x10^3 µg/L)	

(Mohan et al., 2015)	**CuO NPs** Cupric oxide nanoparticles	De-ionized double distilled water	2.0-10.0	20-60	0.25-2.5	0-5.8	5-50	Cr(VI)	98.8% 50.0 (250 mg/L)	Mono elemental
			7.0	25	1.0	0-5.8	30		~35% (2.5-5.8 h) ~8 (2.5-5.8 h)	
			7.0	25	1.0	2.5	5, 10, 15, 20, 25, 30, 35, 40, 45, 50		21.9-91.0% (5 x10^3 µg/L) 3.5-8.55 (25 x10^3 µg/L)	
			2, 3, 4, 5, 6, 6, 7, 8, 9, 10	25	1.0	2.5	25		20-73.2% (pH 4) 4-14.07 (pH 4)	
			4.0	25	0.25, 0.50, 0.75, 1.0, 1.25, 1.5, 1.75, 2.0, 2.25, 2.5	2.5	25		50-80% (1250 mg/L) 7.93-50.0 (250 mg/L)	
			4.0	20, 25, 30, 35, 40, 45, 50, 55, 60	1.25	2.5	25		13.3-86.5% (40ºC) 2.5-16.63 (40ºC)	
			3.81	37.1	1.28		22.5		98.8%	
(Paul et al., 2015)	**TiO_2 NPs** Titania nanoparticles	Deionized (MilliQ) water	2.0-12.0	28	0.010-0.50	0.083-0.75	5-100	Cr(VI)	85.85 (20 x10^3 µg/L)	Mono elemental
			2, 5, 7, 9, 12						75.47 (pH 7)	
						0.083, 0.17, 0.25, 0.33, 0.50, 0.75			79.24 (0.5 h)	
					0.010, 0.050, 0.10, 0.20, 0.50				83.01 (100 mg/L)	
			7.0		0.10	0.50	5, 10, 20, 50, 100		85.85 (20 x10^3 µg/L)	
(Watts et al., 2015)	**BnM** Biogenic nano-magnetite	Ultrapure water	12	20	0.75 Anoxic	0-350	Model solution	Cr(VI)	32	Mono elemental
		Contaminated groundwater	11.9	20	0.66 Anoxic 0.66 Oxic	0-200	16.69	Cr(VI)	24 7	Multi elemental

(Guan et al., 2015)	**PAA@VTES@Fe_3O_4 NPs** Magnetite nanoparticles coated with silane coupling agent (VTES) grafted with polyacrylic acid (PAA)	Ultrapure water	2-6	20-40	1.0-6.5	0-24	170	Cr(III)	92.5% (pH 6, 5000-6500 mg/L) 80.6 (40ºC)	Mono elemental
			2, 2.5, 3, 3.5, 4, 4.5, 5, 5.5, 6	30	5.0	4.0	170		56.2-92.5% (pH 6)	
			6	30	1.0, 2.0, 3.5, 4.0, 5.0, 5.5, 6.0, 6.25, 6.5	4.0	170		66.5-92.5% (5000-6500 mg/L)	
			6	20, 30, 40	5.0	0-24	170		54.1 (20ºC), 61.4 (30ºC), 80.6 (40ºC)	
				30						
		Tannery effluent	6		5.0	4.0	170	Total Cr	94.0%	Multi elemental
(Ataabadi et al., 2015)	**Fe_3O_4 NPs** Magnetite nanoparticles	Deaerated deionized water	2-10	25-45	1.0-5.0	0-3.0	0-120	Cr(VI)	100% (pH 2, 4000 mg/L, 20 x10^3 µg/L, 40ºC)	Mono elemental
			2, 3, 4, 6, 8, 10			0-3.0			35.7-100% (pH 2)	
					1.0, 2.0, 3.0, 4.0, 5.0	0-3.0			29.1-100% (4000 mg/L)	
						0-3.0	20, 50, 70, 100		30-100% (20 x10^3 µg/L)	
				25, 30, 35, 40		0-2.0			73.8-100% (40ºC)	
			2	40	4.0	2.0	20		100%	
							20	Cr(VI)	80-100% (depending on the type and concentration of interfering anion)	Multi elemental

(Kumari et al., 2015)	**Fe_3O_4 nanospheres** Mesoporous magnetite nanospheres	Double distilled water	2-7	25-45	1.0-3.0	1.0-72	5–100	Cr(VI)	44% (1h, 2000 mg/L) 8.90 (45ºC)	Mono elemental
			2, 3, 4, 5, 6, 7	25	1.0		10		~ 27-42% (pH 2)	
			4	25	1.0, 2.0, 3.0	1.0, 48, 72	10		44% (1h, 2000 mg/L)	
			4	25	2.0		5 10 20		1.99 4.35 6.55	
			4	25, 35, 45	2.0		10		4.35 (25ºC), 4.50 (35ºC), 4.72 (45ºC)	
			4	25, 35, 45	2.0				6.64 (25ºC), 7.31 (35ºC), 8.90 (45ºC)	
		Groundwater	4	25	2.0	48	10	Cr(VI)	65%	Multi elemental
(Parsons et al., 2014)	**Fe_3O_4 NPs** Magnetite nanoparticles		2-6		2.5	0.083-1.0	0.10-10	Cr(III) Cr(VI)	100% (pH 4, 0.25 h) / 0.555 100% (pH 4, 0.33 h) / 1.705 (depending on the material type)	Mono elemental
			2, 3, 4, 5, 6		2.5	1.0	0.10	Cr(III) Cr(VI)	0-100% (pH 4, depending on the material type) 50-100% (pH 4, depending on the material type)	
					2.5	0.083, 0.17, 0.25, 0.33, 0.5, 1.0	0.10	Cr(III) Cr(VI)	~10-100% (0.25 h, depending on the material type) ~70-100% (0.33 h, depending on the material type)	
			4	r.t. (21)	2.5	1.0	0.25, 0.50, 1, 5, 10	Cr(III) Cr(VI)	0.555 1.208/1.705 (depending on the material type)	
					2.5	1.0	0.10	Cr(III) Cr(VI)	~60-100% ~25-100 % (depending on the material type and on the type and concentration of interenfence anion)	Multi elemental

(Cantu et al., 2014)	**Mn_3O_4** Manganese oxide nanomaterial		2-6	4-45	2.5	0.17-4.0	0.30-1000	Cr(III) Cr(VI)	90% (pH 2)/ 54.4 (45ºC) 85% (pH 2) / 5.8 (45ºC)	Mono elemental
			2, 3, 4, 5, 6	25	2.5	1.0	0.30	Cr(III) Cr(VI)	~60-90% (pH 2) ~20-85% (pH 2)	
			4	4, 26, 45	2.5	1.0	0.30, 3, 30, 300, 1000	Cr(III) Cr(VI)	~7-10 ~3	
			4	4, 21, 45	2.5	1.0	0.30-1000	Cr(III) Cr(VI)	18.7 (4ºC), 41.7 (21ºC), 54.4 (45ºC) 2.5 (4ºC), 4.3 (21ºC), 5.8 (45ºC)	
(Lan et al., 2014)	**PMMNs** Polyacrylamide modified iron oxide nanoparticles		1-8	30	20	0-2.0	50-1000	Cr(VI)	~99% (pH 3, 100 x10^3 µg/L) 35.186	Mono elemental
			1, 2, 3, 4, 5, 6, 7, 8	30	20	0.67	100		~65-97% (pH 3)	
			3	30	20	0-2.0	100		~99%	
			3	30			50-1000		64.20-98.30% (50 x10^3 µg/L) 35.186	
			3	30		0.67	100	Cr(VI)	~94-98% (depending on the type and concentration of salt)	Multi elemental
(Shahriari et al., 2014)	**Fe_3O_4 NPs** Iron oxide magnetic nanoparticles	Artificial wastewater	3-9	25	250-1500 mg (volume not mentioned)	0.25-1.5	250-1000	Cr(III)	99.9% (pH 9)	Mono elemental
			3, 5.5, 7.5, 9	25	1000 mg	1.0	500		32.7-99.9% (pH 9)	
			5.5		250, 500, 750, 1000, 1500 mg		500		56.9-98.5% (1500 mg)	
			5.5	25	750 mg	0.25, 0.42, 0.50, 0.75, 1.0, 1.5	500		71.2-88.7% (1.5 h)	
			5.5	15, 20, 25, 30	750 mg	0.75	500		70.7-92.9% (30ºC)	
			6	25	1000 mg	0.75	250, 500, 750, 1000		96.96-99.1% (250 x10^3 µg/L)	

(Behnajady and Bimeghdar, 2014)	**NiO NPs** Mesoporous nickel oxide nanoparticles	Distilled water	4.7-9	30	1.0-7.0	0-0.83	10-50	Cr(VI)	~100% (10 x10^3 µg/L, 7000 mg/L) / ~5 (50 x10^3 µg/L)	Mono elemental
			4.7	30	6.0		10, 20, 30, 40, 50, 60		~40-100% (10 x10^3 µg/L) ~0-5 (50 x10^3 µg/L)	
			4.7	30	1.0, 2.0, 3.0, 4.0, 5.0, 6.0, 7.0		20		~20-100% (7000 mg/L) ~3-4.5 (2000 mg/L)	
			4.7, 7, 9	30	6.0		20		~94-98% (4.7)	
			4.7	30	6.0		20		4.73	
(Uygun et al., 2013)	**Cr(VI)-imprinted poly(HEMAH) NPs** Chromium(VI)-imprinted hydroxyethylmethacrylate (HEMA) polymeric nanoparticles	Milli-Q ultrapure water	2-6	25	Information not mentioned	0-2	1000-11 000	Cr(VI)	3830.58	Mono elemental
			2, 3, 4, 5, 6	25			7000		~1700-3830.58 (pH 4)	
			4	25		0, 0.33, 0.66, 1.0, 2.0	7000		3830.58 (1-2 h)	
			4	25			1000, 2000, 3000, 4000, 5000, 6000, 7000, 9000, 11 000		0-3830.58 (7000 x10^3 µg/L)	
			4	25			7000		3830.58	
(Guo et al., 2013)	**TiO_2 NPs** Titania nanoparticles		4.0	25	0.10	0-2.5	0-80	Cr(VI)	21.92	Mono elemental
			4.0	25	0.10	2.0	0-80		~13.5-21.76 (16.83 x10^3 µg/L)	
			4.0	25		0.67			21.92	
(Biswal et al., 2013)	**Fe_3O_4-loaded seeds** Magnetite nanoparticles loaded natural seeds sabja		2	Information not mentioned	1000 mg (volume not mentioned)	0, 0.25, 0.50, 0.75, 1.0, 1.5, 2.0	1 5 20 30 50	Cr(VI)	~100% 97% ~85% ~80% ~75%	Mono elemental
							50	Cr(VI)	80%	Multi elemental
(Chen et al., 2013)	**Fe_3O_4/CNT NPs** Carbon nanotubes loaded with magnetite nanoparticles		2-12	20-80	1.0	0.083-120	100-1000	Cr(VI)	95% (pH 2) / 60 (pH 2)	Mono elemental
			2, 4, 6, 8, 10, 12		1.0		100		~75-95% (pH 2) 50-60 (pH 2)	
			6	20, 40, 60, 80			100-800		47.98-83.54 (80ºC)	

(Luther et al., 2013)	**Fe_3O_4 NPs** Iron(II/III) oxide or magnetite or ferrite nanoparticles		2-10	4-50	2.5	1.0	0.30-100	Cr(III) Cr(VI)	100% (Fe_3O_4, pH 6/7) 10.638 100% ($MnFe_2O_4$, pH 2/3) 3.455	Mono elemental
	$MnFe_2O_4$ NPs Magnanese(II) iron (III) oxide or jacobsite or manganese ferrite nanoparticles		2, 3, 4, 5, 6, 7, 8, 9, 10		2.5	1.0	0.30	Cr(III) Cr(VI)	~0-100% Fe_3O_4 (pH 6/7) ~0-80% $MnFe_2O_4$ (pH 6) ~0-60% Fe_3O_4 (pH 3/4) ~0-100% $MnFe_2O_4$ (pH 2/3)	
			6 3	23	2.5	1.0	0.30, 1, 5, 10, 25, 50, 100	Cr(III) Cr(VI)	10.638 Fe_3O_4 7.189 $MnFe_2O_4$ 3.455 Fe_3O_4 3.211 $MnFe_2O_4$	
(Mao et al., 2012)	**Magnetic PS-EDTA resin** Magnetic chelating resin with EDTA functionality		2-12	30	0.20-2.0	0.083-10	5-1000	Cr(VI)	100 % (pH 4, 10 h, 1000 mg/L, 5-40 x10^3 µg/L) 250.00	Mono elemental
			2, 4, 6, 8, 10, 12	30	1.0	6.0	30		30-100% (pH 4)	
			4	30	1.0	0.083-10	30		~100% (10 h)	
			4	30	1.0	10	5-1000		0-240.23 (1000 x10^3 µg/L) ~25-100% (5-40 x10^3 µg/L)	
			4	30	0.20, 0.60, 1.0, 1.4, 1.8, 2.0	10	30		~91-100% (1000 mg/L)	
			4						250.00	
(Akoz et al., 2012)	Semicarbazone derivatives of calix[4]arene immobilized onto magnetic nanoparticles (Fe_3O_4): **MN-C1**, **MN-C2**, **MN-C3**	Deionized water	1.5-4.5	30	2.5	1.0	5.2-20.8	Cr(VI)	90% (MN-C2, pH 1.5)	Mono elemental
			1.5, 2.5, 3.5, 4.5						~30-70% MN-C1 (pH 1.5) ~70-90% MN-C2 (pH 1.5) ~60-80% MN-C3 (pH 1.5)	
			2.5	30	2.5	1.0	5.2, 10.4, 15.6, 20.8		~48-82% MN-C2 (5.2 x10^3 µg/L)	

(Moradi and Baniamerian, 2012)	**NC** Nanoporous carbon **Ni-NC** Nickel oxide onto nanoporous carbon **Fe-NC** Iron oxide onto nanoporous carbon	Ultrapure water	2-10	20, 30, 40	0.20	0-6.0	10-100	Cr(VI)	60.8 (Fe-NC, r.t.)	Mono elemental
			2, 3, 4, 5, 6, 7, 8, 9, 10	30	0.20		100		~20.8 NC (pH 5) ~46.8 Ni-NC (pH 4) ~52.0 Fe-NC (pH 4)	
				r.t.	0.20	6.0			~15.6 NC 44.7 Ni-NC 60.8 Fe-NC	
(Pang et al., 2011)	**PEI-γ-Fe_2O_3@Fe_3O_4 NPs** Polyethylenimine-modified magnetic nanoparticles		2-9	15-35	4.0	0-2.0	50-500	Cr(VI)	98.2% (100 x10^3 µg/L) 83.33 (15ºC)	Mono elemental
			2, 3, 4, 5, 6, 7, 8, 9	25	4.0	0.50	100		~98-55 % (pH 2)	
			2.2	25	4.0	0-2.0	100 200 400 500		98.2% 92.6% 72.5% 64.6%	
				15, 25, 35			50-500		83.33 (15ºC), 78.13 (25ºC), 74.07 (35ºC)	
			2.2	25	4.0	0.50	100	Cr(VI)	~98-100%	Multi elemental
		Wastewater			2.67	0.50	37.98	Cr(VI)	99.0%	
(Kaya et al., 2011)	**GMDFe** Nanosized ferric oxide loaded glycidyl methacrylatebased polymer		2-10	r.t. (25)	4.0	Equilibrium time	30	Cr(VI)	98% (24 h) 163.47 (pH 2)	Mono elemental
			2, 4, 6, 8, 10	25	4.0		30		163.47 (pH 2), 157.52 (pH 4), 94.38 (pH 6), 77.94 (pH 8), 27.37 (pH 10)	
			4	25	4.0	0-24	30		0-98% (24 h)	
			4	25	1000 mg (volume not mentioned)		30		138.84	
(Li et al., 2011)	**CeO_2 NPs** Monodisperse ceria nanospheres	Simulated wastewater	Information not mentioned	r.t.	1.0	0-2.0	4.8 8	Cr(VI)	94.5% / ~4.5 94.1% / 7.52	Mono elemental

(Chen et al., 2011)	**magMCM-41** Magnetic MCM-41 nanosorbents	Deionized, distilled water	2-7	r.t. (25)	1.0	Information not mentioned	106-156	Cr(VI)	98.8 (pH 2), 83.2 (pH 5)	Mono elemental
		Deionized, distilled water	2-5 5.0				 156	Cr(VI)	67.6 67.6	Multi elemental
		Tap water	5.2				114	Cr(VI)	46.8	
		Mountain stream water	5.4 2, 5, 8				122	Cr(VI)	31.2 97% (pH 2), 97% (pH 5), 86% (pH 8)	
		River water	5.5				106	Cr(VI)	41.6	
(Sayin and Yilmaz, 2011)	**BHCB-MN** 5,11,17,23-tetra-tert-butyl-25,27-di(benzhydrazidylmethoxy)-26,28-dihydroxy-calix[4]arene immobilized silica-based magnetic nanoparticles	Deionized water	1.5 2.5 3.5 4.5	25	2.5	1	5.2	Cr(VI)	66% ~64% 11% ~0%	Mono elemental
(Saikia et al., 2011)	**$Cu_2CO_3(OH)_2$ NPs** Malachite nanoparticles	Milli-Q water	4-9	10-40	5.0-20	1-16	20-500	Cr(VI)	82.2 75% (pH 5, 50 x10^3 µg/L)	Mono elemental
			4, 5, 6, 7, 8, 9		5.0		100		~2-15 (pH 4)	
			5	30	5.0, 10, 15, 20		100		~4-15 (20 000 mg/L)	
			5	30	5.0	1-16	20, 100, 200, 500		82.2	
				10-40			100		11.4-15.6 (40ºC)	
			5				50		75%	
			5				50	Cr(VI)	70%	Multi elemental

(Debnath et al., 2010)	**NHTO** Nanoparticles of hydrous titanium(IV) oxide	Distilled water	2.0	30	1000-3000 mg (packed column)	0.013-0.026	8.0-32.0	Cr(VI)	12.94 [e] (32.0 x10^3 µg/L)	Mono elemental
			2.0	30	1000 2000 3000	0.013 0.026 0.039	16.0		10.13 [e] 11.75 [e] 12.53 [e]	
			2.0	30	2000	0.026	8.0 16.0 32.0		7.31 [e] 11.75 [e] 12.94 [e]	
		Industrial effluent wastewater	2.06	30	4000	0.026	15.67	Cr(VI)	~100%	Multi elemental
(Liu et al., 2010)	**α-Fe_2O_3 NPs** Hematite nanoparticles	Dilute simulated	3-8	20-35	0.50-3.0	0-24	20-200	Cr(VI)	~90% (pH 3)	Mono elemental
		landfill leachate			1.0	0-24 5.0	20 50 100 200		86.5% 77.0% 69.3% 57.0%	
			3.0, 4.0, 5.0, 6.0, 7.0, 8.0						~20-90% (pH 3)	
			6.7	20	0.50, 1.0, 2.0, 3.0	0-24	20		57.2% (500 mg/L), 63.5% (1000 mg/L), 82.5% (2000 mg/L), 88.0% (3000 mg/L)	
			6.7				20	Cr(VI)	~50%	Multi elemental
(Chowdhury and Yanful, 2010)	**Fe_3O_4-γ-Fe2O3 NPs** Magnetite-maghemite nanoparticles	De-ionized water	2-14	r.t.	0.40	0.17-4	1-2	Cr(VI)	96% (pH 2, 1 x10^3 µg/L) 4.45 (pH 2, 2 x10^3 µg/L)	Mono elemental
			2-14	r.t.	0.40	24	1 2		0-96% (pH 2) / 0-2.4 (pH 2) 0-85% (pH 2) / 0-4.45 (pH 2)	
			3		0.40	0.17-4	1 2		70-92% (2 h) 60-85% (2 h)	
			4		0.40			Cr(VI)	35-90%	Multi elemental

(Hu et al., 2007)	Magnetic NPs:	Milli-Q water	2.0-9.3	22.5	5.0	0-1.0	20-100	Cr(VI)	100% ($MnFe_2O_4$, 0.083 h)	Mono elemental
	$MnFe_2O_4$		2.0	22.5	5.0	0-1.0	100		~100% (0.083 h)	
	$MgFe_2O_4$								~85% (0.75 h)	
	$ZnFe_2O_4$								~60% (0.5 h)	
	$CuFe_2O_4$								~50% (0.33 h)	
	$NiFe_2O_4$								~30% (0.25 h)	
	$CoFe_2O_4$								~20% (1 h)	
	$MnFe_2O_4$		2-9.3		5.0				99.5% (pH 2)	
	$MgFe_2O_4$								~10-85% (pH 2)	
	$ZnFe_2O_4$								~5-60% (pH 2)	
	$CuFe_2O_4$								~5-50% (pH 2)	
	$NiFe_2O_4$								~0-30% (pH 2)	
	$CoFe_2O_4$								~0-20% (pH 2)	

[a]Nonlinear Pseudo-second-order model. [b]Pseudo-second-order model. [c]Langmuir type 4 capacity. [d]Langmuir type 1 capacity. [e]Thomas model column capacity. [f]Room temperature.

Note that,
the conditions that are shaded correspond to the best uptake capacity or removal efficiency obtained;
in general, when the type of water is not referred, the authors may have used distilled or milli-Q water;
in the column correspondent to “Cr starting specie”, total chromium concentration was quantified in the works that refer it; in the other works no mention is made regarding the specie or if it is total concentration;
in the column correspondent to “Uptake capacity (mg/g) or removal efficiency (%)”, when the value does not present units, it is the uptake capacity; otherwise, it is the removal efficiency;
the value presented in parentheses in the column “Uptake capacity (mg/g) or removal efficiency (%)” corresponds to the condition that gave rise to the value of uptake capacity or removal efficiency presented;
the uptake capacity values which do not presented a subscript were obtained either experimentally or by Langmuir model;
sometimes, the authors refer to experimental conditions of experiments whose results they do not present;
from column “Type of water” until “Cr starting specie”, the conditions mentioned are the same for the below lines